République Algérienne Démocratique et Populaire

Ministère de l'Enseignement Supérieur et de la Recherche Scientifique

UNIVERSITÉ DE RELIZANE

Faculté des Sciences et Technologies

Département d'Électrotechnique et d'Automatique

THÈSE DE DOCTORAT LMD 3ème CYCLE

Filière : Electrotechnique

Spécialité : Énergies Renouvelables

Titre de thèse

Etude d'un convertisseur DC-DC à haut gain avec MPPT basé sur l'intelligence artificielle pour les applications photovoltaïques

Présenté et soutenu publiquement par :

MOHAMMED BELHADJ SOUHEYB

Soutenue le 24 janvier 2026, devant le jury composé de :

Président	BENAIRED Noreddine	Prof.	Univ. de Relizane
Directeur de thèse	MELIANI Bouziane	Prof.	Univ. de Relizane
Examinateur	BOUNADJA Elhadj	Prof.	Uni, de Chlef
Examinateur	KHOUIDMI Houari	Prof.	Uni, de Chlef
Examinateur	MOSTEFA TOUNSI Mahmoud	MCA.	Uni, de Relizane

Année Universitaire : 2025/2026

République Algérienne Démocratique et Populaire

Ministère de l'Enseignement Supérieur et de la Recherche Scientifique

UNIVERSITÉ DE RELIZANE

Faculté des Sciences et Technologies

Département d'Électrotechnique et d'Automatique

PHD THESIS – LMD 3rd CYCLE

Field: Electrical Engineering

Specialization: Renewable Energies

Thesis Title

Study of a high-gain DC-DC converter with MPPT based on artificial intelligence for photovoltaic applications

Defended by

MOHAMMED BELHADJ SOUHEYB

Defended on 24 January 2026, before the jury composed of :

President:	BENAIRED Noreddine	Prof.	Univ. of Relizane
Thesis Supervisor:	MELIANI Bouziane	Prof.	Univ. of Relizane
Examiner:	BOUNADJA Elhadj	Prof.	Uni, of Chlef
Examiner:	KHOUIDMI Houari	Prof.	Uni, of Chlef
Examiner:	MOSTEFA TOUNSI Mahmoud	MCA.	Uni, of Relizane

Academic Year : 2025/2026

Dedication

To my beloved **parents**,
whose love, guidance, and unwavering support have been my greatest source of strength. You have stood by me in both joy and hardship, believing in me even when I doubted myself. Every page of this thesis is a reflection of your sacrifices and encouragement. This achievement is as much yours as it is mine.

To my dear sisters, **Zineb** and **Assia**, and my brother, **Abderrahim**,
for your kindness, patience, and constant encouragement throughout this journey.

To my supervisor, **Professor Bouziane Meliani**,
for his valuable guidance, trust, and mentorship, and to my colleague **Nassr-Allah Guezouli**, as well as all those who have supported me directly or indirectly during this work — my heartfelt gratitude.

To all those who continue to pursue their goals despite obstacles,
may you always find the strength to persevere and the courage to dream.

Finally, I dedicate this work to **myself**,
for the endurance to face challenges, the resilience to overcome them, and the determination to achieve this milestone. Through this journey, I have discovered not only knowledge but also patience, growth, and self-belief. May this be the beginning of a lifelong pursuit of learning, purpose, and fulfillment.

Acknowledgments

First and foremost, I would like to express my deepest gratitude to
Allah, the Most Gracious and the Most Merciful,
for granting me the strength, courage, and perseverance
to overcome challenges and successfully complete this research work.

This doctoral thesis, carried out within the
Industrial Engineering and Sustainable Development Laboratory (GIDD),
Department of Automation and Electrical Engineering,
Faculty of Technology, **University of Relizane**,
has been made possible through the invaluable guidance and support of
Professor Bouziane Meliani, my thesis supervisor.
His insightful advice, encouragement, and continuous support
have been instrumental in shaping the direction and quality of this work.
I owe him my sincerest thanks and profound respect.

I would also like to express my heartfelt appreciation to
Professor Marco Rivera,
from the **Power Electronics, Machines and Control (PEMC) Research Group**
at the **University of Nottingham**,
for kindly accepting me into the laboratory and providing the opportunity
to conduct experimental studies.
His expertise and guidance have been extremely valuable
to my academic and professional development.

My deepest gratitude goes to my **parents, sisters, and brother**,
whose unconditional love, patience, and encouragement
have been a constant source of motivation throughout this journey.
Their sacrifices and unwavering belief in me
have given me the strength to persevere and achieve this milestone.

I extend my sincere thanks to **Professor Noreddine Benaired**,
who kindly accepted to chair the defense committee of this thesis.
My appreciation also goes to **Professor Abdellah Chaouch**,
Professor Elhadj Bounadja, **Professor Houari Khouidmi**,
and **Mr. Mahmoud Mostefa Tounsi**,
for graciously agreeing to serve as examiners
and for their valuable remarks and constructive feedback
that have enriched this work.

Finally, I would like to thank all those who have, in one way or another,
contributed to the completion of this research.
Your support and collaboration have been truly appreciated.

الملخص

أدى الطلب المتزايد على الطاقة النظيفة والمستدامة إلى تركيز الاهتمام العالمي على توليد الطاقة المتجددة، حيث برزت الطاقة الشمسية الكهروضوئية كتقنية رائدة due إلى وفرتها وقابليتها للتوسع وتأثيرها البيئي المنخفض. ومع ذلك، فإن أنظمة الطاقة الشمسية مقيدة بعدم انتظام موارد الطاقة الشمسية المتأصل، وانخفاض كفاءة الخلايا، والخصائص غير الخطية للتيار والجهد. تتطلب هذه القيود استراتيجيات متقدمة لتتبع نقطة الطاقة القصوى ومراحل تحويل طاقة ذات كسب عالٍ لضمان استخراج طاقة فعال ومستقر.

تتناول هذه الأطروحة هذه التحديات من خلال دمج الابتكارات في تصميم المحولات مع تقنيات التحكم الذكية. تم اقتراح محول رافع تيار مستمر تربيعي ثلاثي المستويات جديد كمساهمة أساسية في العتاد. يحقق هذا المحول الرافع كسب جهد عالٍ جداً عند نسب تشغيل معتدلة مع تحقيق توازن تلقائي لجهود المكثفات، مما يقلل من إجهاد أشباه الموصلات ويحسن الكفاءة الإجمالية. هذا التصميم مناسب بشكل خاص لربط مصفوفات الطاقة الشمسية منخفضة الجهد مع نواقل التيار المستمر عالية الجهد في التطبيقات المنفصلة عن الشبكة والمتصلة بها.

على جانب التحكم، تم تطوير شبكة عصبية غير خطية ذاتية الانحدار بمُدخلات خارجية كخوارزمية متقدمة لتتبع نقطة الطاقة القصوى. يتنبأ المتحكم المقترح نقطة التشغيل المثلى من خلال استغلال الأنماط الزمنية في سلوك الخلايا الشمسية، مما يمكن من التقارب السريع وتقليل التذبذب تحت ظروف الإشعاع ودرجة الحرارة المتغيرة. تم إجراء دراسات مقارنة ضد خوارزميات تتبع نقطة الطاقة القصوى الكلاسيكية للتوصيل التدريجي والمنطق الضبابي. تظهر نتائج المحاكاة أن المتحكم المطور يتفوق على الطرق الحالية من حيث سرعة الاستجابة والمتانة ودقة التتبع، محققاً عائداً طاقياً أعلى مع تقليل تموج الطاقة.

تؤكد نتائج هذا العمل أن الجمع بين المحول الرافع المبتكر واستراتيجية تتبع نقطة الطاقة القصوى المطورة يوفر حلاً موثوقاً وفعالاً لأنظمة الطاقة الشمسية من الجيل التالي. لا تساهم الأطروحة فقط في تقدم محولات التيار المستمر ذات الكسب العالي والمتحكمات الذكية، ولكنها تدعم أيضاً الجهود الأوسع لتعزيز القدرة التنافسية للطاقة الشمسية ضمن التحول العالمي نحو الطاقة المستدامة.

الكلمات المفتاحية :الأنظمة الكهروضوئية؛ تتبع نقطة الطاقة القصوى؛ المحول الرافع التربيعي ثلاثي المستويات؛ محولات التيار المستمر ذات الكسب العالي؛ الشبكة العصبية ذاتية الانحدار بمُدخلات خارجية؛ التحكم بالمنطق الضبابي؛ التحكم الذكي؛ الطاقة المتجددة؛ إلكترونيات القدرة.

Abstract

The increasing demand for clean and sustainable energy has intensified the global focus on renewable power generation, with solar photovoltaics (PV) emerging as a leading technology due to their abundance, scalability, and low environmental impact. However, PV systems are constrained by the inherent intermittency of solar resources, low cell efficiency, and nonlinear current–voltage characteristics. These limitations necessitate both advanced maximum power point tracking (MPPT) strategies and high-gain power conversion stages to ensure efficient and stable energy extraction.

This thesis addresses these challenges by integrating innovations in converter design with intelligent control techniques. A novel three-level quadratic DC–DC boost (TLQBC) converter is proposed as the central hardware contribution. The TLQ-boost achieves very high voltage gain at moderate duty ratios while inherently balancing capacitor voltages, thereby reducing semiconductor stress and improving overall efficiency. This architecture is particularly suitable for interfacing low-voltage PV arrays with higher-voltage DC buses in standalone and grid-connected applications.

On the control side, a Nonlinear Autoregressive Neural Network with Exogenous inputs (NARX-NN) is developed as an advanced MPPT algorithm. The proposed NARX-based controller predicts the optimal operating point by exploiting temporal patterns in PV behavior, enabling rapid convergence and minimal oscillation under varying irradiance and temperature conditions. Comparative studies are conducted against classical Incremental Conductance (IC) and fuzzy-logic MPPT algorithms (type-1 and type-2). Simulation results demonstrate that the NARX-NN controller outperforms existing methods in terms of response speed, robustness, and tracking accuracy, achieving higher energy yield with reduced power ripples.

The outcomes of this work confirm that the combination of the TLQ-boost converter and NARX-NN MPPT strategy provides a reliable and efficient solution for next-generation PV systems. The thesis not only contributes to the advancement of high-gain DC–DC converters and intelligent controllers but also supports broader efforts to enhance the competitiveness of solar energy within the global transition to sustainable power.

Keywords: Photovoltaic (PV) systems; Maximum Power Point Tracking (MPPT); Three-Level Quadratic Boost Converter (TLQBC); High-gain DC–DC converters; NARX neural network; Fuzzy logic control; Intelligent control; Renewable energy; Power electronics.

Résumé

La demande croissante en énergie propre et durable a intensifié l'attention mondiale sur la production d'électricité renouvelable, le photovoltaïque (PV) émergeant comme une technologie de premier plan en raison de son abondance, de son extensibilité et de son faible impact environnemental. Cependant, les systèmes PV sont limités par l'intermittence inhérente de la ressource solaire, le faible rendement des cellules et les caractéristiques non linéaires courant-tension. Ces limitations nécessitent à la fois des stratégies avancées de suivi du point de puissance maximal (MPPT) et des étages de conversion de puissance à haut gain pour assurer une extraction d'énergie efficace et stable.

Cette thèse relève ces défis en intégrant des innovations dans la conception des convertisseurs avec des techniques de contrôle intelligentes. Un nouveau convertisseur élévateur DC-DC quadratique à trois niveaux (TLQ-boost) est proposé comme contribution matérielle centrale. Le TLQ-boost atteint un gain de tension très élevé avec des rapports cycliques modérés tout en équilibrant naturellement les tensions des condensateurs, réduisant ainsi la contrainte sur les semi-conducteurs et améliorant l'efficacité globale. Cette architecture est particulièrement adaptée pour l'interfaçage de champs PV basse tension avec des bus DC plus haute tension dans des applications autonomes ou connectées au réseau.

Sur le plan du contrôle, un réseau de neurones non linéaire autorégressif à entrées exogènes (NARX-NN) est développé comme algorithme MPPT avancé. Le contrôleur proposé basé sur NARX prédit le point de fonctionnement optimal en exploitant les modèles temporels du comportement PV, permettant une convergence rapide et des oscillations minimales sous des conditions d'irradiance et de température variables. Des études comparatives sont menées contre les algorithmes MPPT classiques de conductance incrémentale (IC) et de logique floue (type-1 et type-2). Les résultats de simulation démontrent que le contrôleur NARX-NN surpasse les méthodes existantes en termes de rapidité de réponse, de robustesse et de précision de suivi, obtenant un rendement énergétique supérieur avec des ondulations de puissance réduites.

Les résultats de ce travail confirment que la combinaison du convertisseur TLQ-boost et de la stratégie MPPT NARX-NN constitue une solution fiable et efficace pour les systèmes PV de nouvelle génération. La thèse contribue non seulement à l'avancement des convertisseurs DC-DC à haut gain et des contrôleurs intelligents, mais soutient également les efforts plus larges visant à renforcer la compétitivité de l'énergie solaire dans le cadre de la transition mondiale vers une énergie durable.

Mots-clés : Systèmes photovoltaïques (PV) ; Suivi du point de puissance maximal (MPPT) ; Convertisseur élévateur quadratique à trois niveaux (TLQBC) ; Convertisseurs DC-DC à haut gain ; Réseau de neurones NARX ; Commande par logique floue ; Commande intelligente ; Énergie renouvelable ; Électronique de puissance.

Contents

List of Figures

List of Tables

Nomenclature

PV	Photovoltaic
MPPT	Maximum Power Point Tracking
DC–DC	Direct Current–Direct Current
TLQBC	Three-Level Quadratic Boost Converter
AI	Artificial Intelligence
ANN	Artificial Neural Network
NARX	Nonlinear AutoRegressive with Exogenous Inputs
FLC	Fuzzy Logic Controller
T1FLC	Type-1 Fuzzy Logic Controller
T2FLC	Type-2 Fuzzy Logic Controller
P&O	Perturb and Observe
IC	Incremental Conductance
PSO	Particle Swarm Optimization
GWO	Grey Wolf Optimizer
GA	Genetic Algorithm
MPC	Model Predictive Control
RL	Reinforcement Learning
PWM	Pulse Width Modulation
THD	Total Harmonic Distortion
EMI	Electromagnetic Interference

IGBT	Insulated Gate Bipolar Transistor
MOSFET	Metal-Oxide-Semiconductor Field-Effect Transistor
e(k)	Control error at instant (k)
Δe(k)	Change in error
u(k)	Control signal
D(k)	Duty cycle at instant (k)
V	Voltage
I	Current
P	Power
E	Energy
R	Resistance
L	Inductance
C	Capacitance
f	Frequency
T	Period
η_{MPPT}	
ΔV	Voltage ripple
ΔI	Current ripple
P	Power variation
V_{in}	Input voltage
V_{out}	Output voltage
I_{in}	Input current
I_{out}	Output current
P_{pv}	Photovoltaic output power
G	Solar irradiance
T	Cell temperature

General Introduction

General Introduction

The urgent need to address global energy and climate challenges has driven an unprecedented expansion in renewable power. Solar photovoltaics (PV) have emerged as a key contributor to decarbonization: by early 2024 over 1.6 TW of PV capacity was installed worldwide, supplying roughly 8.3% of global electricity and providing "affordable, decarbonized and scalable" power [1]. Renewables are widely recognized as essential for reducing greenhouse gas emissions and mitigating climate change. Solar PV is particularly attractive because it is clean, abundant, and can be deployed at various scales, yet PV systems still face intrinsic limitations. Individual solar cells have relatively modest conversion efficiency (often 15–25%) and incur high material costs [2]. Moreover, PV output is highly variable, depending on irradiance, temperature, and partial shading. Shading or weather fluctuations can drastically reduce power and distort the PV current–voltage curve, so robust power electronics and control are needed to capture available energy. In practice, these issues mean that special techniques must be applied to maximize a PV array's yield under real-world conditions.

A fundamental tool in PV energy harvesting is maximum power point tracking (MPPT), which dynamically adjusts the operating voltage (or duty cycle of a converter) to extract the maximum available power from the panels. Conventional MPPT methods – such as Perturb & Observe (P&O) or Incremental Conductance – are simple and effective under steady conditions, but they often suffer from oscillations around the maximum power point and slow response under rapidly changing irradiance or temperature. Advanced MPPT schemes have been proposed to overcome these limitations, including fuzzy-logic and neural-network controllers, which can provide smoother tracking and faster adaptation. However, these approaches introduce trade-offs in complexity, training effort, and robustness, and their performance is highly sensitive to the underlying power converter dynamics.

High-gain DC–DC converters play a central role in PV systems by stepping up the low, fluctuating panel voltage to the higher DC-link or battery voltage required by loads and inverters. A conventional boost converter is simple but at high duty ratios suffers from large switching losses, increased stress, and poor efficiency [3]. To overcome this, many multi-stage and switched-capacitor topologies have been developed to achieve large voltage gain without extreme duty cycles. Of particular interest are hybrid designs that combine inductors and capacitors (e.g. quadratic boost converters) to multiply the output voltage. These advanced

topologies aim to achieve high gain, maintain balance of capacitor voltages, and reduce ripple. At the same time, the chosen converter architecture directly affects MPPT: a more linear, balanced converter facilitates accurate tracking, especially when intelligent controllers (e.g. AI-based MPPT) are used. Thus, there is a critical research gap at the intersection of converter design and MPPT control. Existing converter topologies either cannot achieve sufficient gain without excessive component stress, or require complex control for capacitor balancing. Similarly, many MPPT algorithms remain suboptimal in very dynamic conditions or incur excessive oscillations, particularly under partial shading or fast irradiance transients. Bridging this gap requires integrated solutions: new power-electronic architectures matched with advanced control strategies.

Motivations and Objectives

The motivation of this thesis is to develop integrated high-performance solutions for solar PV systems. Specifically, it proposes a novel three-level quadratic DC–DC boost converter (TLQ-boost) that combines a quadratic boost core with a multilevel switched-capacitor network, yielding very high voltage gain with intrinsically balanced capacitors. To maximize power extraction from the PV panel, the thesis introduces two advanced AI-based MPPT controllers as core contributions. One is a Nonlinear AutoRegressive Neural Network with exogenous inputs (NARX-NN), which is trained on historical PV data to predict the optimal duty cycle, enabling extremely fast dynamic response with minimal steady-state oscillation. The other is an interval Type-2 fuzzy logic controller (T2FL), which uses fuzzy membership uncertainty to robustly handle changing conditions and achieve very high tracking accuracy (≈99.5% efficiency). Together, the TLQ-boost converter and these intelligent controllers form a high-gain PV power stage with adaptive, data-driven tracking.

- TLQ-Boost Converter: A novel three-level quadratic boost topology combining a quadratic boost principle with a multilevel switched-capacitor network, achieving very high step-up gain and self-balancing capacitor voltages.
- NARX-NN MPPT: A data-driven neural-network controller trained on PV operating data to predict the optimal duty ratio. This AI-based MPPT yields the fastest dynamic response and high efficiency during tracking.
- Type-2 Fuzzy Logic MPPT: An advanced fuzzy-logic controller using interval Type-2 membership functions to handle uncertainty and

nonlinearities. This AI-based MPPT achieves the highest steady-state accuracy (≈99.5% tracking efficiency) under varying conditions.

- Benchmarking and Comparison: A comprehensive performance evaluation of the proposed system against conventional algorithms (incremental conductance, Perturb & Observe, and standard Type-1 fuzzy MPPT) to quantify improvements. Simulation results show that the NARX-NN provides unmatched speed, while the T2FL provides unmatched accuracy.

In addition to these technical novelties, the thesis addresses a key research gap by unifying converter design with intelligent MPPT optimization. Chapter 4's simulations confirm that the TLQ-boost converter reliably produces the expected high voltage gain with no active balancing needed. The new MPPT controllers are shown to dramatically outperform traditional methods: for example, the NARX-NN controller converges to the MPP almost instantaneously, and the Type-2 fuzzy controller maintains tracking efficiencies above 99.5%. Under dynamic irradiance and temperature changes, the combined TLQ–MPPT system consistently extracts over 95% of the available PV power. Together, these advances – the TLQ-boost architecture with passive balancing and two novel AI-based MPPT strategies – significantly enhance the efficiency and robustness of solar energy extraction, marking them as equally important contributions of this work.

Manuscript Organization

This thesis is organized into four chapters. Chapter I surveys existing high-gain DC–DC boost converter topologies, classifying them by operating principles and evaluating their suitability for PV applications. Chapter II reviews state-of-the-art MPPT algorithms, including classical, fuzzy logic, neural network, and metaheuristic approaches, highlighting their strengths and limitations. Chapter III presents the mathematical modeling and design of the proposed TLQ-boost converter, demonstrating its superior performance compared to existing designs. Chapter IV integrates the converter with advanced MPPT strategies—Incremental Conductance, type-1 fuzzy logic, type-2 fuzzy logic, and the proposed NARX-NN—and evaluates their performance under varying irradiance and temperature. The General Conclusion then synthesizes the findings, discusses broader implications, and identifies directions for future research.

CHAPTER I HIGH GAIN DC–DC BOOST CONVERTER TOPOLOGIES

I.1 Introduction

This chapter establishes the theoretical foundation for high-gain DC-DC converter topologies that serve as the cornerstone for artificial intelligence-based maximum power point tracking integration in photovoltaic applications. The investigation focuses specifically on converter architectures capable of achieving substantial voltage gains while maintaining operational characteristics compatible with advanced control system requirements.

The fundamental challenge addressed herein stems from the voltage disparity between photovoltaic panel outputs (12V-48V) and system integration requirements (>400V for grid-tied applications). Traditional boost converters demonstrate acceptable performance for voltage gains below 5:1, but encounter severe limitations at higher ratios due to extreme duty cycle requirements. High duty cycle operation introduces cascading performance degradation including exponential switching losses, elevated thermal stress, enhanced electromagnetic interference, and compromised dynamic response characteristics.

This chapter employs a systematic classification methodology based on six primary dimensions: energy transfer directionality, galvanic isolation implementation, input source characteristics, switching methodology, dynamic response behaviour, and application-specific optimization parameters. This multidimensional approach enables informed topology selection by establishing clear relationships between architectural decisions and performance characteristics critical for AI-based control integration.

The chapter structure progresses through three analytical phases. First, a comprehensive classification framework categorizes high-gain converter topologies according to fundamental operational characteristics. Second, detailed gain enhancement methodologies are examined, encompassing voltage multiplier cells, magnetic coupling techniques, switched-inductor approaches, switched-capacitor systems, and multi-stage architectures. Finally, the analysis synthesizes findings to identify the most promising converter families for photovoltaic applications with AI-MPPT integration.

Particular emphasis is placed on converter characteristics that facilitate intelligent control algorithm integration, including dynamic response behavior, right-half-plane zero characteristics, and input impedance properties affecting maximum power point tracking accuracy under variable irradiance conditions. The comprehensive analysis serves to establish the technical foundation, analytical framework, and systematic comparison methodology essential for optimal topology selection in AI-enhanced photovoltaic systems.

The chapter concludes by identifying superior high-gain converter architectures for AI-MPPT applications, directly informing the detailed design analysis and implementation strategies presented in subsequent chapters. This establishes coherent progression from theoretical foundation through practical implementation within the broader thesis structure.

I.2 Classification Framework for High-Gain DC-DC Converters

The systematic categorization of high-gain DC-DC converter architectures requires a multidimensional classification approach that encompasses operational characteristics, structural configurations, and performance attributes, as presented in Figure 1. This framework facilitates informed topology selection by establishing clear relationships between design parameters and application requirements.

The proposed classification methodology incorporates six primary dimensions: energy transfer direction, galvanic isolation implementation, input source characteristics, switching methodology, dynamic response behaviour, and application-specific optimization. Each dimension contributes distinct performance implications that collectively determine overall system suitability for specific operational scenarios. This taxonomic approach enables designers to navigate the expanding landscape of converter topologies while maintaining focus on application-critical performance metrics.

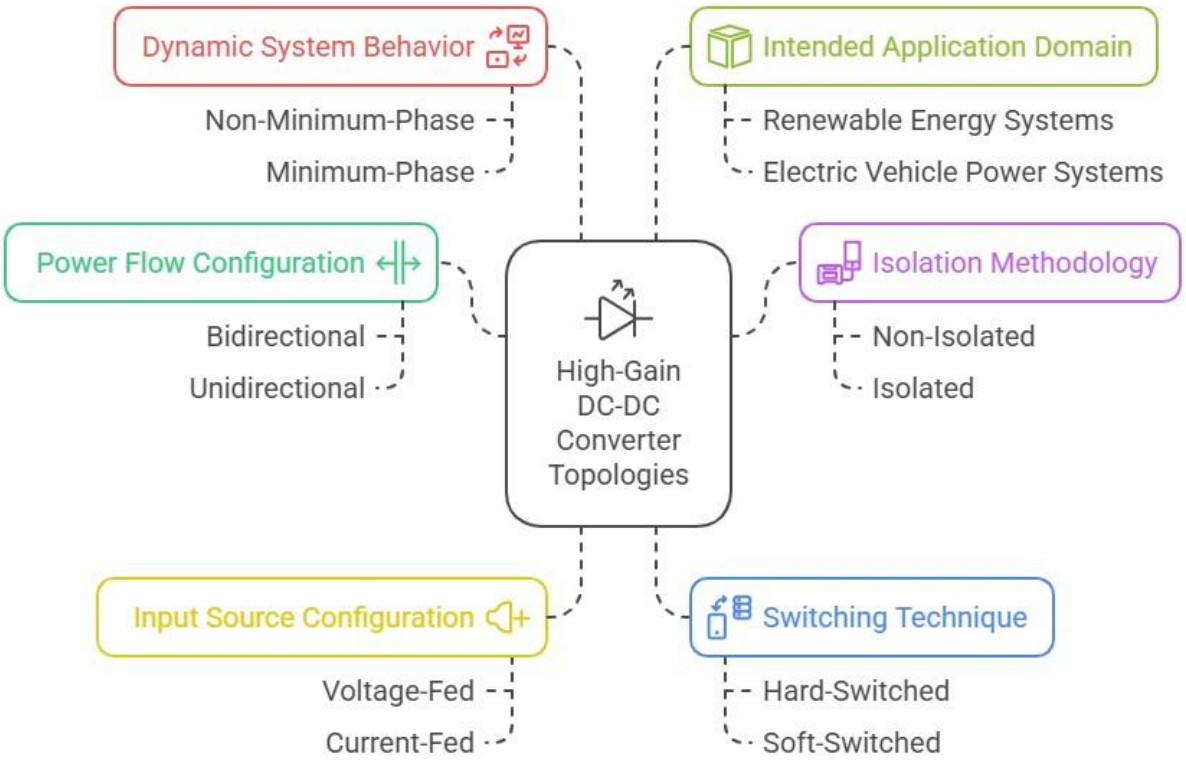

Figure 1 Classification of High-Gain DC–DC Converter topologies

I.2.1 Energy Transfer Configuration Analysis

Modern power conversion systems increasingly demand bidirectional energy flow capabilities, driving the evolution from traditional unidirectional architectures toward more versatile bidirectional implementations. This fundamental distinction shapes component selection, control system complexity, and overall system flexibility.

I.2.1.1 Unidirectional Energy Transfer Systems

Unidirectional converters maintain energy flow exclusively from source to load, implementing this constraint through carefully selected semiconductor configurations and passive component arrangements, as shown in Figure 2(a). These systems demonstrate particular suitability for photovoltaic applications where reverse energy transfer presents minimal operational benefits while introducing unnecessary system complexity [4], [5].

The architectural simplicity of unidirectional systems translates directly into reduced component counts, simplified control algorithms, and enhanced reliability metrics [6]. Conventional implementations utilize MOSFET-diode combinations that inherently prevent reverse current flow while maintaining efficient forward energy transfer. This approach proves particularly advantageous in cost-sensitive applications where bidirectional capability provides insufficient value proposition to justify additional complexity.

Recent developmental efforts have concentrated on extending voltage gain capabilities while preserving the fundamental simplicity advantages [7], [8]. Advanced quadratic configurations achieve substantial gain improvements through cascaded energy transfer stages, enabling voltage amplification ratios exceeding 10:1 without approaching extreme duty cycle regions. These implementations frequently incorporate coupled magnetic elements and voltage multiplier networks to achieve enhanced performance characteristics [9], [10].

The design optimization process for unidirectional systems requires careful consideration of voltage level dependencies. High-voltage applications typically tolerate conventional diode rectification approaches due to proportionally reduced voltage drop impacts. Conversely, low-voltage implementations necessitate synchronous rectification techniques to minimize conduction losses that would otherwise compromise overall efficiency metrics.

I.2.1.2 Bidirectional Energy Management Systems

Bidirectional converter architectures enable energy transfer in both directions, facilitating complex power management scenarios including energy storage integration, regenerative braking systems, and vehicle-to-grid implementations, as illustrated in Figure 2(b) [11], [12].

These systems employ symmetrical switch configurations, typically arranged in anti-series MOSFET pairs, enabling controlled current flow in either direction based on operational requirements.

The implementation complexity inherent in bidirectional systems manifests through dual control loop requirements, increased semiconductor counts, and sophisticated protection mechanisms [13], [14]. However, these investments yield significant system-level benefits including consolidated hardware requirements, enhanced operational flexibility, and improved overall system efficiency through elimination of redundant conversion stages.

For high-power applications requiring galvanic isolation, dual active bridge converter architectures have gained widespread acceptance due to their inherent soft-switching capabilities, symmetrical power transfer characteristics, and robust isolation implementation [15], [16]. These systems demonstrate particular effectiveness in distributed energy systems where power flow direction varies based on generation and consumption patterns.

Advanced control strategies for bidirectional systems continue evolving toward intelligent management approaches that optimize energy transfer efficiency while maintaining system stability across wide operational ranges [13], [16]. Modern implementations incorporate predictive control algorithms that anticipate power flow requirements and adjust operational parameters proactively, resulting in improved transient response and reduced system stress.

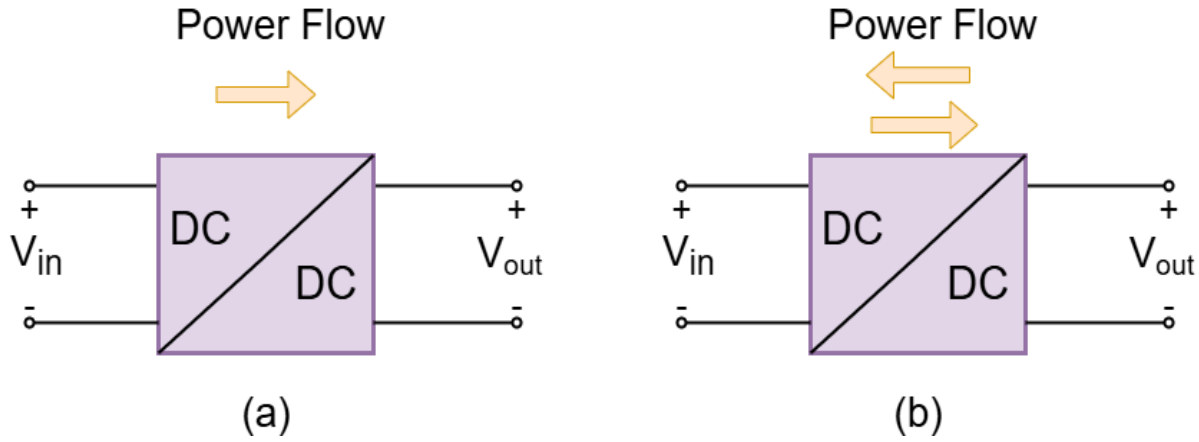

Figure 2 Power flow configuration: (a) Unidirectional converters, (b) Bidirectional converters.

I.2.2 Galvanic Isolation Implementation Strategies

The decision to incorporate galvanic isolation fundamentally influences converter architecture, performance characteristics, and application suitability, as shown in the comparison between Figure 3(a) and Figure 3(b). This choice involves careful evaluation of

safety requirements, electromagnetic compatibility constraints, and performance optimization objectives, as detailed in Table 1.

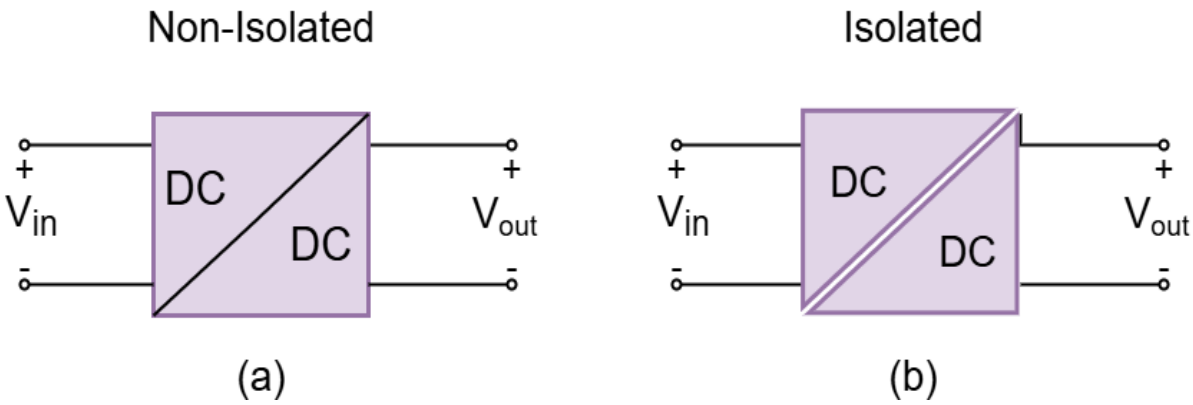

Figure 3 Isolated and Non-isolated DC–DC converter.

I.2.2.1 **Isolated Converter Architectures**

Isolated DC-DC converters employ high-frequency transformers to establish complete electrical separation between input and output domains while enabling efficient energy transfer [17], [18]. This isolation provides essential safety benefits, reduces common-mode noise transmission, and enables flexible voltage level relationships between source and load domains.

The transformer-based isolation approach offers additional voltage transformation capabilities through turns ratio selection, providing a supplementary degree of freedom for achieving desired voltage gains, as demonstrated in Figure 3(b) [19], [20]. This characteristic proves particularly valuable in applications requiring substantial voltage transformation while maintaining reasonable duty cycle operation ranges.

Advanced isolated topologies incorporate sophisticated switching strategies to optimize transformer utilization and minimize magnetic losses [18], [21]. Full-bridge and half-bridge configurations with phase-shifted control enable zero-voltage switching operation, substantially reducing switching losses and electromagnetic interference generation. These soft-switching techniques become increasingly critical as switching frequencies increase to achieve higher power densities [22].

The selection of magnetic core materials and transformer construction techniques significantly impacts overall converter performance [18]. Recent developments in high-frequency core materials enable operation at elevated switching frequencies while maintaining acceptable loss levels. Careful attention to winding techniques, including interleaving and

optimal layer arrangements, minimizes leakage inductance and associated voltage spikes that can compromise device reliability.

I.2.2.2 Non-Isolated Converter Implementations

Non-isolated DC-DC converters eliminate galvanic separation requirements, resulting in simplified architectures with reduced component counts and enhanced efficiency potential, as shown in Figure 3(a) [6]. These systems demonstrate particular effectiveness in applications where isolation is provided elsewhere in the system or where safety requirements permit direct electrical connection between input and output domains.

The architectural simplification achieved through elimination of isolation transformers enables higher power density implementations while reducing electromagnetic interference generation typically associated with high-frequency magnetic coupling [23], [24]. This approach proves especially advantageous in battery-powered systems where every component's contribution to overall efficiency directly impacts operational duration.

Modern non-isolated high-gain topologies employ innovative techniques including coupled inductor networks, switched-capacitor stages, and voltage-lift mechanisms to achieve substantial voltage gains without transformer-based amplification [25]-[28]. These approaches often demonstrate superior dynamic response characteristics compared to transformer-coupled alternatives due to reduced magnetic energy storage requirements and associated response delays.

The development of hybrid topologies combining multiple gain enhancement techniques within non-isolated frameworks represents a significant advancement in converter technology [29], [30]. These systems achieve ultra-high voltage gains while maintaining excellent efficiency metrics and simplified control requirements, making them particularly attractive for renewable energy applications where cost-effectiveness remains paramount [31].

I.2.3 Input Source Configuration Characteristics

The characteristics of the input energy source significantly influence optimal converter architecture selection, with particular emphasis on voltage stability and current profile requirements, as illustrated in Figure 4. This consideration proves especially critical in renewable energy applications where source characteristics exhibit substantial variability [32], [33].

Table 1Comparative Analysis of Isolated and Non-Isolated High-Gain DC–DC Converter Topologies.

Design Criterion	**Isolated DC–DC Converters**	**Non-Isolated DC–DC Converters**
Galvanic Isolation	Provides electrical isolation via a high-frequency transformer, ensuring safety and noise immunity.	Absence of isolation; input and output share a common ground, requiring external protection if needed.
Voltage Gain Capability	Achieves very high voltage gain through transformer turns ratio and advanced modulation schemes.	Moderate to high voltage gain achieved through coupled inductors, switched-capacitor, or hybrid techniques.
Safety and Compliance	Superior safety characteristics, suitable for safety-critical applications (e.g., medical or grid-connected systems).	Limited safety without isolation; less suitable for high-risk environments unless additional protection is incorporated.
Circuit Complexity	Structurally more complex due to transformer design, multiple switching devices, and control requirements.	Relatively simple architecture with fewer components and straightforward control schemes.
Conversion Efficiency	May suffer reduced efficiency due to core losses and transformer leakage inductance.	Typically higher efficiency under moderate power levels due to minimal magnetic losses.
Control Strategy Requirements	Requires advanced control methods (e.g., phase-shift, ZVS/ZCS) to minimize switching losses and manage isolation.	Often compatible with conventional PWM control; simpler regulation and feedback design.
Electromagnetic Interference (EMI)	Better EMI mitigation due to isolation and differential-mode suppression.	Greater susceptibility to EMI; requires additional filtering for noise-sensitive applications.
Typical Applications	Medical electronics, industrial automation, grid-tied PV inverters, electric vehicle fast chargers.	Portable devices, consumer electronics, LED drivers, low-power PV systems, and battery charging circuits.

I.2.3.1 **Voltage-Fed Input Configurations**

Voltage-fed converters utilize parallel input capacitance to maintain stable input voltage characteristics while accommodating load variations and switching transients, as shown in Figure 4(a) [34]. This configuration demonstrates particular effectiveness with fuel cell systems and battery sources where voltage stability represents a primary design objective.

The implementation of voltage-fed architectures typically incorporates substantial input capacitance to minimize voltage ripple and provide instantaneous energy for load transients. This approach enables rapid response to load changes while maintaining acceptable input voltage stability metrics. The control system design for voltage-fed converters emphasizes output voltage regulation through pulse-width modulation techniques with feedback-based duty cycle adjustment [34].

Recent developments in voltage-fed converter technology focus on minimizing input capacitor requirements while maintaining performance standards. Advanced control algorithms incorporate predictive elements that anticipate load changes and adjust operational parameters proactively, reducing reliance on passive energy storage components [35].

I.2.3.2 **Current-Fed Input Architectures**

Current-fed converter implementations employ series input inductance to establish controlled input current characteristics, providing particular advantages in photovoltaic applications where smooth current profiles enhance maximum power point tracking accuracy and reduce system stress, as demonstrated in Figure 4(b) [33].

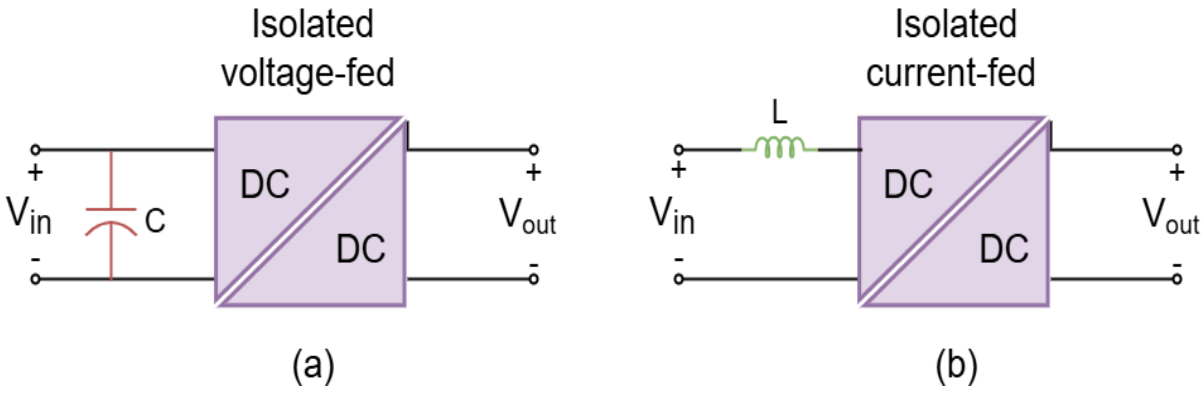

Figure 4 Isolated voltage-fed and current-fed converter.

The series inductor configuration inherently provides current limiting functionality, offering protection against short-circuit conditions while enabling gradual startup characteristics that reduce component stress [32]. This approach demonstrates superior

compatibility with current-based maximum power point tracking algorithms commonly employed in photovoltaic systems.

The design of current-fed systems requires careful consideration of inductor sizing to balance current ripple minimization with dynamic response requirements. Larger inductance values reduce current ripple but may compromise transient response speed, necessitating optimization based on application-specific priorities [33].

I.2.4 Switching Methodology Classification

The switching technique employed in DC-DC converters fundamentally determines efficiency characteristics, electromagnetic interference generation, and component stress levels. This classification dimension particularly influences high-frequency operation capabilities and thermal management requirements.

I.2.4.1 Hard-Switching Implementation

Hard-switching converters operate by activating power switches while both voltage and current exist across the switching elements, resulting in simultaneous voltage and current overlap during transition periods [36]. This operational mode generates substantial switching losses that increase proportionally with switching frequency, limiting high-frequency operation capabilities.

The simplicity of hard-switching control implementation and the minimal auxiliary component requirements make this approach attractive for cost-sensitive applications where moderate efficiency levels are acceptable [36]. Modern hard-switching implementations often incorporate optimized gate drive timing and snubber networks to minimize switching losses and electromagnetic interference generation.

The thermal management requirements for hard-switching systems scale directly with switching frequency and load current levels. Effective heat sink design and thermal interface optimization become critical factors in achieving reliable high-power operation. Advanced thermal simulation tools enable optimization of component placement and cooling system design to maximize power density while maintaining acceptable operating temperatures.

I.2.4.2 Soft-Switching Implementation

Soft-switching methodologies enable power switch transitions to occur under either zero-voltage or zero-current conditions, substantially reducing switching losses and electromagnetic interference generation [22]. These techniques facilitate higher switching frequency operation while maintaining excellent efficiency characteristics.

Zero-voltage switching implementations create resonant conditions that force switch voltage to zero before turn-on transitions occur. This approach eliminates turn-on switching losses while reducing electromagnetic interference generation associated with rapid voltage transitions. The implementation typically requires additional resonant components that increase system complexity but provide substantial performance benefits [22].

Zero-current switching techniques ensure that switch current reaches zero before turn-off transitions occur, eliminating turn-off switching losses and reducing device stress [37], [38]. These implementations often demonstrate superior performance in high-current applications where turn-off losses would otherwise dominate overall loss calculations.

Advanced soft-switching topologies combine multiple resonant elements to achieve both zero-voltage and zero-current switching conditions across wide operational ranges [26], [38]. These implementations represent the current state-of-the-art in high-efficiency converter design, achieving efficiency levels exceeding 98% in optimized implementations.

I.2.5 Dynamic Response Characteristics

The dynamic behaviour of high-gain DC-DC converters significantly influences their suitability for applications involving variable input conditions or rapid load changes, as classified in Table 2. This characteristic proves particularly critical in photovoltaic applications where irradiance variations can occur rapidly and unpredictably [39].

I.2.5.1 Minimum-Phase System Behaviour

Minimum-phase converters exhibit control-to-output transfer functions with all zeros located in the left-half plane of the complex frequency domain. This characteristic ensures that output response moves in the same direction as control input changes, facilitating straightforward controller design and aggressive bandwidth implementation.

The absence of right-half-plane zeros in minimum-phase systems enables higher control bandwidth implementation without stability concerns, resulting in superior transient response characteristics and improved disturbance rejection capabilities [40]. This behaviour proves particularly beneficial in photovoltaic applications where rapid irradiance changes require quick system response to maintain optimal power extraction.

Modern controller design techniques for minimum-phase systems can achieve bandwidth limitations approaching the switching frequency divided by ten, enabling excellent dynamic response while maintaining adequate stability margins [40]. The implementation of advanced

control algorithms including model predictive control and sliding mode techniques becomes significantly more straightforward in minimum-phase systems.

Table 2 Dynamic Behaviour Classification of High-Gain DC–DC Converters

Dynamic Category	**Converter Examples**	**Characteristic Dynamics**	**Control / Practical Implications**
Non-Minimum-Phase	Boost, Buck–Boost (CCM), Quadratic Boost.	Presence of RHPZ; initial response opposite to control input.	Bandwidth severely limited; compensation must be conservative; MPPT may suffer under rapid irradiance changes [9], [10], [41].
Minimum-Phase	Flyback (DCM), Current-Mode Controlled Converters.	All zeros in left-half-plane; no “wrong-way” transient.	Easier and more robust control design; better transient response [42].
Resonant / Quasi-Resonant	LLC, Series-Resonant, Quasi-Resonant Boost.	Soft-switching, smoother transient transitions, reduced overshoot/undershoot.	Can support faster dynamics with moderate control complexity; favourable for high-efficiency designs [43], [44].
Multilevel / Switched-Capacitor	Three-Level Boost, SC-Based High-Gain Converters	Multiple reactive elements and topology states lead to complex transient interactions	Requires advanced or digital control (MPC, AI, sliding mode) to ensure stability under dynamic load shifts
Isolated High-Gain	Dual Active Bridge (DAB), Transformer-Resonant Converters	Often minimum-phase; avoids RHPZ; supports bidirectional power flow and precise current control	Well suited for EV charging and renewable interaction in dynamic environments

I.2.5.2 **Non-Minimum-Phase System Behaviour**

Non-minimum-phase converters contain right-half-plane zeros in their control-to-output transfer functions, creating initial "wrong-way" response characteristics where output initially moves opposite to the desired direction before eventually settling to the correct steady-state value [45]. This behaviour severely constrains achievable control bandwidth and complicates controller design.

The presence of right-half-plane zeros typically limits control bandwidth to approximately one-half the zero frequency to maintain adequate phase margin and system

stability [39]. This limitation becomes particularly problematic in high-gain boost converters where right-half-plane zero frequency decreases with increasing voltage gain, further constraining dynamic response capabilities.

Advanced control techniques for non-minimum-phase systems include feedforward compensation, pole-zero placement optimization, and adaptive control strategies that adjust parameters based on operating conditions, as illustrated in Figure 5. These approaches can partially mitigate the limitations imposed by right-half-plane zeros but require increased controller complexity and careful stability analysis [46].

I.2.6 Application-Oriented Design Considerations

The selection and optimization of high-gain DC-DC converter topologies must consider specific application requirements that extend beyond basic voltage transformation functionality. These considerations include environmental conditions, reliability requirements, electromagnetic compatibility constraints, and integration complexity.

I.2.6.1 Renewable Energy System Integration

Renewable energy applications impose unique requirements including wide input voltage ranges, environmental robustness, and compatibility with maximum power point tracking algorithms. The converter topology must accommodate substantial input voltage variations while maintaining stable output characteristics across diverse operating conditions.

Photovoltaic system integration requires converters capable of handling rapid input changes while maintaining maximum power point tracking accuracy [32]. The converter's impedance characteristics must remain compatible with MPPT algorithms across the full operational range to ensure optimal energy extraction under variable irradiance conditions.

The environmental conditions typical of renewable energy installations necessitate robust design approaches that can withstand temperature extremes, humidity variations, and vibration exposure. Component selection must emphasize long-term reliability under these challenging conditions while maintaining acceptable performance metrics throughout the operational lifetime [31].

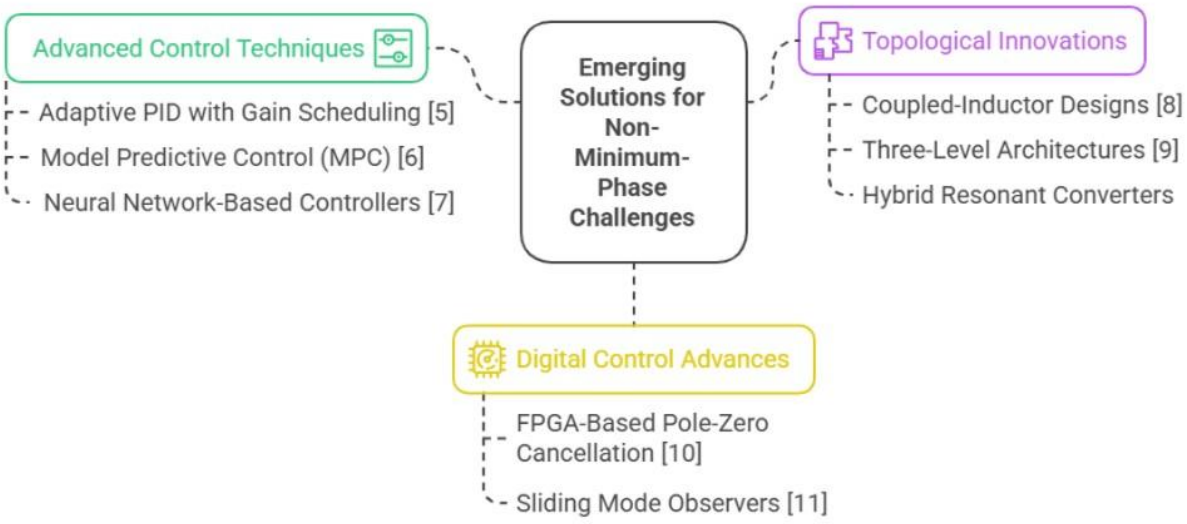

Figure 5 Emerging solutions for non-minimum-phase challenges in power electronics.

I.2.6.2 **Electric Vehicle Power System Applications**

Electric vehicle applications demand converters with exceptional power density, lightweight construction, and bidirectional energy flow capabilities to accommodate diverse operational scenarios including propulsion, regenerative braking, and vehicle-to-grid interactions.

The space and weight constraints inherent in automotive applications require optimization approaches that maximize power density while maintaining thermal management effectiveness [12]. Advanced packaging techniques and component integration strategies become critical factors in achieving competitive performance metrics within automotive constraints.

The safety requirements for electric vehicle applications necessitate comprehensive fault detection and protection capabilities that can respond rapidly to abnormal operating conditions. The converter control system must incorporate multiple protection mechanisms while maintaining normal operational efficiency and performance.

I.3 High-Gain Enhancement Methodologies

The achievement of substantial voltage gains in DC-DC converter applications requires systematic implementation of specialized enhancement techniques that extend beyond conventional duty cycle manipulation, as categorized in Figure 6. These methodologies address the fundamental limitations of traditional boost topologies while introducing innovative

approaches to voltage amplification that maintain efficiency and reliability standards appropriate for demanding applications [7], [8].

Contemporary high-gain converter design emphasizes the integration of multiple enhancement techniques within unified architectures, creating synergistic effects that exceed the performance capabilities of individual methods [47]-[49]. This approach enables the development of converter systems capable of achieving voltage gains exceeding 20:1 while operating at moderate duty cycles and maintaining excellent efficiency metrics.

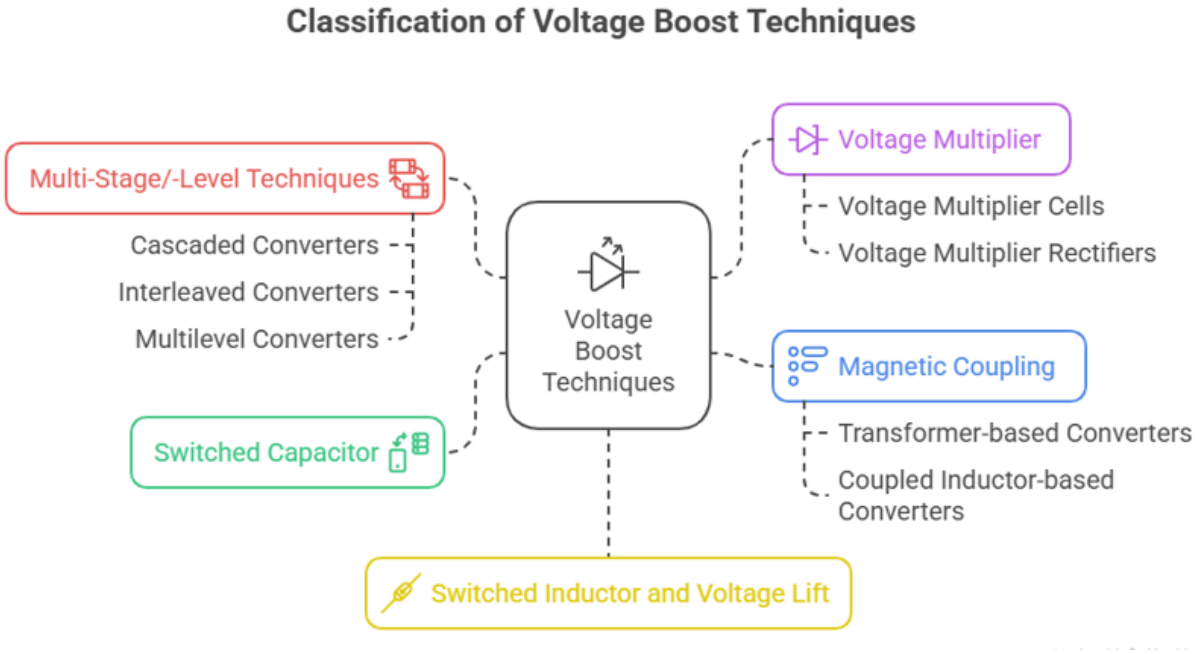

Figure 6 Classification of voltage boost topologies.

I.3.1 Voltage Multiplier Cell Integration

Voltage multiplier cells represent modular building blocks that provide incremental voltage amplification through capacitive charge redistribution mechanisms, as illustrated in Figure 7 [50]. These cells demonstrate exceptional versatility through their ability to integrate seamlessly with various converter topologies while providing predictable voltage gain enhancement characteristics.

The fundamental operation of voltage multiplier cells relies on sequential charging and discharging of capacitors arranged in diode-capacitor ladder configurations [51]. During each switching cycle, energy redistribution occurs between capacitive stages, resulting in progressive voltage amplification that accumulates across multiple stages. This mechanism

enables substantial voltage gains through relatively simple circuit modifications to existing converter architectures.

Modern voltage multiplier implementations incorporate advanced techniques to minimize the traditional drawbacks associated with capacitive charge-pump systems [9], [41]. Innovative designs address current spike generation through soft-charging mechanisms, reduce component count through integrated magnetic-capacitive approaches, and improve voltage regulation through enhanced control strategies.

The integration of voltage multiplier cells with switching converters creates hybrid systems that combine the continuous energy transfer advantages of inductive systems with the high-gain capabilities of capacitive charge-pump mechanisms [40], [52]. These implementations demonstrate particular effectiveness in applications requiring both high voltage gain and excellent dynamic response characteristics, as summarized in Table 3.

Recent research developments have focused on optimizing voltage multiplier cell configurations for specific applications [41], [53], [54]. Advanced topologies incorporate coupled magnetic elements with voltage multiplier networks, creating systems that achieve ultra-high voltage gains while maintaining compact physical implementations and excellent efficiency characteristics.

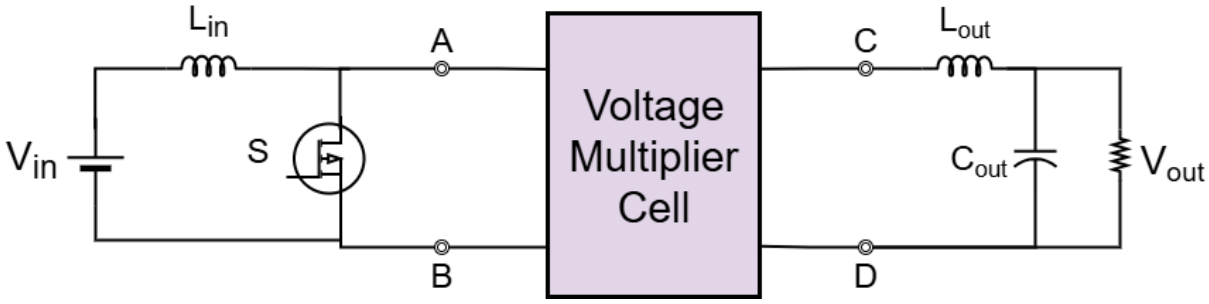

Figure 7 Schematic of a high gain DC–DC converter with an integrated VMC.

Table 3 summarizes recent VMC-integrated converter topologies

Ref	Operating Principle	Key Benefits	Limitations
[10]	Interleaved boost with winding-cross-coupled inductors and integrated VMCs	High gain (~11×) without extreme duty cycle; Zero-current switching (ZCS); Balanced phase currents and reduced ripple; High efficiency (97.4%)	Increased circuit complexity; Requires accurate inductor coupling and phase synchronization

Ref	Operating Principle	Key Benefits	Limitations
[9]	Quadratic boost with 3-winding coupled inductor and VMC under soft-switching	Ultra-high gain (~16×); ZCS switching, reduced losses and stress; Common ground between input and output; Reduced current ripple and voltage spikes	Larger component count; More complex control due to quadratic and soft-switching integration
[41]	Review of non-isolated VMC-integrated converters	Summarizes numerous efficient designs; Highlights modular and scalable topologies for PV	No unified analysis model; Efficiency and performance are topology-dependent
[52]	Diode-capacitor VMC with switched inductor network	High gain with simple diode–capacitor ladder; Low device voltage stress; Broad design adaptability	High component count; Efficiency drops under partial load; Requires feedback for good regulation

I.3.2 Magnetic Coupling Techniques

Magnetic coupling represents one of the most effective approaches for achieving substantial voltage gains in DC-DC converter applications. These techniques exploit magnetic field relationships between coupled windings to provide voltage amplification while enabling efficient energy transfer and component stress reduction, as compared in Table 4.

Table 4 Comparison of Transformer-Based and Coupled-Inductor Converters.

Feature	Transformer-Based	Coupled-Inductor
Isolation Capability	Full galvanic isolation	No isolation
Voltage Gain	High	Moderate to high
Leakage Management	Requires snubbers/active clamps	Easier integration
Power Density	Lower (due to transformer size)	Higher
Typical Applications	Grid-tied, medical, industrial systems	Automotive, renewables

I.3.2.1 Transformer-Based Voltage Amplification

Transformer-based DC-DC converters utilize high-frequency magnetic coupling to achieve galvanic isolation while providing substantial voltage transformation capabilities through turns ratio selection, as shown in Figure 8 [19], [20], [55]. These systems offer exceptional design flexibility through the combination of turns ratio and duty cycle control, enabling optimization for specific voltage gain requirements.

The implementation of transformer-based high-gain converters requires careful attention to magnetic design considerations including core material selection, winding configuration optimization, and leakage inductance minimization [18]. Advanced transformer design techniques incorporate interleaved winding structures and optimal layer arrangements to minimize parasitic effects while maximizing power transfer efficiency.

Modern transformer-based converter topologies integrate sophisticated switching strategies to optimize magnetic utilization and minimize losses [21], [18]. Phase-shifted full-bridge configurations with zero-voltage switching enable operation at high switching frequencies while maintaining excellent efficiency metrics. These techniques prove particularly effective in high-power applications where transformer size and weight represent significant design constraints.

The development of planar magnetic structures enables substantial improvements in power density and thermal management compared to conventional transformer construction approaches [18]. These techniques facilitate integration of multiple magnetic functions within compact structures while providing excellent thermal coupling to cooling systems.

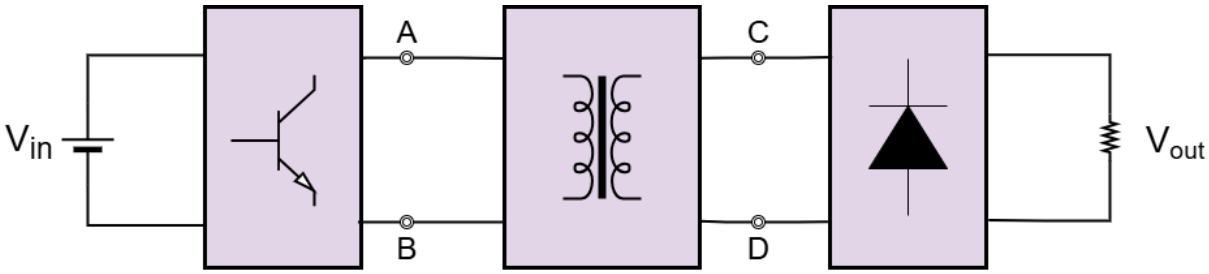

Figure 8 Basic structure of a transformer-based isolated DC–DC converter.

I.3.2.2 **Coupled-Inductor Implementations**

Coupled-inductor converters achieve voltage amplification through magnetic coupling between windings sharing common magnetic cores, as demonstrated in Figure 9 [10], [23], [56]. This approach provides voltage gain enhancement without requiring galvanic isolation, enabling simplified control strategies while achieving substantial voltage transformation capabilities.

The design of coupled-inductor systems requires optimization of magnetic coupling coefficients to achieve desired voltage gain characteristics while maintaining acceptable leakage inductance levels [37]. The coupling coefficient directly influences both voltage gain and energy transfer efficiency, necessitating careful consideration of core geometry and winding arrangement.

Advanced coupled-inductor topologies incorporate multiple windings with optimized turns ratios to achieve complex voltage transformation relationships [57]. These implementations often include auxiliary windings for energy recycling and voltage clamping, improving overall efficiency while reducing component stress levels.

The integration of coupled inductors with additional gain enhancement techniques creates hybrid systems with exceptional voltage amplification capabilities [25]. These approaches combine magnetic coupling with switched-capacitor networks or voltage-lift mechanisms to achieve ultra-high gains while maintaining excellent dynamic response characteristics.

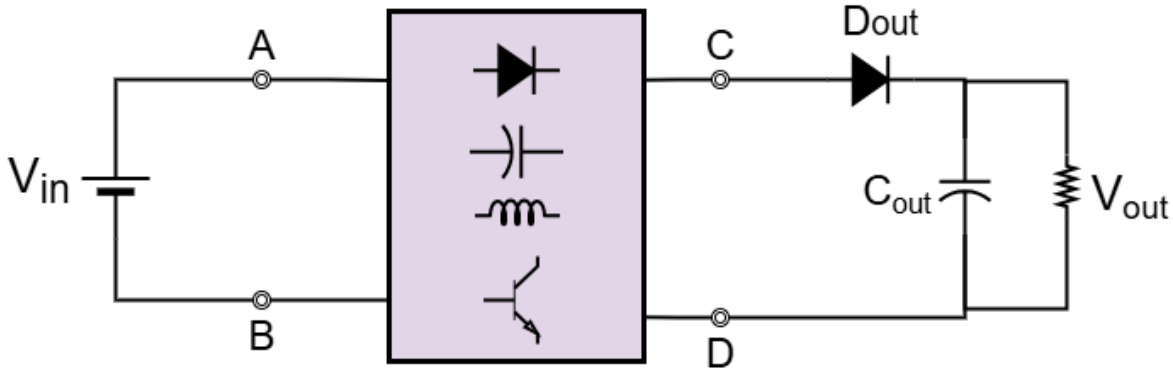

Figure 9 Simplified structure of a coupled-inductor-based DC–DC converter.

I.3.3 Switched-Inductor and Voltage-Lift Methodologies

Switched-inductor and voltage-lift techniques provide effective approaches for voltage gain enhancement through innovative rearrangement of energy storage elements during different switching intervals, as illustrated in Figure 10. These methods achieve substantial voltage amplification while maintaining relatively simple control requirements and good dynamic response characteristics [27], [58].

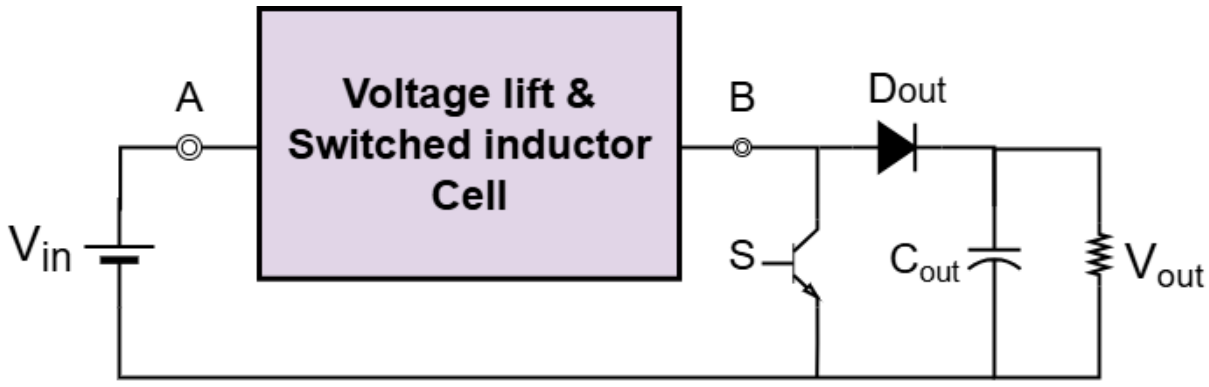

Figure 10General structure of a hybrid switched-inductor and voltage-lift cell.

I.3.3.1 **Switched-Inductor Configurations**

Switched-inductor techniques reconfigure inductor connections between parallel arrangements during energy storage intervals and series arrangements during energy transfer intervals. This reconfiguration multiplies the effective voltage delivered to the output while distributing current stress across multiple magnetic elements.

The implementation of switched-inductor systems typically involves multiple inductors and switching elements arranged to provide the required series/parallel reconfiguration. Advanced implementations incorporate coupled magnetic structures to reduce component count while maintaining the voltage multiplication benefits of the switching arrangement [58].

Interleaved switched-inductor configurations distribute switching stress across multiple phases while reducing input and output ripple currents [59], [60]. These implementations demonstrate particular effectiveness in high-power applications where current distribution and thermal management represent primary design concerns.

The optimization of switched-inductor systems requires careful consideration of magnetic design parameters including inductance values, current ratings, and core loss characteristics [61]. Advanced design techniques incorporate integrated magnetic structures that combine multiple inductor functions while minimizing size and weight penalties.

I.3.3.2 **Voltage-Lift Implementation Strategies**

Voltage-lift techniques utilize capacitive charge storage and series addition mechanisms to achieve voltage amplification without requiring magnetic coupling or complex switching arrangements [62]. These approaches demonstrate excellent compatibility with existing converter topologies while providing predictable voltage gain enhancement.

The fundamental voltage-lift operation involves charging capacitors to specific voltage levels during one switching interval and connecting them in series with the main power path during subsequent intervals [28]. This mechanism provides additive voltage effects that accumulate to achieve substantial overall voltage gains.

Advanced voltage-lift implementations incorporate multiple capacitive stages with optimized charging and discharging sequences. These configurations achieve high voltage gains while minimizing capacitor voltage stress and reducing ripple current requirements. The modular nature of voltage-lift cells enables scalable implementations tailored to specific voltage gain requirements [27].

The integration of voltage-lift mechanisms with other gain enhancement techniques creates powerful hybrid systems capable of achieving exceptional voltage transformation ratios. These approaches often combine voltage-lift capacitors with coupled magnetic elements to achieve ultra-high gains while maintaining excellent efficiency and dynamic response characteristics [28], [29].

I.3.4 Switched-Capacitor

Switched-capacitor techniques implement pure capacitive energy transfer mechanisms that achieve voltage amplification without requiring magnetic elements [30]. These approaches demonstrate particular effectiveness in applications requiring compact implementations with minimal electromagnetic interference generation.

The operation of switched-capacitor systems relies on precise timing of capacitor charging and discharging sequences to achieve desired voltage transformation ratios. Advanced control strategies optimize switching sequences to minimize current spikes while maximizing energy transfer efficiency between capacitive stages [47], [63].

Modern switched-capacitor implementations incorporate soft-charging techniques that reduce current spikes and improve efficiency compared to traditional hard-switched charge-pump approaches. These methods utilize controlled current ramp rates and optimized switching transitions to minimize losses while maintaining rapid energy transfer capabilities [30].

The integration of switched-capacitor networks with inductive elements creates hybrid systems that combine the high-gain capabilities of charge-pump mechanisms with the continuous energy transfer advantages of magnetic systems [25]. These approaches achieve exceptional voltage gains while maintaining good dynamic response and load regulation characteristics.

I.3.5 Multi-Stage and Multilevel Architectures

Multi-stage converter systems achieve high voltage gains through cascaded arrangements of individual converter stages, each contributing incremental voltage amplification to achieve substantial overall transformation ratios. These architectures provide excellent scalability and enable optimization of individual stages for specific performance objectives.

I.3.5.1 Cascaded Configuration Strategies

Cascaded converter arrangements connect multiple converter stages in series to achieve cumulative voltage gains that exceed the capabilities of individual stages, as shown in Figure

11 [48], [64]. These implementations enable the use of moderate duty cycles in each stage while achieving overall voltage gains that would require extreme duty cycles in single-stage configurations.

Quadratic cascaded converters achieve voltage gains proportional to the square of individual stage gains, enabling exceptional overall transformation ratios through relatively modest individual stage requirements, as demonstrated in Figure 12 [7], [48]. These configurations demonstrate particular effectiveness in applications requiring ultra-high voltage gains while maintaining reasonable component stress levels.

Advanced cascaded implementations incorporate different converter topologies within individual stages to optimize overall system performance [49], [64]. These approaches might combine boost configurations for voltage amplification with buck-boost stages for isolation or specialized gain-enhancement topologies for maximum voltage transformation.

The control of cascaded converter systems requires coordination between individual stage controllers to achieve optimal overall performance. Advanced control strategies incorporate feedforward compensation and inter-stage communication to minimize interaction effects while maintaining excellent dynamic response characteristics.

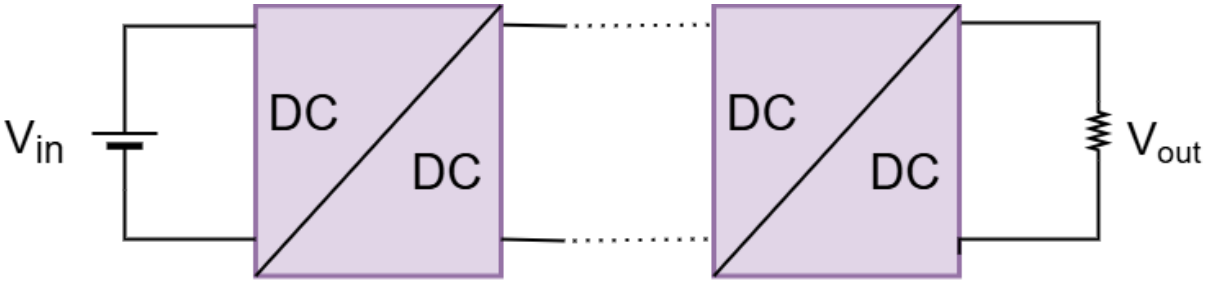

Figure 11 Basic layout of cascaded converter.

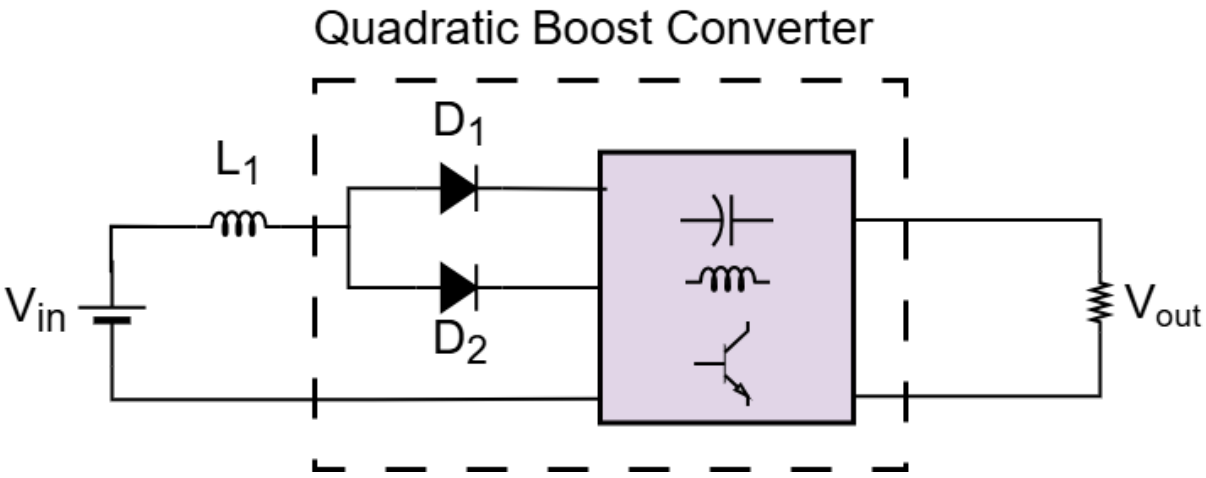

Figure 12 Basic structure of Quadratic boost converter.

I.3.5.2 **Interleaved Parallel Architectures**

Interleaved converter configurations distribute power processing across multiple parallel-connected converter stages operating with phase-shifted switching sequences, as illustrated in Figure 13. This approach reduces input and output ripple currents while increasing overall power handling capability and improving thermal management through power distribution.

The implementation of interleaved systems requires precise timing coordination between phases to achieve optimal ripple cancellation and current sharing [38]. Advanced control systems incorporate current balancing mechanisms and phase synchronization techniques to maintain uniform power distribution across all phases.

Multi-phase interleaved converters with specialized gain enhancement techniques create systems capable of handling high power levels while achieving substantial voltage gains [37]. These implementations often incorporate coupled magnetic elements or integrated voltage multiplier networks to maximize power density while maintaining excellent performance metrics.

The scalability of interleaved architectures enables system optimization for specific power and voltage requirements through phase count adjustment [60], [61]. Additional phases improve ripple performance and power handling capability while increasing system complexity and control requirements.

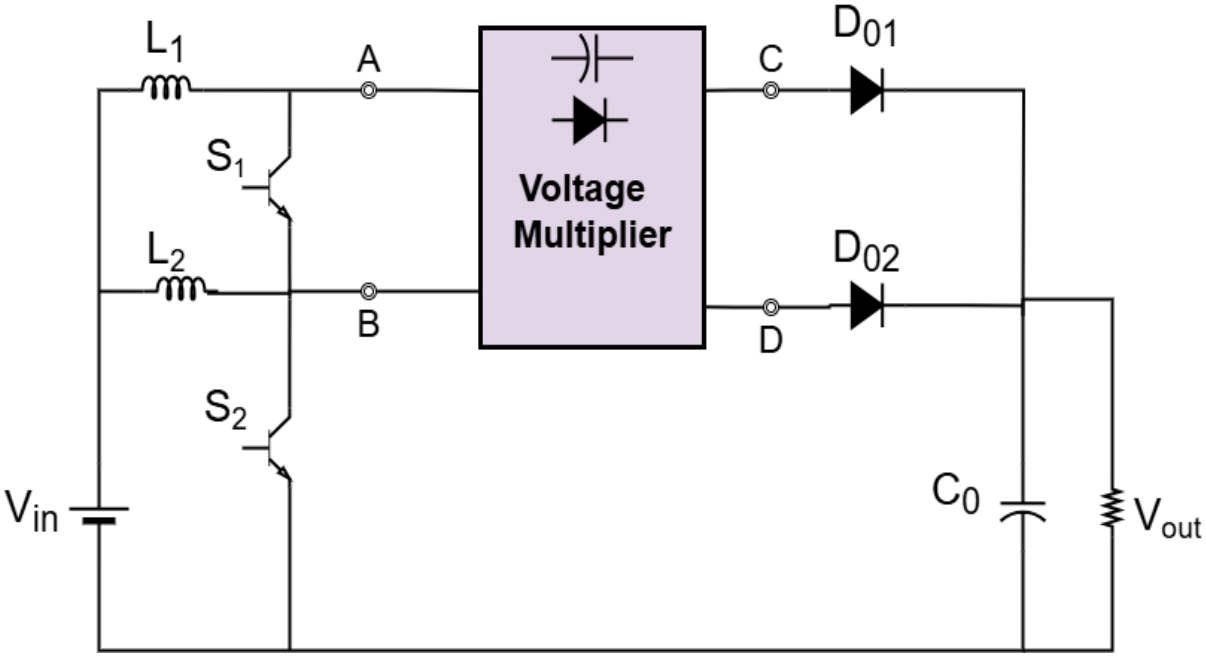

Figure 13 Structure of an interleaved cascaded converter.

I.3.5.3 **Multilevel Voltage Synthesis**

Multilevel converter architectures generate multiple discrete voltage levels that can be combined to achieve high-resolution voltage synthesis while minimizing individual component voltage stress, as shown in Figure 14 [65], [66]. These systems demonstrate particular effectiveness in high-voltage applications where component voltage ratings represent significant design constraints.

Modular multilevel converters utilize multiple identical submodules connected in series to achieve high voltage capabilities while distributing stress across many components. This approach enables the use of lower-voltage components while achieving exceptional overall voltage ratings and excellent fault tolerance characteristics.

Cascaded multilevel configurations with independent DC sources enable distributed power processing with individual maximum power point tracking for each source, as illustrated in Figure 15. This approach proves particularly effective in photovoltaic applications where individual panel or string optimization maximizes overall system energy harvest [67].

The control of multilevel converter systems requires sophisticated voltage balancing and modulation strategies to maintain uniform stress distribution while achieving desired output voltage characteristics. Advanced control techniques incorporate predictive algorithms and real-time optimization to maximize performance while ensuring component protection [66].

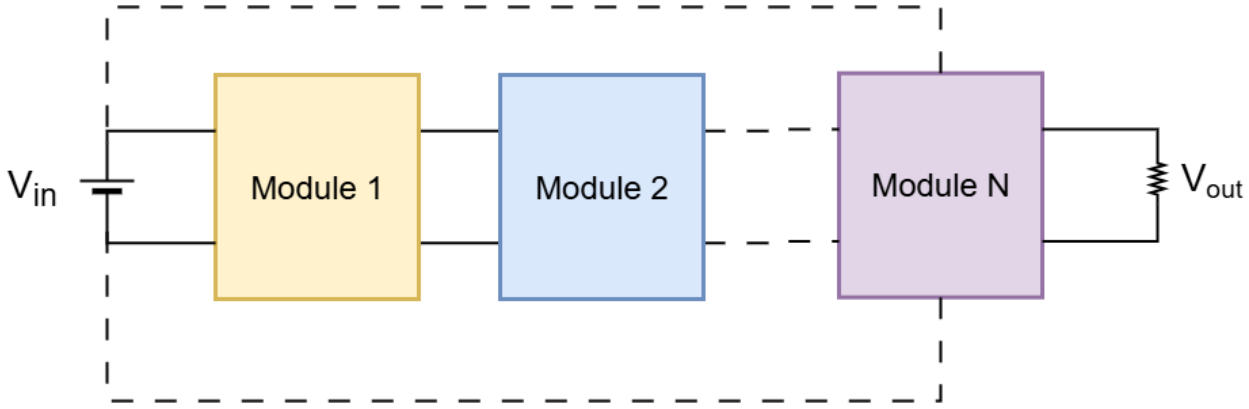

Figure 14 Modular multilevel converter (MMC).

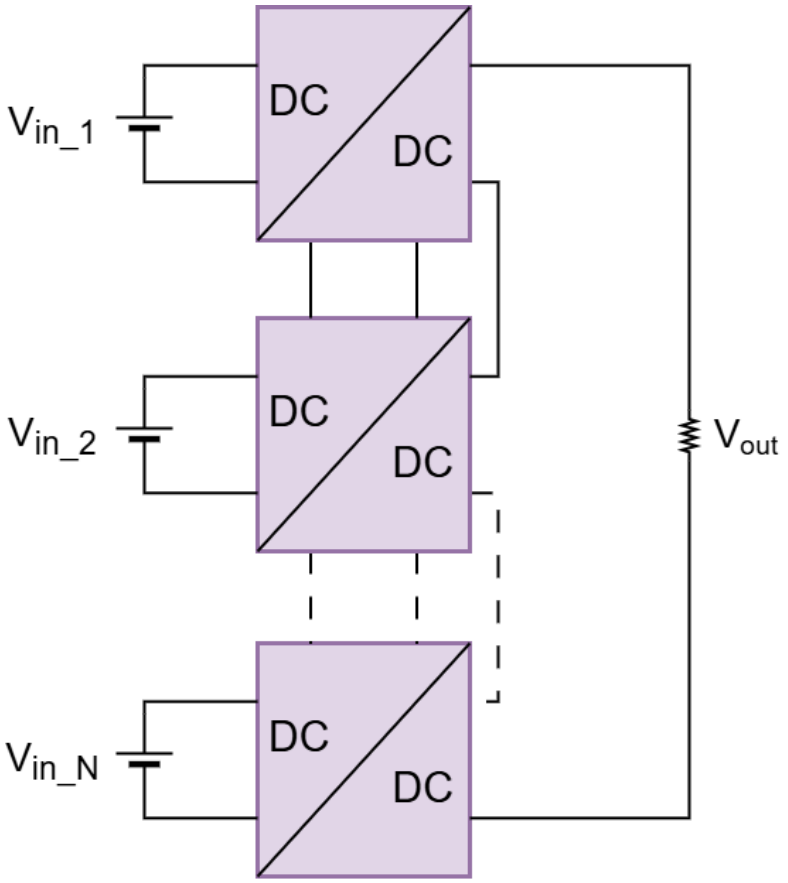

Figure 15 Cascaded multilevel converter with multiple DC sources.

I.4 Conclusion

The comprehensive analysis of high-gain DC-DC converter topologies reveals a sophisticated landscape of technological solutions designed to address the evolving demands of modern power electronic applications. The systematic classification framework presented demonstrates that optimal converter selection requires careful consideration of multiple interdependent factors including energy transfer directionality, isolation requirements, input source characteristics, switching methodologies, dynamic response behavior, and application-specific constraints.

The investigation of voltage gain enhancement techniques illustrates the substantial progress achieved through innovative circuit architectures that transcend the limitations of traditional boost converter approaches. Voltage multiplier cells, magnetic coupling techniques, switched-inductor and voltage-lift methodologies, switched-capacitor systems, and multi-stage architectures each contribute unique advantages that can be synergistically combined to achieve exceptional performance characteristics.

For photovoltaic applications incorporating artificial intelligence-based maximum power point tracking systems, the most promising converter families demonstrate several critical characteristics: exceptional capability to accommodate wide input voltage variations without compromising tracking accuracy, robust dynamic response suitable for rapid irradiance changes, minimal right-half-plane zero influence to enable aggressive control bandwidth implementation, and inherent stability characteristics that facilitate integration with advanced control algorithms.

The coupled-inductor hybrid topologies emerge as particularly attractive candidates due to their excellent balance of high voltage gain capability, moderate component stress levels, and dynamic response characteristics compatible with AI-based control systems. These architectures enable the implementation of sophisticated MPPT algorithms while maintaining the efficiency and reliability standards required for commercial photovoltaic installations.

Future developments in high-gain converter technology will likely emphasize further integration of enhancement techniques within unified architectures, optimization for specific renewable energy applications, and enhanced compatibility with intelligent control systems. The continued advancement of semiconductor technologies, magnetic materials, and control system capabilities will enable even more sophisticated converter implementations that push the boundaries of efficiency, power density, and dynamic performance.

This foundational understanding of high-gain converter topologies and enhancement methodologies provides the essential framework for subsequent detailed analysis of specific architectures and their integration with artificial intelligence-based maximum power point tracking systems, establishing the groundwork for optimal photovoltaic system design and implementation.

CHAPTER II OPTIMIZATION METHODS FOR PHOTOVOLTAIC SYSTEMS

II.1 Introduction

The inherent nonlinearity of photovoltaic module characteristics, manifested through complex power-voltage and current-voltage relationships, presents fundamental challenges for energy extraction optimization across diverse operational environments. These characteristic curves demonstrate singular global maxima under uniform irradiance conditions, yet evolve into multipeaked landscapes exhibiting numerous local optima when subjected to partial shading phenomena or rapid environmental fluctuations. This complexity necessitates sophisticated algorithmic approaches that transcend conventional linear control methodologies to ensure reliable maximum power point acquisition.

The evolution of maximum power point tracking methodologies reflects a sophisticated progression from elementary perturbation-based techniques toward increasingly intelligent optimization paradigms. Contemporary research encompasses three distinct categorical domains: conventional algorithms characterized by computational simplicity yet operational limitations, artificial intelligence-based approaches offering adaptive learning capabilities with enhanced computational requirements, and bio-inspired metaheuristic methods providing robust global search mechanisms at the expense of convergence velocity.

Conventional algorithms, including Perturb and Observe, Incremental Conductance, and Constant Voltage methodologies, maintain dominance in commercial photovoltaic installations due to their minimal hardware requirements and straightforward implementation on basic microcontroller platforms. However, these approaches exhibit fundamental limitations including steady-state oscillations around optimal operating points, susceptibility to local maxima entrapment under partial shading conditions, and inadequate response characteristics during rapid environmental transitions.

Artificial intelligence paradigms introduce model-free adaptability through fuzzy logic controllers, artificial neural networks, and nonlinear autoregressive architectures. These methodologies demonstrate superior dynamic response characteristics and enhanced tracking precision, particularly under variable operational conditions. The adaptive learning capabilities inherent in these approaches enable autonomous optimization without explicit system modeling, though computational overhead requirements necessitate more sophisticated processing platforms.

Bio-inspired metaheuristic algorithms, exemplified by Particle Swarm Optimization, Genetic Algorithms, Grey Wolf Optimization, and Cuckoo Search techniques, exploit natural

phenomena principles to achieve global optimization capabilities. These methodologies excel in partial shading environments where conventional approaches fail, yet typically require extended convergence periods and substantial computational resources for real-time implementation.

Hybrid optimization strategies emerge as particularly promising approaches, combining complementary algorithmic strengths to achieve superior performance characteristics. These methodologies seek to balance tracking accuracy, convergence velocity, and implementation complexity through strategic integration of multiple optimization paradigms.

This chapter establishes comprehensive theoretical foundations for photovoltaic optimization methodologies, with particular emphasis on compatibility with high-gain DC-DC converter architectures examined in Chapter 1. The systematic analysis progresses through conventional optimization principles, artificial intelligence-based approaches, bio-inspired metaheuristic techniques, hybrid methodologies, and comparative performance evaluation. The investigation culminates in identification of optimal strategies for integration with intelligent power conversion systems, providing the analytical framework for subsequent chapters addressing artificial intelligence-based maximum power point tracking implementation.

II.2 Conventional Optimization Methodologies

Conventional MPPT methods remain the most widely used in commercial PV systems due to their simplicity, low computational requirements, and ease of implementation on low-cost microcontrollers. This subsection summarizes the principal algorithms — Perturb and Observe (P&O), Incremental Conductance (IncCond) and Constant Voltage (CV) approaches — and discusses their performance and limitations when applied to high-gain DC–DC converters. The instantaneous power delivered by a PV array is:

$$P = VI \tag{1}$$

And the MPP satisfies:

$$\frac{dP}{dV} = 0 \tag{2}$$

Conventional maximum power point tracking algorithms exploit the fundamental relationship that power derivative with respect to voltage equals zero at the optimal operating point. These methodologies achieve optimization through iterative perturbation of converter operating parameters while monitoring resulting power variations, implementing hill-climbing strategies that converge toward local optima.

The mathematical foundation underlying these approaches recognizes that photovoltaic power output P=VI reaches maximum when dP/dV=0. Conventional algorithms estimate this derivative through discrete sampling of voltage and current measurements, subsequently adjusting converter duty cycles to approach optimal operating conditions.

II.2.1 Perturb and Observe (P&O)

The Perturb and Observe methodology implements a straightforward hill-climbing approach through systematic perturbation of photovoltaic array voltage or converter duty cycle while monitoring corresponding power variations. When power increases following perturbation, the algorithm continues in the same direction; conversely, power reduction triggers directional reversal, as illustrated in Figure 16.

This algorithmic approach requires no explicit photovoltaic modelling or additional sensing beyond standard voltage and current measurements, contributing to its widespread commercial adoption. Implementation simplicity enables deployment on basic microcontroller platforms with minimal computational overhead, making it particularly attractive for cost-sensitive applications where sophisticated processing capabilities are economically prohibitive [68].

The perturbation magnitude represents a critical design parameter influencing both tracking accuracy and dynamic response characteristics. Smaller perturbation steps reduce steady-state oscillations around the maximum power point but compromise tracking velocity during rapid environmental changes. Conversely, larger steps enhance dynamic response at the expense of increased power losses due to oscillatory behaviour around optimal operating points.

Despite its simplicity and widespread implementation, the Perturb and Observe algorithm exhibits fundamental limitations that constrain its effectiveness in complex operational environments. Under steady irradiance conditions, the algorithm demonstrates persistent oscillations around the true maximum power point, resulting in continuous power losses that accumulate over extended operational periods. More critically, the methodology cannot distinguish between local and global maxima, leading to convergence at suboptimal operating points under partial shading conditions [69].

The algorithm's susceptibility to environmental variation represents another significant limitation. During rapid irradiance changes, the correlation between perturbation direction and power variation may be compromised, potentially causing the algorithm to pursue incorrect

optimization directions. This phenomenon, commonly referred to as the drift problem, can result in substantial tracking errors and reduced energy harvest efficiency.

In high-gain DC-DC converter applications, the Perturb and Observe algorithm's oscillatory behavior interacts with converter dynamic characteristics, potentially inducing system instability or compromising control loop performance. The algorithm's inability to handle multiple power peaks fundamentally limits its effectiveness in applications requiring robust global optimization capabilities.

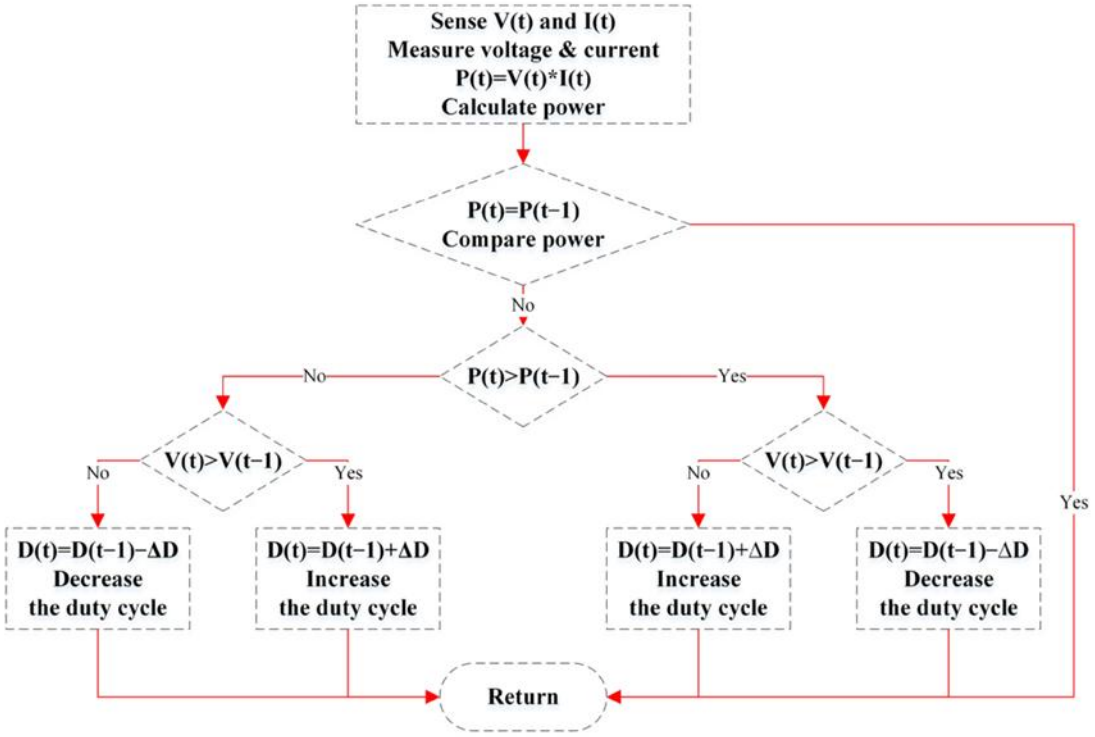

Figure 16 Flowchart of the P&O MPPT algorithm

II.2.2 Incremental Conductance (IncCond)

The Incremental Conductance methodology enhances conventional perturbation-based approaches through exploitation of the power-voltage curve derivative relationship. This algorithm compares instantaneous conductance (I/V) with incremental conductance (dI/dV) to determine maximum power point location, as depicted in Figure 17.

The theoretical foundation recognizes that at the maximum power point:

$$\frac{dP}{dV} = I + V\frac{dI}{dV} \tag{3}$$

This condition yields the relationship:

$$\frac{dI}{dV} = -\frac{I}{V} \quad (4)$$

The algorithm evaluates these quantities through discrete measurements, determining whether the operating point lies to the left (dI/dV > -I/V), right (dI/dV < -I/V), or at the maximum power point (dI/dV = -I/V).

Incremental Conductance methodology theoretically eliminates steady-state oscillations by detecting exact maximum power point location and halting perturbations accordingly. This characteristic represents a significant advantage over Perturb and Observe approaches, potentially reducing power losses associated with continuous oscillatory behaviour around optimal operating points.

The algorithm requires both voltage and current measurements plus derivative computations, resulting in marginally increased complexity compared to basic perturbation methods. However, the computational overhead remains manageable for most microcontroller implementations, maintaining the accessibility advantages of conventional approaches [70].

Despite theoretical advantages, practical Incremental Conductance implementations face challenges related to measurement noise and discrete sampling effects. Derivative calculations based on finite differences can introduce errors that compromise exact maximum power point detection, potentially reintroducing oscillatory behaviour. Additionally, the methodology maintains susceptibility to local maxima entrapment under partial shading conditions, similar to Perturb and Observe limitations.

Dynamic response characteristics during environmental transitions remain comparable to basic perturbation methods, as the algorithm employs similar step-based approaches during transient conditions. The primary advantage emerges during steady-state operation, where accurate maximum power point detection enables oscillation elimination [71].

II.2.3 Constant Voltage Algorithm

The Constant Voltage methodology exploits the empirical relationship between maximum power point voltage and open-circuit voltage, typically expressed as V_mpp≈b.V_oc, where the proportionality constant k ranges from 0.71 to 0.78 for silicon photovoltaic modules [72]. The Fractional Open-Circuit Voltage implementation periodically disconnects the photovoltaic array to measure open-circuit voltage, subsequently establishing operating voltage as a predetermined fraction of this measurement, as illustrated in Figure 18.

This approach offers exceptional simplicity and rapid response characteristics, requiring no iterative search procedures or complex computational operations. Implementation demands minimal processing resources and can achieve virtually instantaneous tracking following open-circuit voltage measurement, making it particularly suitable for applications prioritizing simplicity over precision [73].

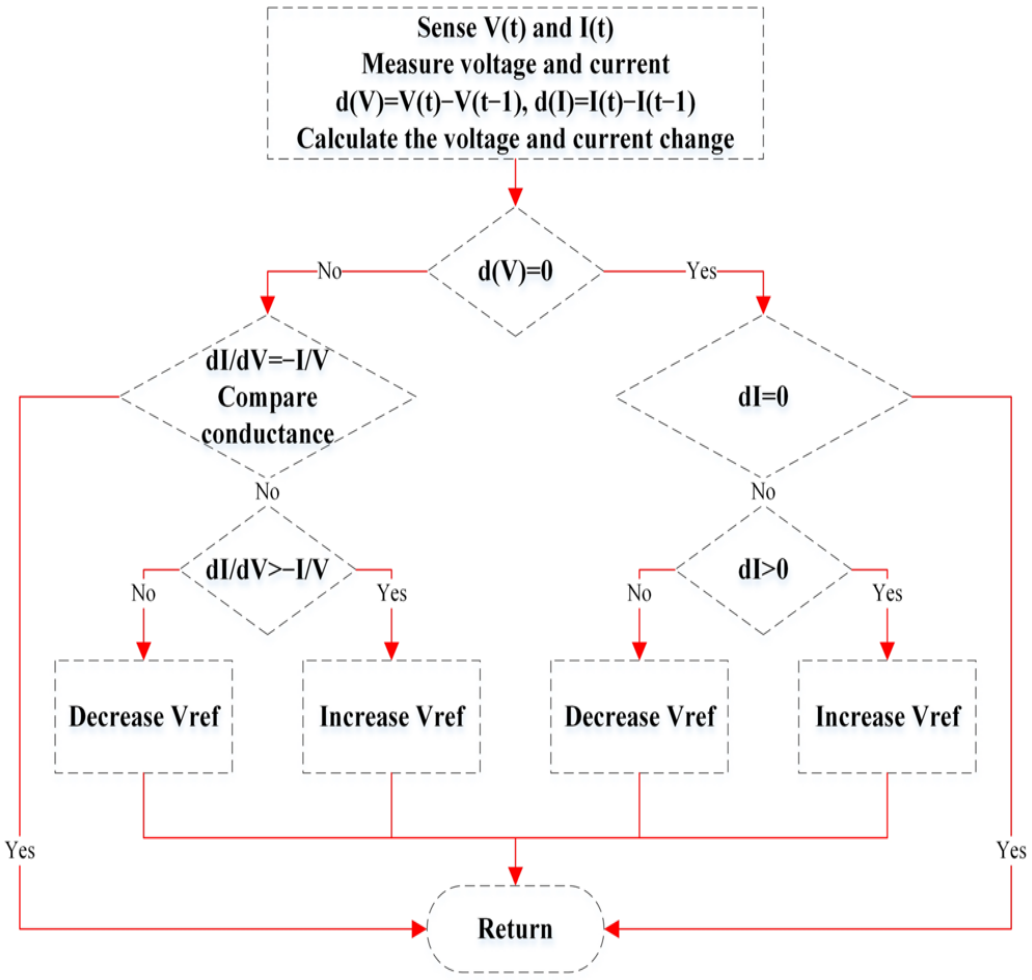

Figure 17 Flowchart of the IncCond MPPT algorithm.

The Constant Voltage approach demonstrates poor performance under partial shading conditions, as the fractional relationship assumes uniform irradiance distribution across the array. Multiple peak conditions invalidate the fundamental assumption underlying the methodology, potentially resulting in significant energy harvest losses.

In high-gain converter applications, the Constant Voltage method provides excellent compatibility due to its non-oscillatory nature and predictable behaviour. However, the reduced

tracking accuracy and inability to handle complex irradiance patterns limit its applicability in demanding operational environments requiring precise optimization [74].

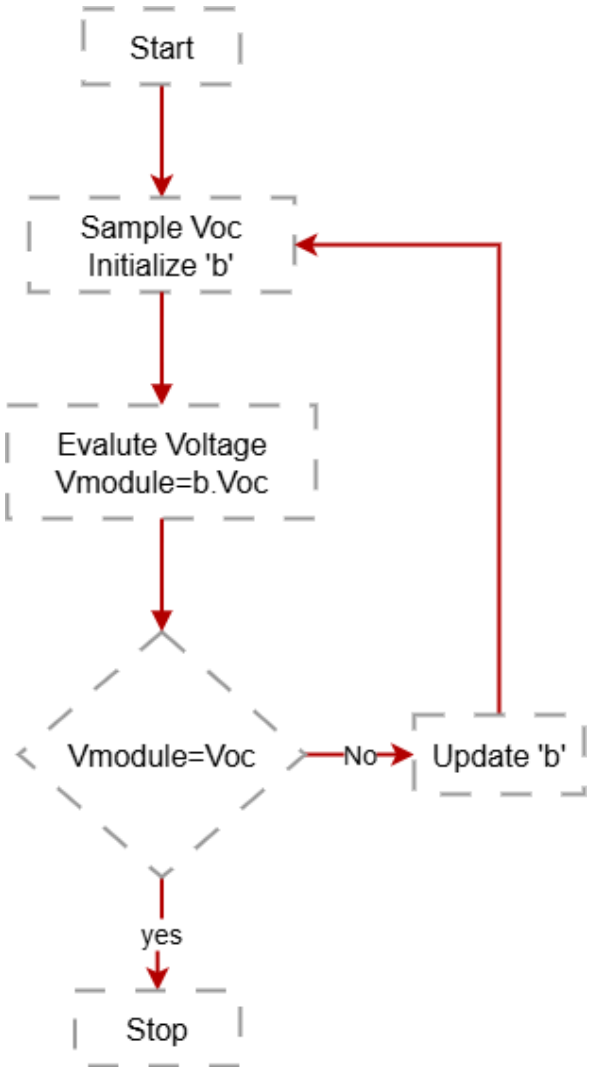

Figure 18 Flowchart of the FOCV-based MPPT algorithm.

II.3 Artificial Intelligence-Based Optimization Methods

The inherent limitations of conventional algorithms in handling nonlinear photovoltaic characteristics and complex environmental conditions have driven the development of artificial intelligence-based optimization approaches. These methodologies exploit machine learning principles, adaptive reasoning, and pattern recognition capabilities to achieve superior tracking performance without requiring explicit system modelling.

Artificial intelligence paradigms offer fundamental advantages including model-free operation, adaptive learning capabilities, and enhanced robustness under uncertain operating conditions. These characteristics prove particularly valuable in photovoltaic applications where

environmental variability, component aging, and partial shading create complex optimization landscapes that challenge conventional approaches.

II.3.1 Fuzzy Logic Control Systems

Fuzzy logic control represents a paradigmatic departure from conventional binary logic systems, embracing partial membership concepts that mirror human reasoning processes under uncertainty. This approach proves particularly well-suited for photovoltaic applications where imprecise measurements, environmental variability, and component tolerances create inherently uncertain operational conditions.

II.3.1.1 Type-1 Fuzzy Logic Controller

A Type-1 fuzzy logic systems utilize membership functions to transform crisp input variables into linguistic representations, subsequently applying rule-based inference mechanisms to generate control actions. The fundamental architecture encompasses four primary components: fuzzification, knowledge base, decision-making logic, and defuzzification, as depicted in Figure 19.

The fuzzification process converts measured photovoltaic parameters, typically including power error and power change rate, into fuzzy variables characterized by membership functions. These functions, commonly implemented as triangular or trapezoidal shapes, define the degree of membership for each input within predetermined linguistic categories such as Negative Large, Negative Medium, Zero, Positive Medium, and Positive Large.

The knowledge base incorporates expert understanding of photovoltaic system behavior through rule sets expressed in linguistic form. These rules typically follow the structure: "If power error is Positive Medium and power change is Negative Small, then duty cycle change is Negative Medium." The rule base encapsulates optimization strategy without requiring explicit mathematical modeling of system dynamics.

Decision-making logic implements inference mechanisms to evaluate active rules and determine appropriate control actions. Common approaches include Mamdani (max-min), Larsen (max-product), and Zadeh (sum-product) methods, each offering distinct characteristics regarding computational complexity and output smoothness.

Defuzzification converts the aggregated fuzzy output into crisp control signals suitable for converter duty cycle adjustment. Popular methods include centroid calculation, maximum criterion, and weighted average techniques, with centroid approaches generally providing superior performance at increased computational cost.

Type-1 fuzzy logic controllers demonstrate excellent dynamic response characteristics and superior tracking accuracy compared to conventional methods. The adaptive nature of fuzzy reasoning enables effective handling of nonlinear photovoltaic characteristics and environmental variations without explicit system identification [75].

Implementation complexity remains moderate, requiring storage of membership functions and rule sets plus execution of inference mechanisms. Modern microcontrollers can readily accommodate these requirements, making fuzzy logic controllers practical for commercial photovoltaic applications [76].

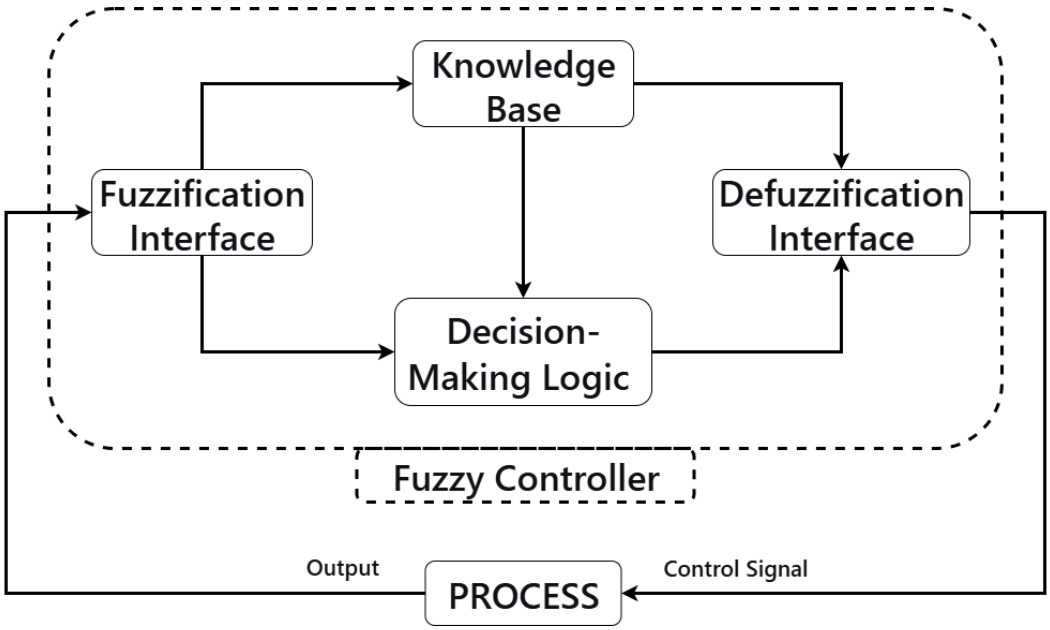

Figure 19 General Block Diagram of a Fuzzy Controller.

II.3.1.2 Type-2 Fuzzy Logic Enhancement

The Type-2 fuzzy logic builds on conventional (Type-1) fuzzy sets by embedding uncertainty directly into the membership functions. Instead of a single crisp curve, each Type-2 fuzzy set $\tilde{A}$ is defined over a footprint of uncertainty (FOU), bounded by an upper membership function (UMF) and a lower membership function (LMF). Mathematically, the FOU can be expressed as [77].

$$\tilde{A} = \int_{x \in X} \int_{u \in j_x} \mu_{\tilde{A}}(x,u)/(x,u), j_x \in [0,1] \quad (5)$$

Where X is the universe of discourse for the primary variable $x, j_x \subseteq$ is the secondary membership domain at x, and $\mu_{\tilde{A}}(x,u)$ denotes the secondary grade at (x,u).

The membership function itself can take simple forms, such as the symmetric triangular secondary MF:

$$\tilde{\mu}(x) = \begin{cases} 1 - \dfrac{|x-a|}{b}, & if\, a-b < x < a+b \\ 0, & else \end{cases} \quad (6)$$

Where a and b define the center and half-width of the triangle, respectively.

Type-2 fuzzy logic extends the standard Type-1 framework by embedding uncertainty directly into each membership function, resulting in a three-dimensional fuzzy set structure. In this paradigm, the primary Type-1 membership curve is "blurred" into an Upper Membership Function (UMF) and a Lower Membership Function (LMF), which together define the Footprint of Uncertainty (FOU). Figure 20 illustrates these components: Figures 20 (a) and 20 (b) display a triangular Type-1 set at the core, flanked by the LMF and UMF that articulate the permissible variation around the nominal membership values.

By displacing the left and right vertices of the original Type-1 triangle, the FOU encapsulates all secondary membership grades between the LMF and UMF. This blurring operation transforms a crisp Type-1 controller into a Type-2 controller without altering the underlying linguistic rule base or inference mechanism. The resulting Type-2 Fuzzy Logic System (T2FLS) therefore retains the intuitive appeal and rule structure of its Type-1 counterpart while offering enhanced capacity to model sensor noise, parameter drift, and environmental disturbances.

In practical MPPT applications, this additional dimension captures uncertainties arising from sensor noise, parameter drift, and irradiance fluctuations, yielding more robust control under partial shading and rapid environmental changes. Compared to Type-1 controllers, Type-2 FLCs maintain higher tracking accuracy and superior stability by accommodating a range of feasible membership grades rather than a single crisp value [78].

The control architecture adds a type-reduction stage between inference and defuzzification, as depicted in Figure 21. During type reduction, the three-dimensional secondary memberships collapse into an interval set, which is then defuzzified to produce a crisp control action.

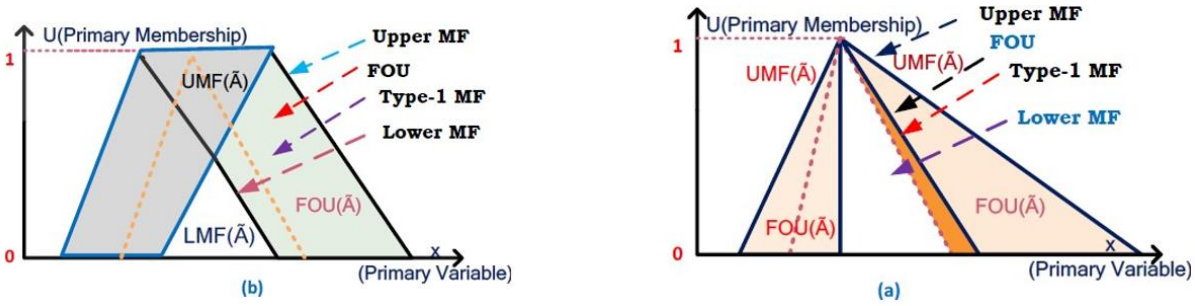

Figure 20 Footprint of uncertainty for a Type-2 fuzzy set, showing the upper membership function (UMF), lower membership function (LMF), and the primary Type-1 membership curve.

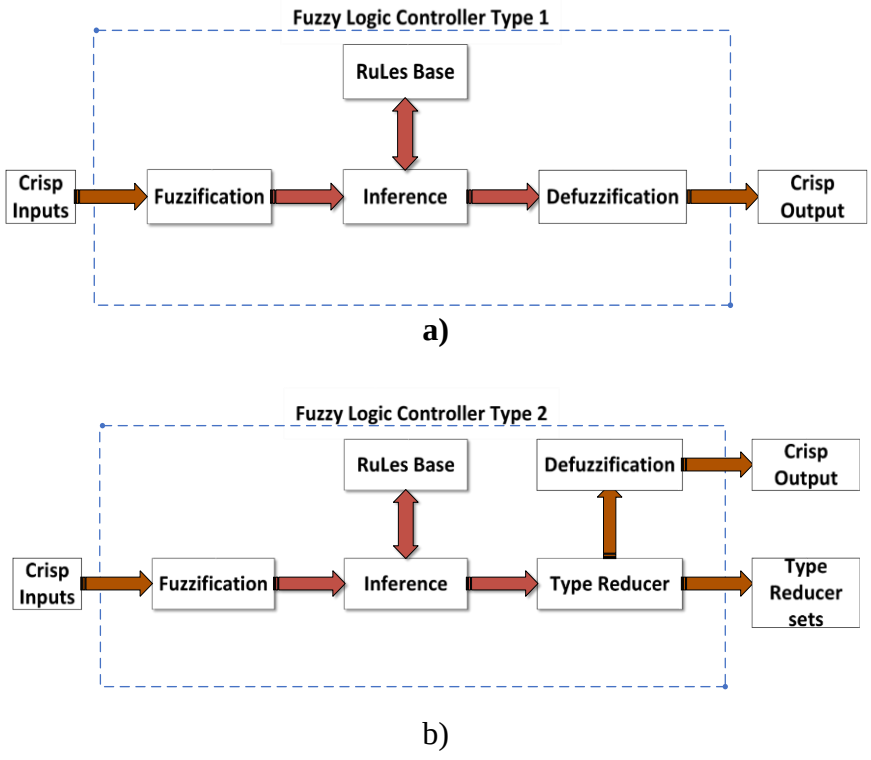

Figure 21 Schematic representation of T1FLC and T2FLC systems

II.3.2 Artificial Neural Networks

Artificial neural networks provide powerful pattern recognition and nonlinear mapping capabilities that prove exceptionally well-suited for photovoltaic optimization applications. These systems learn optimal control strategies through training on historical data, subsequently applying learned patterns to achieve rapid and accurate maximum power point tracking.

II.3.2.1 Feedforward Neural Networks

Feedforward neural networks implement direct mapping from input parameters, typically including irradiance, temperature, voltage, and current measurements, to optimal control

outputs such as duty cycle or reference voltage. As shown in Figure 22, the network first normalizes these inputs, then propagates them through multiple hidden layers with nonlinear activation functions to capture the nonlinear relationship between environmental conditions and the maximum power point. Recent studies report that well-trained feedforward models achieve over 98% tracking efficiency with response times under 100 ms during rapid irradiance transients [79].

Training procedures utilize historical data sets encompassing diverse operational conditions to establish network weights that minimize tracking errors. Supervised learning algorithms, including backpropagation and Levenberg-Marquardt techniques, iteratively adjust network parameters to achieve optimal performance across the training dataset.

Once trained, feedforward networks provide virtually instantaneous maximum power point determination, eliminating iterative search procedures required by conventional algorithms. This characteristic enables exceptional dynamic response capabilities, particularly valuable during rapid environmental transitions.

The training data quality significantly influences network performance, requiring comprehensive datasets encompassing anticipated operational conditions including partial shading scenarios. Inadequate training data can result in poor generalization and suboptimal performance under conditions not represented in the training set.

Implementation requirements include storage of network weights and execution of matrix multiplication operations for forward propagation. Modern microcontrollers and digital signal processors readily accommodate these computational demands, making neural network implementations practical for real-time applications.

II.3.2.2 Nonlinear Autoregressive Networks with Exogenous Inputs (NARX)

The Nonlinear AutoRegressive Network with eXogenous inputs (NARX) is one of the best and most reliable ways to deal with dynamic and nonlinear systems among many intelligent control paradigms. Its recurrent architecture lets it capture how the behaviour of a system changes over time, which makes it perfect for PV applications where the conditions change all the time because of changes in temperature and irradiance.

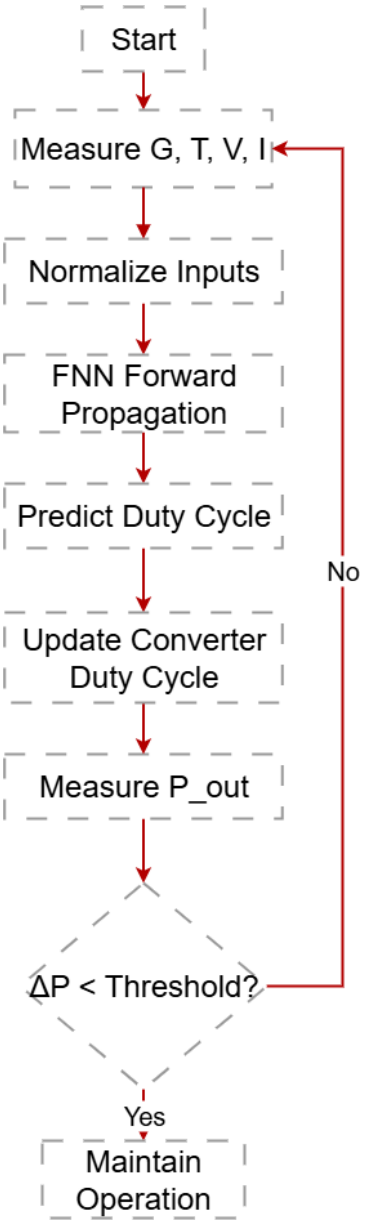

Figure 22 Flowchart of FNN-MPPT Algorithm.

The NARX model is a dynamic recurrent neural network architecture conceptually derived from the classical Autoregressive with Exogenous Input (ARX) model. However, unlike the linear ARX structure, the NARX model introduces nonlinearity through a neural mapping function, enabling it to model complex system dynamics with high precision. The general NARX formulation can be expressed as [3]:

$$y(t) = f[y(t-1), \ldots., y(t-m\_y), x(t-1), ., x(t-m_x)) \quad (7)$$

where y(t) and x(t) denote the system output and input at time t, respectively; m_x and m_y are the output and input lag orders; and f is a nonlinear mapping function approximated by the neural network.

The model's main strength is that it can use historical sequences of both system outputs and inputs from outside the system. This lets the NARX network learn and copy the nonlinear and transient behaviours that are typical of PV systems. As a result, it can figure out the best control actions to make sure that the MPPT works correctly and in real time. Backpropagation keeps the hidden neurones up to date all the time, which lowers the mean squared error (MSE) between the predicted and actual power outputs. Weight matrices and bias parameters are optimised over and over again to make sure that the system converges quickly and runs smoothly.

As depicted in Figure 23, the NARX neural network consists of three primary layers: an input layer featuring time-delayed input signals, a hidden layer that performs nonlinear transformations via weighted connections, and an output layer that forecasts the subsequent system output. The incorporation of input and feedback delays allows the model to maintain temporal relationships, hence enhancing prediction accuracy and robustness in real-time control.

The overall design process includes data acquisition and preprocessing, model training and validation, and performance evaluation, as illustrated schematically in figure 24 [80].

(1) NARX MPPT Model Configuration

The model utilizes the hyperbolic tangent sigmoid (tansig) activation function in both hidden and output layers. Unlike conventional multilayer perceptron networks, the NARX structure incorporates feedback connections between layers, allowing the system to process temporal dependencies effectively. This recurrent feature makes it exceptionally suitable for PV systems, where past behavior influences future system dynamics.

(2) Data Acquisition and Preprocessing

The dataset used for model training comprises key operational parameters such as solar irradiance, cell temperature, PV voltage, and PV current, with the converter duty cycle serving as the target output. To ensure data reliability and optimal training performance, several preprocessing steps were applied:

- Data cleaning: Removal of outliers and inconsistent samples to improve accuracy.
- Normalization: Scaling of input and output data to accelerate convergence and enhance generalization.

- Structured formatting: Organizing datasets for efficient model training, validation, and testing.

Both historical and real-time PV data were collected to capture a wide range of environmental variations, ensuring that the model learned the full spectrum of system dynamics.

(3) Training and Validation Process

The NARX-NN training process is designed to ensure robustness and predictive accuracy in MPP tracking. Input variables—irradiance, temperature, PV voltage, and PV current—were mapped to the corresponding optimal duty cycle values. Data were partitioned into training (70%), validation (15%), and testing (15%) subsets.

Training was conducted using backpropagation through time (BPTT) with mean squared error (MSE) as the objective function. Adaptive optimization algorithms were employed to accelerate convergence, and an early stopping criterion was introduced to prevent overfitting. Model generalization capability was further verified using K-fold cross-validation, ensuring consistent performance across different data segments.

(4) Performance Evaluation

The effectiveness of the NARX-based MPPT controller was assessed through a set of quantitative performance metrics, including the Root Mean Squared Error (RMSE), Mean Absolute Percentage Error (MAPE), and the Coefficient of Determination (R^2). These metrics are defined as follows:

$$RMSE = \sqrt{\frac{1}{n}\sum_{i=1}^{n}(\hat{y}_i - y_i)^2} \tag{8}$$

$$MAPE = \frac{1}{n}\sum_{i=1}^{n}\frac{|\hat{y}_i - y_i|}{y_i} \times 100 \tag{9}$$

$$R^2 = 1 - \frac{\sum_{i=1}^{n}(y_i - \hat{y}_i)^2}{\sum_{i=1}^{n}(y_i - \bar{y}_i)^2} \tag{10}$$

Where *n* denotes the number of observations, y_i the measured values, $\hat{y}_i$the predicted outputs, and $\bar{y}_i$ the mean of the observed data. High R^2 values, coupled with low RMSE and MAPE scores, indicate strong model fidelity and precise prediction of the maximum power point.

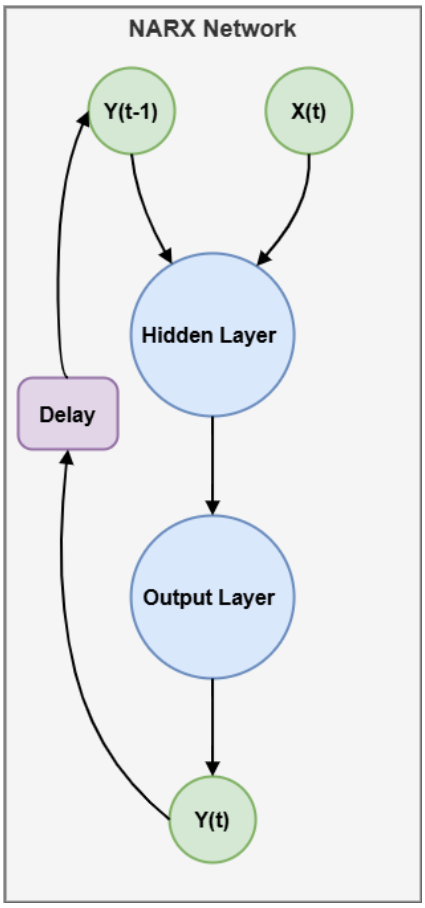

Figure 23 Diagram of the NARX-NN Strategy.

Figure 24 Flowchart of NARX MPPT strategy

II.4 Bio-Inspired Metaheuristic Optimization Methods

Bio-inspired algorithms exploit natural phenomena principles to achieve global optimization capabilities that surpass conventional gradient-based approaches. These methodologies demonstrate particular effectiveness in photovoltaic applications where partial shading creates multiple local optima that challenge traditional optimization strategies.

II.4.1 Particle Swarm Optimization (PSO)

Particle Swarm Optimization (PSO) draws inspiration from collective behaviour in bird flocks and fish schools, employing a population of particles—each defined by position and velocity vectors—to search for the global maximum power point. In PSO-based MPPT [81]:

1. Initialize a swarm of particles with random positions (duty-cycle or voltage settings) and velocities.
2. At each iteration, compute each particle's fitness by evaluating the PV array's power output at its current position.
3. Update each particle's personal best (pBest) and the swarm's global best (gBest).
4. Adjust velocities:

$$v_i(t+1) = wv_i + c_1 r_1[pBest_i - x_i(t)] + c_2 r_2[pBest_i - x_i(t)] \quad (11)$$

Moreover, positions:

$$x_i(t+1) = x_i(t) + v_i(t+1) \quad (12)$$

Where w is inertia weight, $c_1$and c_2 are acceleration coefficients, and r_1,r_2~U(0,1).

5. Repeat until the termination criterion is met—typically a convergence threshold or maximum iterations.

The social learning component lets particles share information about high-power regions, enabling escape from local maxima caused by partial shading. Adaptive tuning of w, $c_1$and c_2 balances exploration and exploitation, accelerating convergence while avoiding premature stagnation.

Although PSO incurs added computational overhead for population management and velocity/position updates, its global optimization capability and resilience to multimodal power landscapes justify its use in demanding PV environments.

II.4.2 Genetic Algorithm Implementation

Genetic Algorithms emulate evolutionary principles through selection, crossover, and mutation operations applied to populations of candidate solutions. This approach demonstrates exceptional robustness in navigating complex optimization landscapes characterized by multiple local optima [82].

The algorithmic framework, as presented in figure 25 begins with random population initialization, where each chromosome represents a potential duty cycle or operating voltage. Fitness evaluation determines each individual's survival probability based on corresponding photovoltaic power output.

Selection mechanisms probabilistically choose superior individuals as parents for subsequent generation creation. Common approaches include tournament selection, roulette wheel selection, and rank-based selection, each offering distinct characteristics regarding selection pressure and diversity maintenance.

Crossover operations combine genetic material from parent chromosomes to create offspring solutions. Single-point, multi-point, and uniform crossover strategies provide different mixing mechanisms, with appropriate selection depending on problem characteristics and desired exploration behavior.

Mutation introduces random variations to maintain population diversity and prevent premature convergence to local optima. Mutation probability represents a critical parameter balancing exploration and exploitation, typically requiring adaptive adjustment based on population convergence characteristics.

Genetic Algorithms demonstrate exceptional global search capabilities and robust performance under partial shading conditions. However, convergence velocity typically exceeds that of conventional algorithms, particularly during initial generations when population diversity remains high.

Parameter sensitivity regarding population size, crossover probability, and mutation rate requires careful tuning to achieve optimal performance. Multi-objective optimization variants have been developed to simultaneously optimize multiple criteria including tracking accuracy, convergence speed, and implementation complexity.

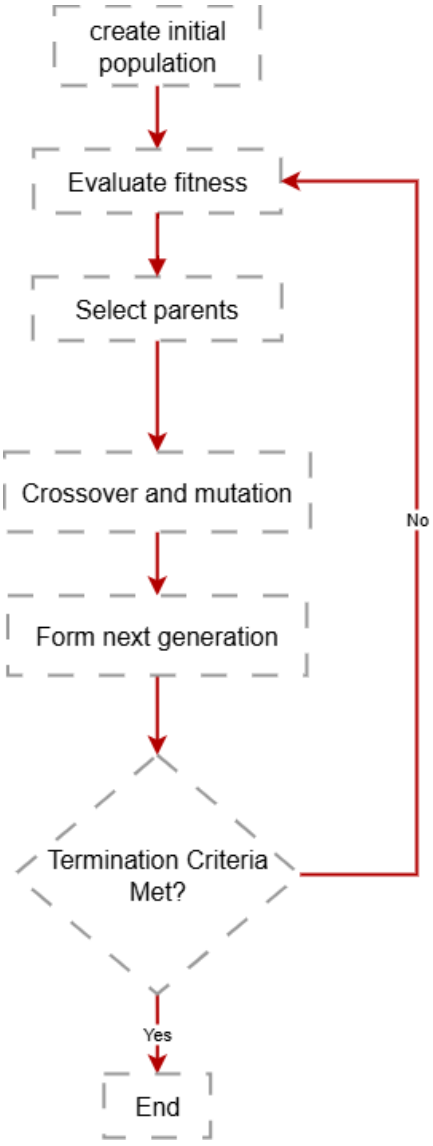

Figure 25 Genetic Algorithms flowchart.

II.4.3 Grey Wolf Optimizer

The GWO is a recent metaheuristic algorithm inspired by the hierarchical leadership and hunting strategies of grey wolves. This algorithm imitates the pack hierarchy of grey wolves, where α, β, and δ wolves lead the search, and the ω wolves follow their guidance.

As illustrated in Figure 26, the GWO algorithm follows a structured workflow: initializing the wolf pack, evaluating fitness, selecting the alpha, beta, and delta leaders, updating positions based on their guidance, and iterating until termination criteria are met. This hierarchical structure provides effective balance between exploration and exploitation through differentiated leadership roles, where alpha wolves represent the optimal current solutions, beta wolves provide secondary guidance, and delta wolves contribute tertiary influence.

Position updating follows the mathematical formulation:

$$x(t+1) = \frac{x_1 + x_2 + x_3}{3} \tag{13}$$

Where x_1, x_2 and x_3 represent positions calculated based on alpha, beta, and delta wolf influences respectively.

The algorithm demonstrates rapid convergence characteristics compared to other population-based methods, typically requiring fewer iterations to achieve satisfactory solutions. This characteristic proves advantageous for real-time MPPT applications where computational resources impose constraints on algorithm execution time. GWO has demonstrated superior performance in photovoltaic applications, achieving high tracking accuracy and robust global search capabilities while maintaining reasonable computational complexity. The algorithm's adaptive search mechanism proves particularly effective under varying environmental conditions and partial shading scenarios [83].

II.4.4 Cuckoo Search Algorithm

Cuckoo Search exploits the brood parasitism breeding strategy observed in cuckoo species, combined with Lévy flight patterns for efficient search space exploration. This combination provides effective balance between local and global search capabilities.

The algorithmic implementation generates new solutions through Lévy flights, which follow heavy-tailed probability distributions enabling both local exploitation and global exploration. The Lévy flight mechanism proves particularly effective for escaping local optima and discovering promising search regions.

Host nest discovery probability governs the abandonment and replacement of poor solutions, maintaining population diversity while focusing search efforts on promising regions. This mechanism prevents premature convergence while ensuring computational resources concentrate on viable solution candidates.

Mathematical formulation of Lévy flights follows:

$$x_i(t+1) = x_i(t) + \alpha \oplus Lévy(\lambda) \tag{14}$$

Where α represents step size and λ controls the Lévy distribution characteristics.

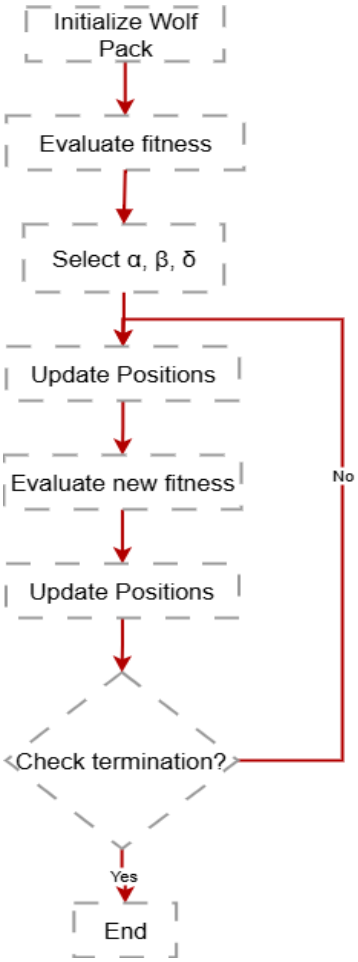

Figure 26 GW Optimization Algorithm Flowchart.

Cuckoo Search demonstrates excellent global optimization capabilities with relatively simple implementation requirements. The algorithm typically converges faster than genetic algorithms while maintaining superior exploration characteristics compared to gradient-based methods [84].

Parameter sensitivity primarily involves discovery probability and Lévy flight characteristics, requiring less extensive tuning compared to other metaheuristic approaches. This characteristic enhances practical applicability while maintaining robust optimization performance.

II.5 Hybrid Optimization Strategies

Hybrid methodologies combine complementary algorithmic strengths to achieve superior performance characteristics that exceed individual method capabilities. These approaches typically balance global search capabilities with local refinement precision, convergence speed with tracking accuracy, and implementation complexity with performance requirements.

II.5.1 Particle Swarm Optimization-Perturb and Observe Integration

Hybrid algorithms combining Particle Swarm Optimization (PSO) with the Perturb and Observe (P&O) method have been proposed to exploit the complementary strengths of global search and local refinement. In such approaches, PSO first scans the duty-cycle (or voltage) search space to approximate the vicinity of the maximum power point (MPP). Once the swarm converges sufficiently close to the true peak, the P&O algorithm takes over to perform fine adjustments, achieving rapid and precise settling at the MPP.

Hybrid PSO–P&O algorithms can achieve steady-state tracking efficiencies exceeding 99% under uniform and partially shaded conditions, with dynamic recovery times below 25 ms following abrupt irradiance changes. Comparative studies report up to 40% fewer iterations required to converge within 0.1% of the true MPP compared to standalone PSO, thereby reducing computational overhead in real-time applications [85].

II.5.2 Fuzzy Logic-Perturb and Observe Enhancement

Fuzzy logic is used to adjust or adapt the P&O algorithm. For example, a hybrid controller might use fuzzy rules to select a perturbation step size based on current error, combining fuzzy adaptability with P&O's simplicity. One study introduced a novel P&O with Fuzzy MPPT whose fuzzy controller inputs were Delta V and Delta P. The hybrid achieved a 99.7% success rate in locating MPP, significantly better response time, and higher tracking efficiency than either standalone P&O or fuzzy logic . This illustrates that fuzzy adaptation can eliminate much of P&O's oscillation and response delay. The trade-off is additional computation for the fuzzy inference. Overall, Fuzzy–P&O hybrids can dramatically improve speed and accuracy relative to each component, with moderate added complexity [86].

II.5.3 Adaptive Neuro-Fuzzy Inference Systems

ANFIS architectures combine neural network learning capabilities with fuzzy logic interpretability, creating adaptive systems that optimize membership functions and rule parameters through training procedures. This hybrid approach achieves superior performance while maintaining transparent decision-making processes.

In fact, ANFIS achieved faster settling and higher tracking accuracy than pure ANN controllers under the same conditions. This makes ANFIS a popular choice for MPPT: it retains fuzzy logic's interpretability while automatically optimizing membership functions. Complexity is high (training and inference) but feasible on modern processors. In summary,

ANFIS hybrids deliver very high accuracy and robustness, combining the best of neural and fuzzy techniques [87].

II.6 Comparative Analysis and Performance Evaluation

Recent comparative studies elucidate the trade-offs among various MPPT techniques in terms of transient response, steady-state efficiency, robustness under shading, and implementation complexity. Conventional methods—such as Constant Voltage (CV), Perturb and Observe (P&O), and Incremental Conductance (IncCond)—continue to serve as baseline approaches. For instance, a buck-boost converter employing CV control achieved the fastest transient response, whereas IncCond on a buck converter delivered the highest steady-state efficiency, although their limited complexity and hardware requirements constrain widespread adoption [88].

In contrast, artificial intelligence (AI) and bio-inspired algorithms typically attain higher efficiencies under nonuniform irradiance and rapid environmental changes. Standard artificial neural network (ANN) controllers have been shown to extract approximately 98% of the available power with rapid convergence dynamics [89]. Improved Particle Swarm Optimization (IPSO) methods consistently exceed 99% tracking accuracy with minimal particle counts and iteration numbers [90]. Under partial shading, genetic-algorithm (GA)-based MPPT successfully locates the global maximum power point where P&O becomes trapped in local optima [91]. Adaptive Neuro-Fuzzy Inference System (ANFIS) controllers further enhance both efficiency and stability over pure ANN implementations [87].

Hybrid controllers, which combine global search and local refinement, demonstrate superior overall performance. The fuzzy–P&O hybrid, for example, achieved a 99.7% success rate in simulated partial-shading scenarios—surpassing either algorithm alone—by exploiting fuzzy logic's adaptability alongside P&O's simplicity [92]. In general, AI and bio-inspired schemes (ANFIS, optimized PSO, GA, and Grey Wolf Optimizer) achieve tracking accuracies in the 98–100% range, compared to 90–98% for conventional methods [93]. Convergence speed is fastest in fuzzy and neural controllers, whereas population-based algorithms require more time unless augmented by enhancements or hybridization.

II.7 Conclusion

This chapter has mapped the spectrum of photovoltaic optimization techniques, from elementary conventional methods to sophisticated hybrid frameworks. Conventional algorithms—such as Constant Voltage, Perturb and Observe, and Incremental Conductance—

remain compelling for applications prioritizing simplicity, cost-effectiveness, and proven reliability under uniform conditions. Artificial intelligence approaches deliver enhanced adaptability and tracking precision through model-free learning, making them well suited to variable and complex operating environments. Bio-inspired metaheuristic methods excel at global maximum power point extraction under partial shading and multimodal landscapes, albeit at the expense of higher computational load and longer convergence times. Hybrid strategies integrate complementary strengths—leveraging global search, local refinement, and adaptive learning—to achieve best-in-class performance with manageable implementation complexity.

The synergy between advanced optimization algorithms and high-gain DC–DC converter architectures (explored in Chapter 1) underpins system-level enhancements in both power conversion efficiency and maximum power point accuracy. Looking ahead, intelligent hybrid systems that dynamically select or combine optimization methods based on real-time environmental assessment will define next-generation MPPT solutions. Continued progress in embedded processing power and machine learning will support ever more sophisticated, yet deployable, photovoltaic optimization strategies across scales and applications.

CHAPTER III MODELLING OF HIGH-GAIN DC-DC CONVERTER FOR PHOTOVOLTAIC APPLICATIONS

III.1 Introduction

The Photovoltaic (PV) energy systems continue to expand rapidly as renewable power sources gain prominence in efforts to decarbonize the electricity sector. However, the inherently low voltage of individual PV modules necessitates power electronic converters that can elevate these levels to match grid or load requirements while maximizing energy extraction. Conventional boost converters suffer from limited step-up ratios, excessive duty-cycle stress, and efficiency losses when tasked with high voltage gains. Consequently, the development of advanced high-gain DC–DC converter topologies has become critical for compact, efficient, and reliable PV power conversion.

This chapter delivers an in-depth study of high-gain converter architectures suitable for PV applications. It begins by reviewing the single-diode equivalent circuit of a PV cell, establishing the key electrical characteristics—current-voltage (I–V) and power-voltage (P–V) relationships—that underpin converter modeling and control design. Thereafter, the quadratic boost converter (QBC) and three-level boost converter (TLBC) are analyzed in detail, with emphasis on their operating modes, voltage gain derivations, and component stress distribution. Building on these foundational topologies, the chapter then introduces a novel Three-Level Quadratic Boost Converter (TLQBC). By integrating cascaded quadratic gain mechanisms within a three-level configuration driven by a single switch, the TLQBC achieves exceptional voltage multiplication while mitigating voltage stress on semiconductor devices.

Design equations for inductors and capacitors are derived to facilitate practical implementation, and key trade-offs between gain, efficiency, and complexity are discussed. Comparative evaluation demonstrates the TLQBC's superior step-up capability at moderate duty cycles, positioning it as an optimal choice for PV systems requiring high-voltage conversion. The insights and models developed herein establish the groundwork for Chapter 4, which will explore the integration of intelligent maximum power point tracking algorithms with these high-gain converters to enhance overall system performance under dynamic environmental conditions..

III.2 Modellling of photovoltaic generator

A photovoltaic (PV) cell converts incident photons into electrical energy via the photovoltaic effect, first observed by Becquerel in 1839 [94]. When photons with energy exceeding the semiconductor bandgap are absorbed, electron–hole pairs are generated and separated by the intrinsic electric field of a p–n junction. In silicon cells, this junction is formed between a

phosphorus-doped n-region and a boron-doped p-region, producing a voltage difference across the device.

III.2.1 Single-Diode Equivalent Circuit

The electrical behavior of a PV cell is commonly represented by the single-diode model shown in Figure 27. It comprises [95]:

- A current source I_{ph} that models photocurrent, proportional to irradiance and temperature.
- A diode D characterizing the nonlinear I–V relationship.
- Series resistance R_s, accounting for resistive losses in contacts and semiconductor bulk.
- Shunt resistance R_{sh} , representing leakage paths.

The cell's output current I is given by

$$I_{pv} = I_{ph} - I_d - \frac{V + I\,R_s}{R_{sh}} \tag{15}$$

where the diode current follows

$$I_d = I_0\left(\exp\left(\frac{q(V + IR_s)}{K.n.\mathrm{T}}\right) - 1\right) \tag{16}$$

and the photocurrent is

$$I_{ph} = I_{ph,ref}\frac{\mathrm{G}}{G_{ref}}\left[1 + K_i\left(\mathrm{T} - T_{ref}\right)\right] \tag{17}$$

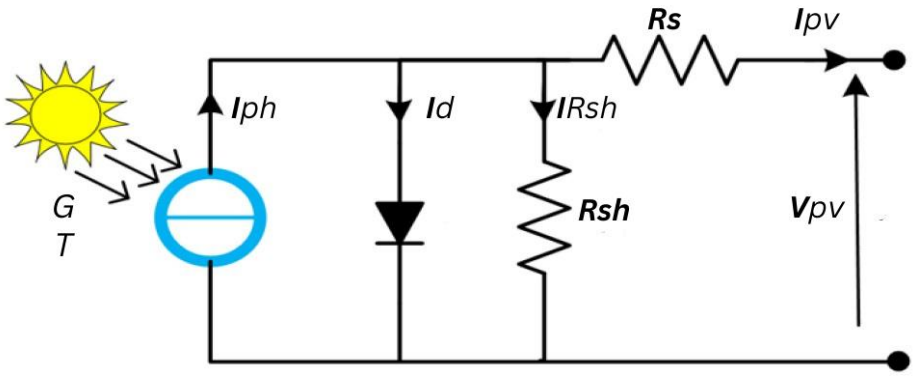

Figure 27 Single-diode equivalent circuit of a PV cell.

Here, q is the electronic charge, K is the Boltzmann constant, n is the diode ideality factor, T is absolute temperature, G is solar irradiance, and subscript "ref" denotes reference conditions.

III.2.2 I–V and P–V Characteristics

The I–V and P–V curves vary with irradiance and temperature. Increased irradiance raises short-circuit current nearly proportionally, while open-circuit voltage shifts modestly. Elevated temperature reduces open-circuit voltage, thus decreasing maximum power. Figure 28 and 29 illustrates these dependencies, highlighting the need for accurate models when designing MPPT algorithms and converter controls.

III.2.3 PV Module and Array Configuration

Practical PV systems employ modules and arrays to meet voltage and current requirements. Series connections increase voltage—the sum of individual cell voltages—while parallel connections raise current by summing individual branch currents (Figures 30 and 31). Bypass diodes mitigate mismatch losses under partial shading by providing alternate current paths, and blocking diodes prevent reverse current flow during low-light conditions [96].

The overall generator efficiency η is defined as the ratio of maximum power P_{max} to incident solar power $G \times A$:

$$\eta = \frac{P_m}{G.A} \tag{18}$$

Where A is the active cell area. Typical silicon modules achieve 15–22% efficiency under standard test conditions (1000 W/m², 25 °C).

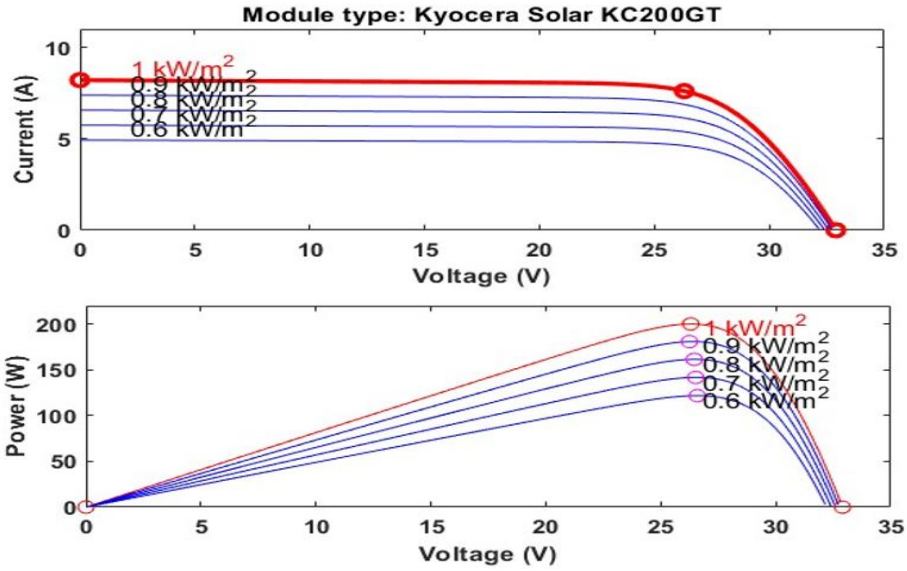

Figure 28 I-V and P-V curves at various levels of irradiance when T=25 °C.

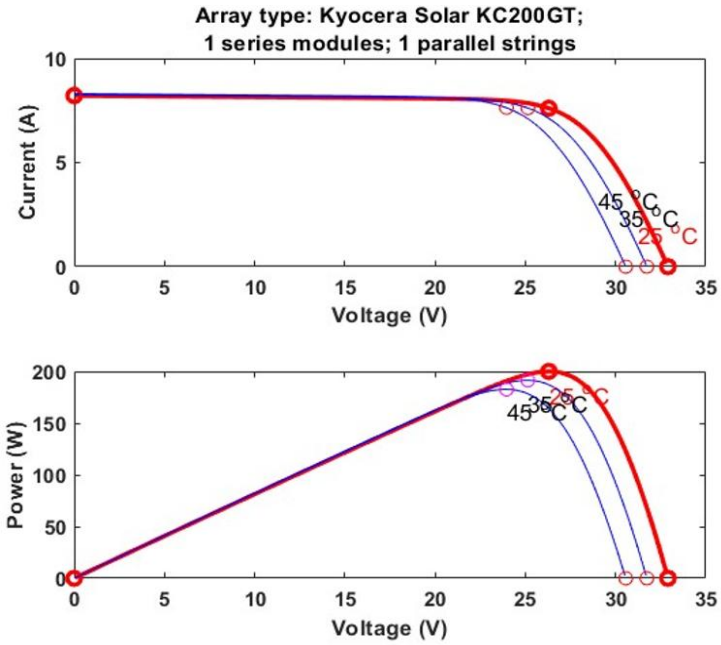

Figure 29 I-V and P-V curves at various levels of T when G=1000 W/m^2.

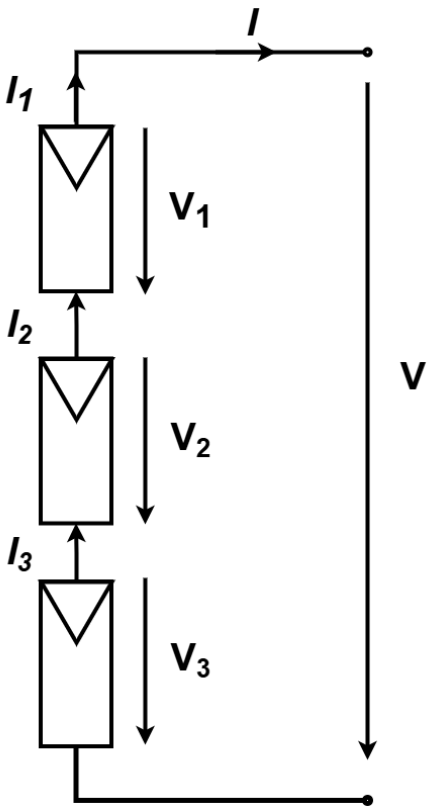

Figure 30 Series connection of PV cells..

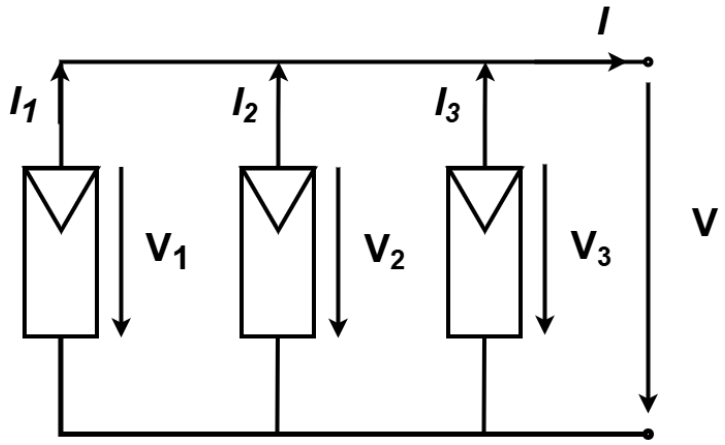

Figure 31 Parallel connection of PV cells and module protection diodes.

III.3 Quadratic Boost Converter

Traditional boost converters are inadequate for achieving high voltage gains due to extreme duty cycle requirements, elevated component stress, and efficiency degradation. The quadratic boost converter (QBC) addresses these limitations by incorporating additional passive elements, delivering a squared voltage gain characteristic that enhances step-up performance without demanding extreme duty cycles [97].

III.3.1 Circuit Description and Operation

The quadratic boost converter comprises two inductors (L_1, L_2), two capacitors (C_1, C_2), three diodes (D_1, D_2 and D_3), and a single controlled switch S, as depicted in Figure 32. This architecture effectively functions as two cascaded boost stages powered by a shared input source, such as a photovoltaic module. The converter operates in continuous conduction mode (CCM) through two distinct switching states:

Mode 1 (Switch ON): When switch S is activated, both inductors store energy from the input source. Diodes D_1 and D_3 remain reverse-biased, isolating their respective branches. Capacitor C_2 discharges to supply the load directly (Figure 33).

Mode 2 (Switch OFF): When Upon switch opening, stored energy in the inductors is released through forward-biased diodes D_1 and D_3. Inductor L_1 transfers energy to charge capacitor C_1, while inductor L_2 charges capacitor C_2. Both capacitors contribute to load supply, elevating the output voltage (Figure 34).

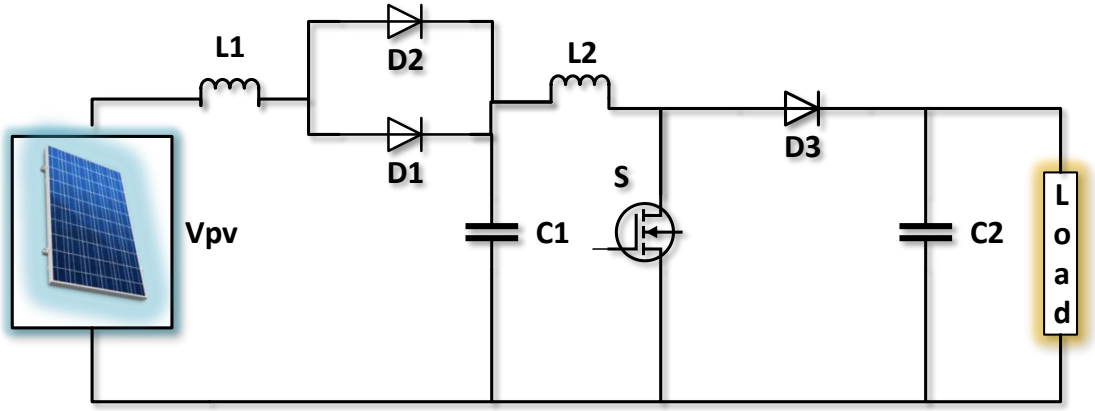

Figure 32 Quadratic Boost Converter topology.

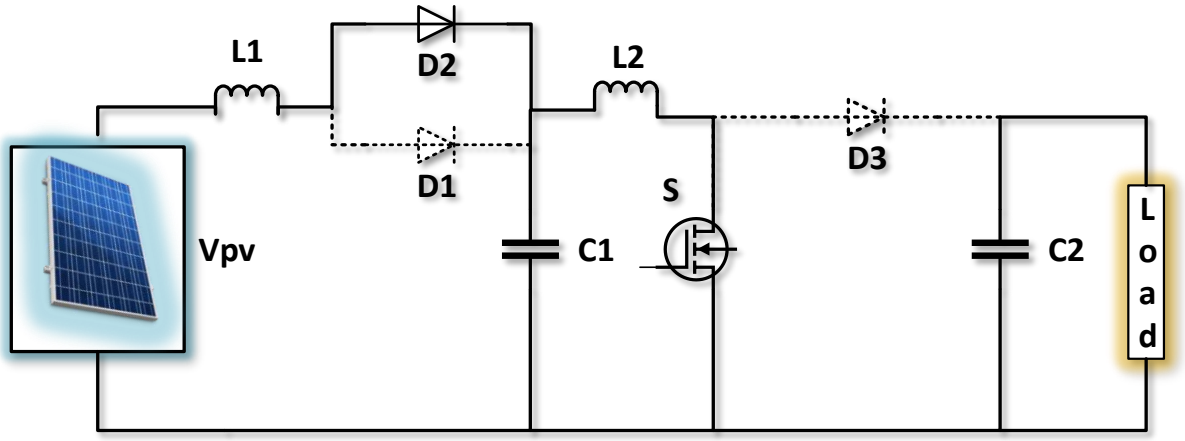

Figure 33 Mode 1 Operation (Switch ON).

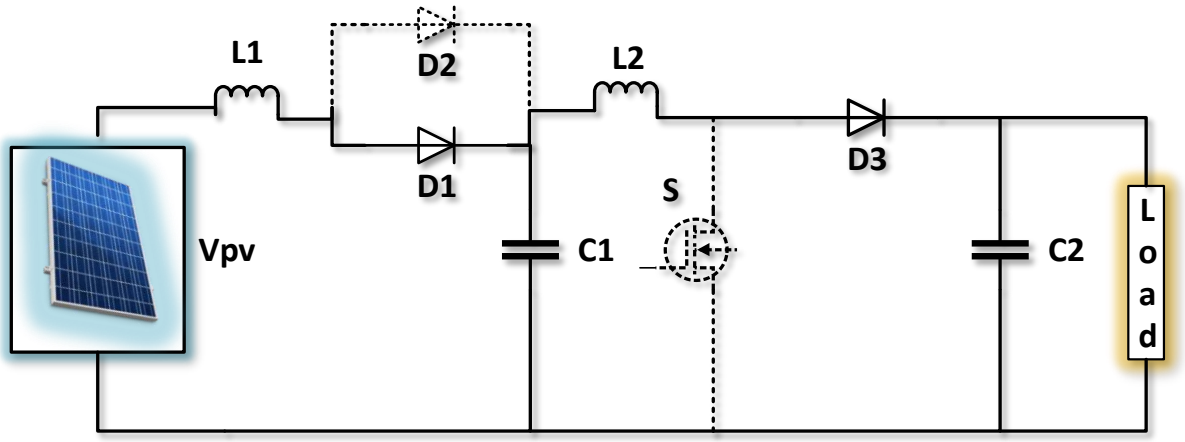

Figure 34 Mode 2 Operation (Switch OFF).

III.3.2 Voltage Gain Derivation

Applying volt-second balance to both inductors under steady-state conditions and assuming ideal components yields the output-to-input voltage relationship:

$$V_{out} = \frac{V_{in}}{(1-D)^2} \tag{19}$$

This quadratic relationship demonstrates significantly enhanced gain compared to conventional boost converters, particularly at moderate duty cycles. The squared denominator characteristic enables high step-up ratios while maintaining reasonable switching duty cycles.

III.3.3 Design Considerations

Despite superior voltage gain, the QBC incorporates additional passive components that increase conduction losses and circuit complexity. However, the topology remains attractive for PV applications due to reduced voltage stress on semiconductor devices and improved efficiency under high-gain operation. Key design parameters can be estimated using:

Inductor Sizing:

$$L = \frac{V_{in}.D}{f_s\,.\Delta i_L} \tag{20}$$

Capacitor Sizing:

$$C = \frac{i_o.D}{f_s\ .\Delta V} \tag{21}$$

Where, f_s is the switching frequency, Δi_L is the peak-to-peak inductor current ripple, and ΔV is the allowable output voltage ripple.

III.4 Three-Level Boost Converter

The three-level boost converter (TLBC) has emerged as an effective topology for achieving high voltage gain while simultaneously reducing voltage stress across the semiconductor devices. This characteristic makes the TLBC particularly attractive for photovoltaic (PV) applications, where efficiency, compactness, and reliability are critical requirements. In addition to mitigating device stress, the TLBC also contributes to reduced switching losses and lower electromagnetic interference (EMI), thereby improving overall system performance [75].

III.4.1 Power Circuit

The circuit configuration of the TLBC is illustrated in Figure 35. Compared with the conventional boost converter, the TLBC can deliver an output voltage that is approximately three

times higher, with the gain being directly influenced by the number of voltage levels. The topology employs a single controlled switch, which simplifies control implementation and reduces circuit complexity. Additional voltage levels are realized by incorporating supplementary capacitors and diodes into the structure, enabling further extension of the voltage gain without significant modification to the core circuit [75].

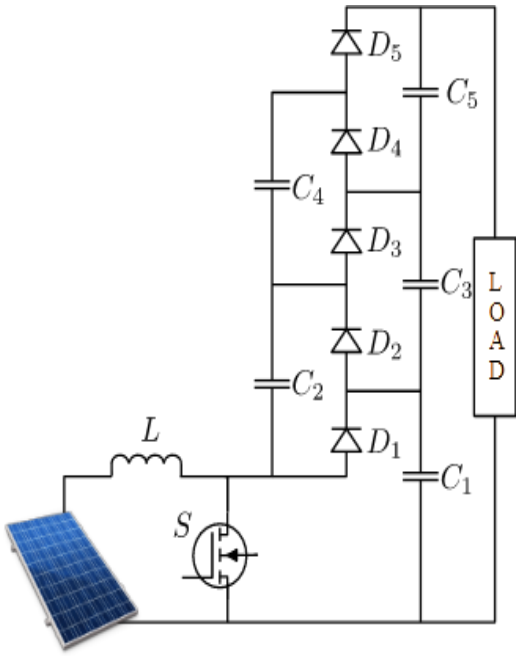

Figure 35 Three-Level Boost DC-DC Converter.

III.4.2 Operational States

When operating in continuous conduction mode (CCM), the three-level boost converter (TLBC) alternates between two distinct switching states, depending on whether the controlled switch S is turned ON or OFF. The sequence of events in each state is described below.

Mode 1 (Switch ON): During the switch-on state, the inductor charges from the source voltage V_{PV}, as illustrated in Figure 36(a). If C_2's voltage is smaller than C_1's voltage then C_1 clamps C_2's voltage through D_2 and the switch S, as depicted in Figure 36(b). If the combined voltage across C_4+C_2 is smaller than the voltage across C_3+C_1, then C_3 and C_1 clamp the voltage across C_6 and C_4 through D_4 and S, as illustrated in Figure 36(c). The TLBC ensures that the output capacitors C_1, C_2, and C_3 maintain equal voltages. Assuming equal capacitances, the total output voltage across the load is given by:

$$V_{C1} = V_{C3} = V_{C5} = V_C \tag{22}$$

$$V_{out} = 3.V_C \tag{23}$$

The differential equations for the inductor current and output voltage in this mode are given by Equations (24) and (25).

$$\frac{di_L}{dt} = \frac{V_{pv}}{L} \tag{24}$$

$$\frac{dV_{out}}{dt} = -3\frac{V_{out}}{R.\mathrm{C}} \tag{25}$$

Mode 2 (Switch OFF): When the switch S is opened, the converter enters the OFF state. In this interval, the inductor current is redirected through the diode network, transferring stored energy into the capacitors. . For instance, Figure 37(a) depicts inductor L_1 delivering energy to capacitor C_1. When D_1 closes, C_2 and the voltage in V_{in} plus the inductor's voltage clamp the voltage across C_3 and C_1 through D_3, as represented in Figures 37(b). Similarly, the voltage across the inductor plus V_{in}, C_2, and C_4 clamps the voltage across C_1, C_3, and C_5 through D_5. Figure 37(c). The corresponding differential equations governing this mode are expressed in Equations (26) and (27), which describe the dynamic relationships between inductor currents and capacitor voltages.

$$\frac{di_L}{dt} = \frac{V_{pv}}{L} - \frac{V_{out}}{3.L} \tag{26}$$

$$\frac{dV_{out}}{dt} = \frac{i_L}{C} - 3\frac{V_{out}}{R.\mathrm{C}} \tag{27}$$

From the state equations of each operating mode, the converter's bilinear model is derived, as expressed in Equation (28). The state vector is defined as $= [i_L \quad V_{out}]^T$, and D denotes the duty cycle provided by the control unit.

$$\dot{x} = \begin{bmatrix} 0 & -\frac{1-D}{3.L} \\ \frac{1-D}{C} & -\frac{3}{R.C} \end{bmatrix} x + \begin{bmatrix} \frac{1}{L} \\ 0 \end{bmatrix} V_{pv} \tag{28}$$

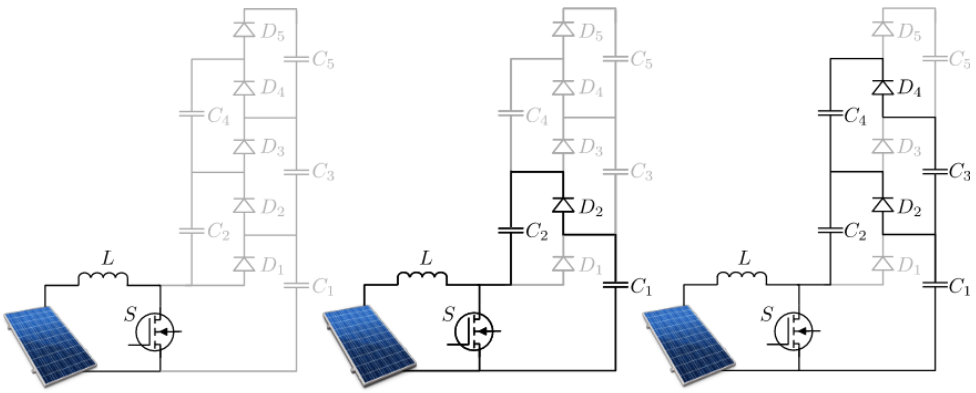

Figure 36 State ON.

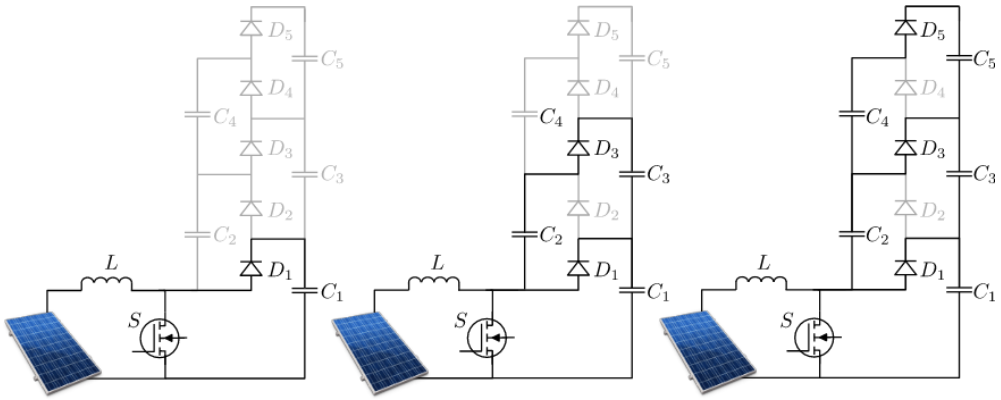

Figure 37 State OFF.

III.4.3 Voltage Conversion Ratio

For an ideal three-level boost converter (TLBC) operating under steady-state conditions, the average voltage across the inductor is zero. This yields the following relation:

$$V_L = D.\left(V_{pv}\right) + (1 - D).\left(V_{pv} - V_c\right) = 0 \tag{29}$$

which simplifies to:

$$V_{pv} = V_c.(1 - D) \tag{30}$$

Since each of the three output capacitors maintains the same voltage V_c, the total output voltage can be expressed as:

$$V_{out} = 3.V_c \tag{31}$$

From these relations, the fundamental voltage conversion ratio is obtained as:

$$M = \frac{V_{out}}{V_{pv}} = \frac{3}{1 - D} \tag{32}$$

When parasitic elements are considered, particularly the equivalent series resistance of the inductor ($R_{esr,L}$), the inductor voltage equation becomes:

$$V_L = D.\left(V_{pv} - i_L.R_{esr,L}\right) + (1 - D).\left(V_{pv} - V_c - i_L.R_{esr,L}\right) = 0 \tag{33}$$

From this, a more comprehensive expression for the conversion ratio can be derived:

$$M = \frac{V_{out}}{V_{pv}} = \frac{1}{\frac{(1 - D)}{3} + \frac{3.R_{esr,L}}{(1 - D).\mathrm{R}}} \tag{34}$$

This analysis indicates that the presence of inductor resistance reduces the achievable voltage gain. Consequently, in practical implementations, the duty cycle D must be increased to maintain the desired output voltage.

III.4.4 Voltage Balancing Across Capacitors

In the TLBC circuit, power transfer to the load occurs through the sequential charging and discharging of capacitors in the switched-capacitor voltage multiplier network. For medium- and high-voltage applications, the voltage drops across switches and diodes are typically small and may be neglected in first-order analysis [75].

As shown in Figure 38, the voltage across capacitor C_2 can be expressed as:

$$V_{C2} = V_{C1} - V_{drop-switch} - V_{drop-Diode} = V_{C1} - 2.V_d \tag{35}$$

During the charging process of capacitor C_4 (Figure 39), the charging current flows through the input inductor and the PV source, rather than through the diode. Since capacitor C_3 charges concurrently with C_1, its voltage can be expressed as:

$$V_{C3} = V_{C1} - 4.V_d \tag{36}$$

Figure 40 demonstrates that beyond the second level, the diode voltage drop no longer affects the capacitor charging sequence. Thus, subsequent capacitors are charged to approximately the same voltage level as C_3. The resulting capacitor voltages can therefore be written as:

$$V_{C5} = V_{C1} - 4.V_d \tag{37}$$

and the total output voltage is given by:

$$V_{out} = V_{C1} + V_{C3} + V_{C5} = 3.V_C - 8.V_d \tag{38}$$

For medium- to high-voltage operation, the capacitor voltage V_C is significantly greater than the diode forward voltage V_D. As a result, the effect of diode voltage drops on the overall output is negligible. This balancing mechanism ensures that capacitors maintain uniform voltage profiles, thereby supporting stable operation and reliable high-gain performance.

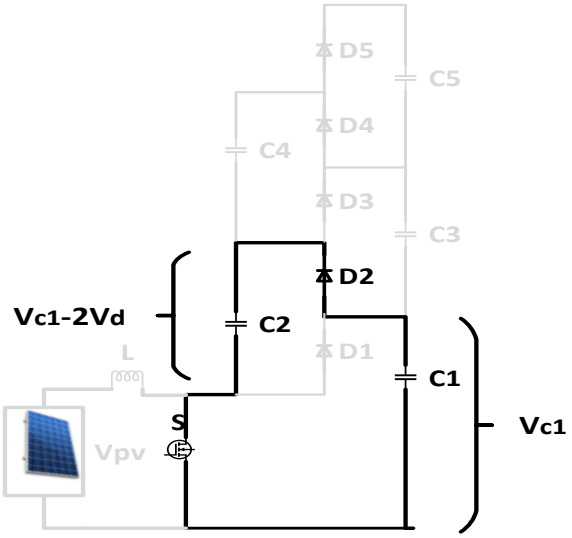

Figure 38 Charging of capacitor C_2 utilizing the voltage drop across the diodes and a switch.

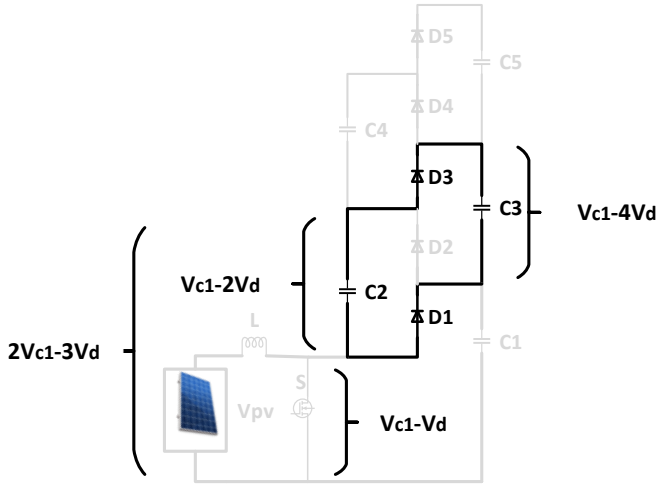

Figure 39 Charging of capacitor C_3 utilizing the voltage drop across the diodes and a switch.

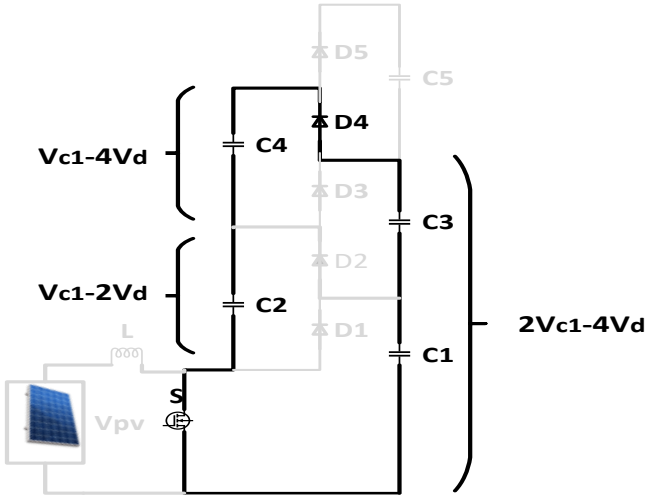

Figure 40 Charging of capacitor C_4 utilizing the voltage drop across the diodes and a switch.

III.5 Proposed Three-Level Quadratic Boost Converter

Building upon the quadratic and three-level boost topologies, the Three-Level Quadratic Boost Converter (TLQBC) synergistically combines their voltage gain mechanisms to achieve exceptionally high step-up ratios with reduced device stress. The TLQBC integrates cascaded inductive stages and stepped capacitor stacking, resulting in a converter capable of interfacing low-voltage PV sources with high-voltage loads while maintaining efficiency and reliability.

III.5.1 Topology Overview

In the proposed configuration, a quadratic boost converter stage is combined with a three-level boost converter incorporating a switched-capacitor network. This configuration not only boosts the possible output voltage but also distributes voltage stress more equally among the

components, hence boosting reliability. A noteworthy strength of the architecture resides in its scalability: additional voltage levels can be produced by integrating extra capacitors and diodes without the need to modify the underlying circuit framework.

For the purpose of analysis, all circuit components are assumed to be ideal. The complete power circuit of the TLQBC is illustrated in Figure 41.

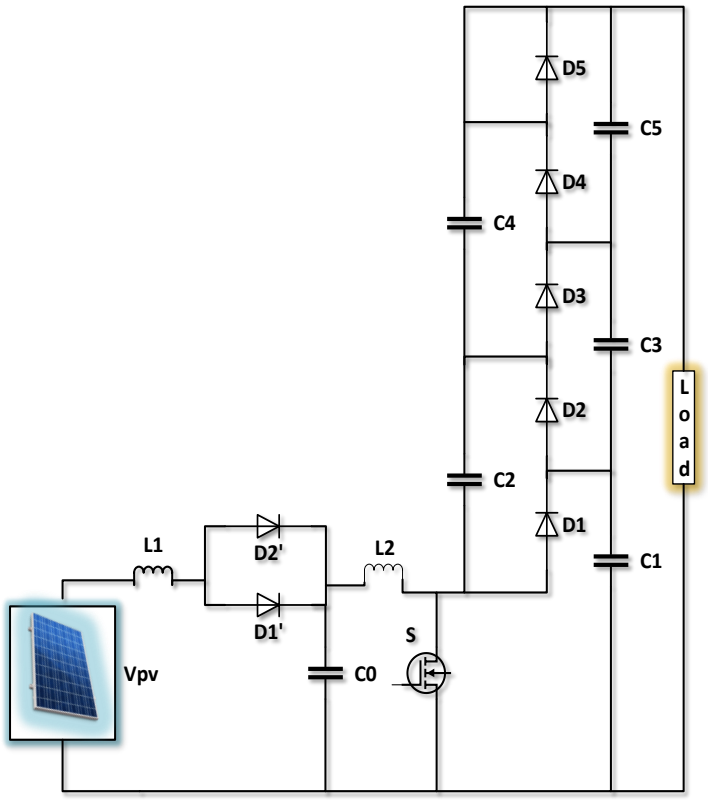

Figure 41 Proposed high gain Boost Converter topology.

III.5.2 Operational States

When operating in continuous conduction mode (CCM), the TLQBC alternates between two switching states depending on whether the main switch S is turned ON or OFF. The operation of each state is outlined below.

Mode 1 (Switch ON): In the switch-on state, the circuit's functionality primarily relies on the TLQBC switch, with the diode D_1' is reverse biased and the diode D_2' is forward biased. The inductor L_1 is charged by the source voltage V_{pv}, while inductor L_2 receives its charge from capacitor C_0, both inductors playing a role in energy storage, as shown in Figure 42a. Should the voltage of C_2 be less than that of C_1, C_1 will clamp C_2's voltage via D_2 and the switch S, as depicted in Figure 42b. Concurrently, if the voltage across C_4+C_2 is lower than that across C_3+C_1, then C_3 and C_1 will clamp the voltage across C_2 and C_4 through D_4 and S, as illustrated in Figure 42c. The

differential equations for output voltage and inductor current in this mode are given by Equation (39):

$$\begin{cases} \dfrac{di_{L1}}{\mathrm{dt}} = \dfrac{V_{pv}}{L_1} \\ \dfrac{di_{L2}}{\mathrm{dt}} = \dfrac{V_{C0}}{L_2} \\ \dfrac{dV_{C0}}{\mathrm{dt}} = -\dfrac{i_{L2}}{C_0} \\ \dfrac{dV_{out}}{\mathrm{dt}} = -\dfrac{3V_{out}}{\mathrm{RC}} \end{cases} \tag{39}$$

Mode 2 (Switch OFF): When the switch SSS is turned OFF, diode D_1' becomes forward-biased while diode D_2' turns reverse-biased. In this condition, capacitor C_0 is recharged using energy supplied by both the source voltage V_{pv} and inductor L_1, while inductor L_2 transfers its stored energy to capacitor C_1, as shown in Figure 43(a).

When diode D_1 conducts, the combined voltage from C_2, the inductors, and the source clamps the voltage across C_3 and C_1 through diode D_3, as depicted in Figure 43(b). Similarly, the voltages from V_{pv}, L_1, L_2 , C_2, and C_4 collectively clamp the voltages of C_1, C_3, and C_5through diode D_5, as shown in Figure 43(c).

The corresponding differential equations for this state are:

$$\begin{cases} \dfrac{di_{L1}}{\mathrm{dt}} = \dfrac{V_{pv}}{L_1} - \dfrac{V_{C0}}{L_1} \\ \dfrac{di_{L2}}{\mathrm{dt}} = \dfrac{V_{C0}}{L_2} - \dfrac{V_{out}}{3L_2} \\ \dfrac{dV_{C0}}{\mathrm{dt}} = -\dfrac{i_{L2}}{C_0} + \dfrac{i_{L1}}{C_0} \\ \dfrac{dV_{out}}{\mathrm{dt}} = -\dfrac{3V_{out}}{\mathrm{R.C}} + \dfrac{i_{L2}}{\mathrm{C}} \end{cases} \tag{40}$$

III.5.3 State-Space Representation

By combining the dynamics of both switching states, the bilinear averaged model of the TLQBC can be derived. The state vector is defined as:

$$x = [i_{L1}, i_{L2}, V_{C0}, V_{out}]^T \tag{41}$$

where D represents the duty cycle controlled by the switching signal.

The averaged model is expressed as:

$$\dot{x} = A(D)x + BV_{pv} \tag{42}$$

with the system matrices defined as:

$$A(D) = \begin{bmatrix} 0 & 0 & -\frac{1-D}{L_1} & 0 \\ 0 & 0 & \frac{1}{L_2} & -\frac{1-D}{3L_2} \\ \frac{1-D}{C_0} & -\frac{1}{C_0} & 0 & 0 \\ 0 & \frac{1-D}{C} & 0 & -\frac{3}{\mathrm{R.C}} \end{bmatrix}, \quad B = \begin{bmatrix} \frac{1}{L_1} \\ 0 \\ 0 \\ 0 \end{bmatrix} \tag{43}$$

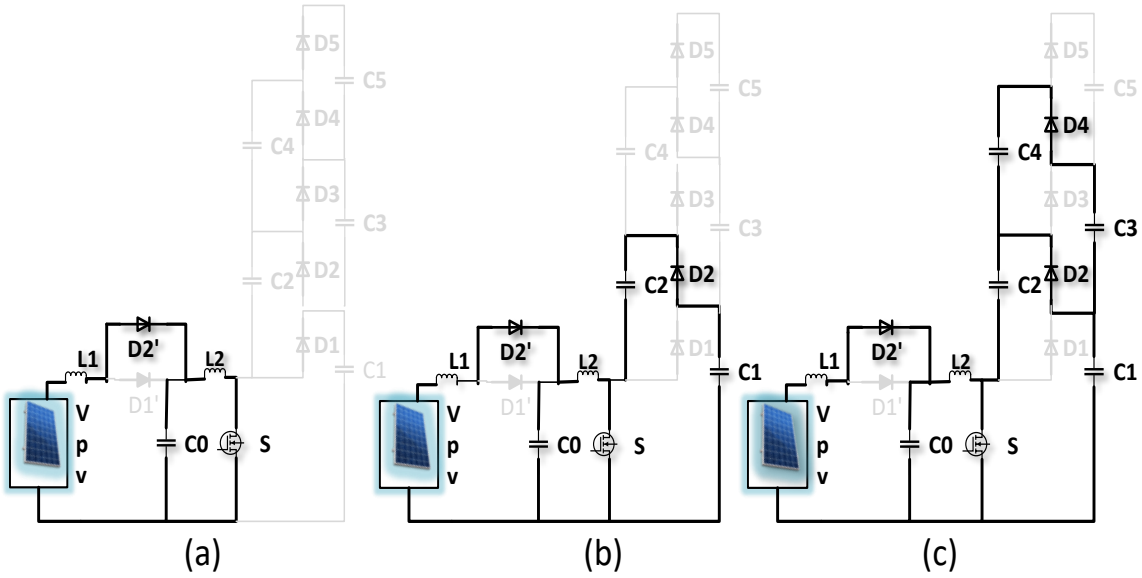

Figure 42 State ON.

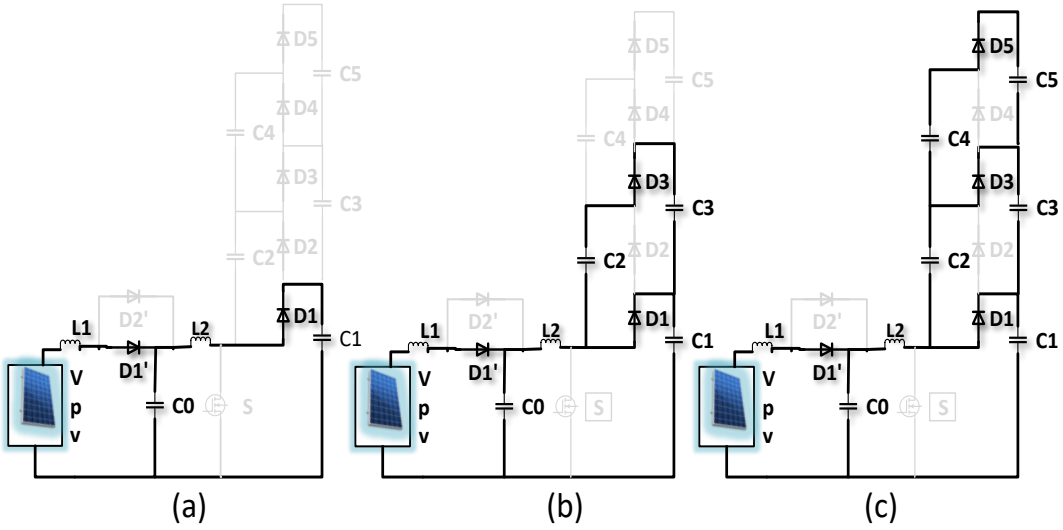

Figure 43 State OFF.

This state-space model provides a useful mathematical framework for analyzing and designing control strategies for the TLQBC under varying operating conditions.

III.5.4 Voltage Conversion Ratio

For an ideal TLQBC, the steady-state voltage across each inductor is zero. This condition leads to the following relationships:

$$V_{L1} = D.\left(V_{pv}\right) + (1 - D).\left(V_{pv} - V_{C0}\right) = 0 \tag{44}$$

$$V_{C0} = \frac{V_{pv}}{(1 - D)} \tag{45}$$

$$V_{L2} = D.(V_{C0}) + (1 - D).(V_{C0} - V_{out} = 0 \tag{46}$$

$$V_{out} = \frac{3\,V_{C0}}{(1 - D)} \tag{47}$$

Since all output capacitors share the same voltage V_C, the overall output voltage becomes V_{out} = $3V_c$. Combining (11) and (13) yields the ideal voltage gain:

$$\mathrm{M} = \frac{V_{out}}{V_{pv}} = \frac{3}{(1 - \mathrm{D})^2} \tag{48}$$

The relationship between the input current, the output voltage, and the output current can then be written as:

$$V_{pv} i_{L1} = V_{out} i_{out} = V_{out} \frac{V_{out}}{R} \tag{49}$$

From which:

$$i_{L1} = \frac{3\,V_{out}}{(1 - D)^2 R} \tag{50}$$

$$i_{L2} = (1 - D) i_{L1} = \frac{3\,V_{out}}{(1 - D) R} \tag{51}$$

III.5.4.1 Practical Considerations with Inductor Resistance

In practice, the inductors are not ideal and exhibit an equivalent series resistance (ESR), denoted as $R_{esr,L}$. Including this effect modifies the inductor voltage equations:

$$V_{L1} = D.\left(V_{pv} - i_{L1}.R_{esr,L1}\right) + (1 - D).\left(V_{pv} - V_{C0} - i_{L1}.R_{esr,L1}\right) = 0 \tag{52}$$

$$V_{pv} = (1-D)V_{C0} + i_{L1}.R_{esr,L1} \tag{53}$$

$$V_{L2} = D.\left(V_{C0} - i_{L2}.R_{esr,L2}\right) + (1-D).\left(V_{C0} - \frac{V_{out}}{3} - i_{L2}.R_{esr,L2}\right) = 0 \tag{54}$$

$$V_{C0} = (1-D)\frac{V_{out}}{3} + i_{L2}.R_{esr,L2} \tag{55}$$

By substituting (16), (17), (19), and (21), the input PV voltage can be expressed as:

$$V_{pv} = \frac{3\,V_{out}}{R}R_{esr,L2} + (1-D)^2\frac{V_{out}}{3} + \frac{3\,V_{out}}{(1-D)^2R}R_{esr,L1} \tag{56}$$

Finally, the generalized voltage conversion ratio including inductor resistance is obtained as:

$$M = \frac{V_{out}}{V_{pv}} = \frac{1}{\frac{(1-D)^2}{3} + \frac{3R_{esr,L1}}{(1-D)^2\mathrm{R}} + \frac{3R_{esr,L2}}{R}} \tag{57}$$

This expression demonstrates that the presence of inductor ESR reduces the effective voltage gain compared with the ideal case ($R_{esr,L}$=0). Consequently, a higher duty cycle is required in practical converters to achieve the same target output voltage.

III.6 Performance Comparison

Table 5 summarizes the performance of the proposed TLQBC in comparison with conventional QBC and TLBC. The comparison highlights key parameters, including voltage gain, component count, and structural complexity.

As illustrated in Figure 44, the TLQBC achieves the highest output voltage gain among the compared converters at the same duty ratio. Figures 44(a) and 44(b) further demonstrate that the TLQBC consistently outperforms the QBC and TLBC across the full duty cycle range. Notably, at a moderate duty cycle (e.g.,D=0.6), the TLQBC delivers a significantly higher voltage gain while avoiding excessive device stress, which is a common limitation of conventional converters.

This superior gain characteristic arises from the combined quadratic and three-level mechanisms, enabling the TLQBC to deliver enhanced voltage boosting with only a single active switch, thus simplifying the control strategy.

Table 5 Comparison between different high gain boost converter.

Converter	**QBC[97]**	**TLBC[75]**	**TLQBC**

Output voltage	$V_{out} = \frac{V}{(1-D)^2}$	$V_{out} = \frac{3V}{(1-D)}$	$V_{out} = \frac{3V}{(1-D)^2}$
Switch	1	1	1
frequency	F	F	F
capacitors	2	5	6
Inductors	2	1	2
Diodes	2	5	7

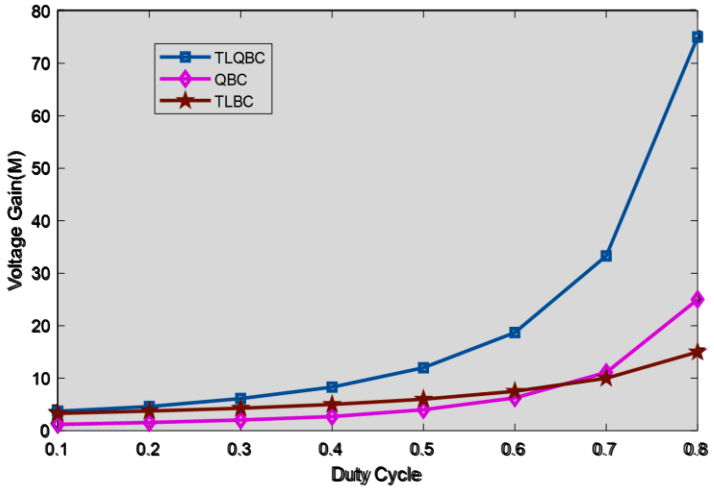

a)

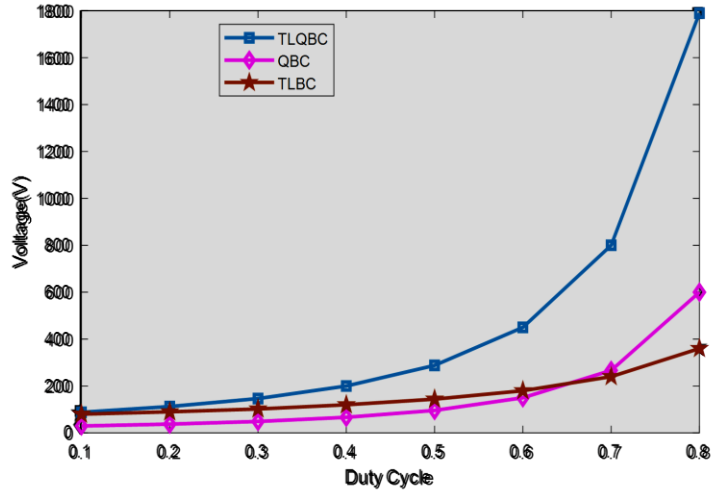

b)

Figure 44 Comparative analysis of output voltage and static gain across different converter topologies.

III.7 Conclusion

This chapter has presented a comprehensive examination of high-gain DC–DC converter architectures tailored for photovoltaic systems. Beginning with the single-diode equivalent model, the electrical behavior of PV cells under varying irradiance and temperature conditions was characterized, establishing a foundation for converter analysis and control design.

Subsequently, the quadratic boost converter (QBC) and the three-level boost converter (TLBC) were introduced. Their operating principles, voltage-gain derivations, and design considerations were detailed, highlighting how the QBC achieves a squared gain characteristic while the TLBC distributes voltage stress across multiple levels. Comparative evaluation revealed inherent trade-offs between voltage gain, component count, and device stress in these topologies.

Building on these insights, the proposed Three-Level Quadratic Boost Converter (TLQBC) was developed. By unifying the quadratic gain mechanism with three-level operation in a single-switch topology, the TLQBC delivers superior voltage amplification while reducing voltage stress on each semiconductor device. Performance comparison across duty-cycle ranges confirmed the TLQBC's highest step-up ratio among the studied converters, achieving substantial gain at moderate duty cycles without compromising component reliability.

Design guidance for inductor and capacitor sizing was provided, and a bilinear averaged model was formulated to support future control synthesis. Practical considerations, including the impact of inductor equivalent series resistance on achievable gain, were also addressed.

In summary, the TLQBC offers a compelling balance of high voltage gain, reduced device stress, and control simplicity, making it well suited for PV applications requiring compact, efficient, and reliable power conversion. The groundwork laid in this chapter paves the way for Chapter 4, which will explore advanced maximum power point tracking algorithms and intelligent optimization strategies integrated with high-gain converter platforms to maximize energy harvesting under dynamic environmental conditions.

CHAPTER IV ADVANCED MPPT STRATEGIES FOR HIGH-GAIN DC–DC CONVERTER-BASED PV SYSTEMS

IV.1 Introduction

Photovoltaic (PV) systems exhibit highly nonlinear electrical characteristics that vary significantly with changes in irradiance and temperature. As a result, they require specialized power electronic interfaces not only to extract energy efficiently but also to regulate it under dynamic operating conditions. Conventional DC–DC converters, often paired with simple maximum power point tracking (MPPT) algorithms such as the incremental conductance (IncCond) method, provide limited voltage gain and exhibit shortcomings in dynamic performance. These limitations typically manifest as high power ripple, overshoot, and slow transient response, which reduce overall system efficiency and reliability.

To address these challenges, this chapter investigates the integration of advanced MPPT strategies with a novel three-level quadratic boost (TLQ-boost) converter, specifically designed for high-gain PV applications. The TLQ-boost topology combines the quadratic boost principle with a multilevel switched-capacitor network, enabling substantial voltage gain while inherently balancing capacitor voltages. This structural advantage reduces voltage stress across switching devices, enhances efficiency, and makes the topology particularly well suited for renewable energy systems that demand compact, scalable, and high-performance conversion stages. A schematic representation of a photovoltaic (PV) system integrated with the proposed TLQBC converter is presented in Figure 45.

Given the variability of solar irradiance and temperature, MPPT control plays a crucial role in ensuring that the PV system consistently operates at its maximum power point. This chapter evaluates the TLQBC when integrated with four distinct MPPT approaches: (i) the conventional incremental conductance (IncCond) algorithm, (ii) a nonlinear autoregressive neural network with exogenous inputs (NARX-NN), and (iii–iv) two fuzzy logic controllers—namely, a standard Type-1 fuzzy logic (T1-FLC) and an interval Type-2 fuzzy logic (IT2-FLC). These controllers are comparatively assessed under uniform test conditions using key performance indicators, including tracking speed (rise time), steady-state accuracy (error and efficiency), output voltage and current ripple, and robustness under environmental disturbances.

The remainder of this chapter is structured as follows. Section 4.2 describes the simulation framework and modeling assumptions. Section 4.3 validates the TLQ-boost converter operation. Section 4.4 presents the selected MPPT strategies, while Section 4.5 details the performance evaluation across various scenarios. Section 4.6 provides a comparative analysis of the controllers,

and Section 4.7 examines the integrated system-level behavior. Section 4.8 offers a critical discussion of the results, and Section 4.9 concludes the chapter with key findings and insights.

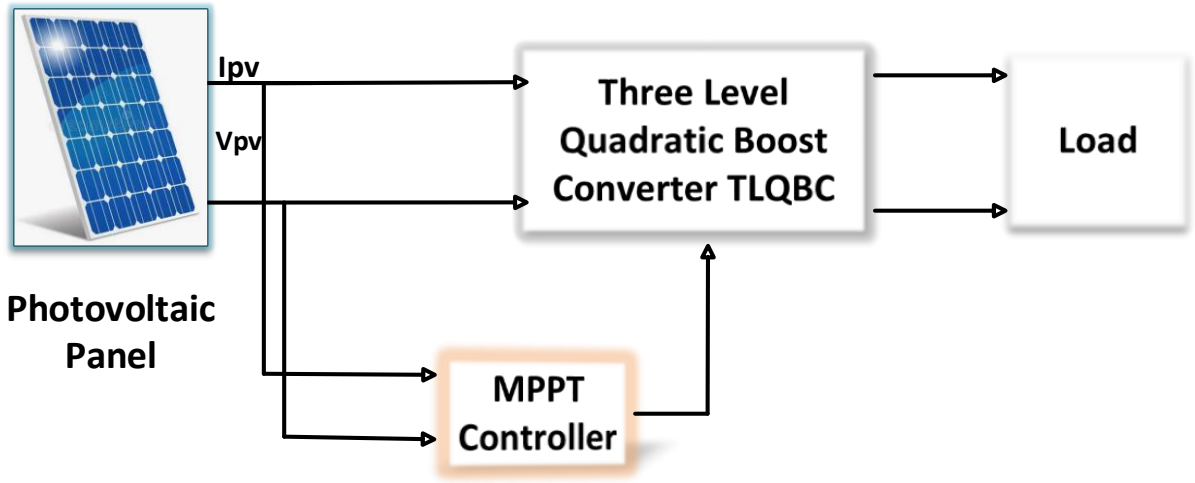

Figure 45 Schematic representation of a photovoltaic (PV) system integrated with the proposed TLQBC topology.

IV.2 Simulation Framework and Modelling Methodology

The comprehensive evaluation of advanced maximum power point tracking strategies integrated with the three-level quadratic boost converter necessitates a sophisticated computational framework capable of accurately representing the complex nonlinear interactions between photovoltaic characteristics, power electronic dynamics, and intelligent control algorithms. The modeling methodology encompasses detailed component-level representations, comprehensive environmental parameter variations, and precise controller implementation specifications to ensure reliable performance assessment across diverse operational scenarios.

IV.2.1 Computational Environment and Software Implementation

The complete system modeling and simulation framework utilizes MATLAB/Simulink R2024a as the primary computational environment, leveraging its advanced numerical solvers and comprehensive power electronics toolboxes to ensure accurate representation of both continuous-time system dynamics and discrete-time control algorithm implementation.

The software implementation encompasses multiple specialized toolboxes to address the diverse computational requirements of the integrated system. The Neural Network Time Series Toolbox facilitates implementation of the nonlinear autoregressive neural network controller, providing advanced training algorithms and recurrent network architectures essential for capturing temporal dependencies in photovoltaic system behaviour. The Fuzzy Logic Toolbox enables

comprehensive implementation of both Type-1 and interval Type-2 fuzzy logic controllers, incorporating sophisticated inference mechanisms and type-reduction algorithms necessary for uncertainty management.

IV.2.2 Photovoltaic Module Characterization

The photovoltaic energy source modeling employs the commercially available Kyocera Solar KC200GT module, selected for its comprehensive documentation in academic literature and representative performance characteristics typical of crystalline silicon photovoltaic technology. This module demonstrates a rated maximum power output of 200.143 W under standard test conditions, corresponding to 1000 W/m² solar irradiance and 25°C cell temperature, as comprehensively detailed in Table 6.

The mathematical representation of photovoltaic characteristics follows the widely-accepted single-diode equivalent circuit model, incorporating series resistance effects, temperature-dependent parameters, and irradiance scaling factors to accurately capture real-world operational behavior across the complete environmental envelope. The model implementation accounts for both irradiance and temperature variations through appropriate physical scaling relationships that maintain thermodynamic consistency throughout the operational range.

Table 6 Parameters of the PV panel Kyocera Solar KC200GT.

Parameters	**Values**
Maximum power (P_{mpp})	200.143 W
Short-circuit current (I_{sc})	8.21 A
Open-circuit voltage (V_{oc})	32.9 V
Current at MPP (I_{mpp})	7.61 A
Voltage at MPP (V_{mpp})	26.3 V
Temperature coefficient of I<α_{sc}>	–0.401 %/°C
Temperature coefficient of V<β_{oc}>	0.025998 %/°C

IV.2.3 Three-Level Quadratic Boost Converter Specification

The three-level quadratic boost converter architecture represents a sophisticated power processing topology specifically engineered to overcome the fundamental duty cycle limitations inherent in conventional boost converter configurations. The converter structural design incorporates dual boost inductors (L_1, L_2) operating in coordinated fashion with a multilevel

switched-capacitor network comprising capacitors C_0 through C_5. The Component parameter specifications, as detailed in Table 7, result from iterative design optimization that balances converter performance, component stress levels, and practical implementation considerations. The design methodology incorporates appropriate safety margins and accounts for component tolerances to ensure robust operation under real-world conditions.

Table 7 Parameters of the TLQBC.

Parameters	**Values**
Capacitors (C0–C5)	220 μF
Inductors (L1, L2)	1.5 mH
Load resistance	30 Ω

IV.2.4 Performance Evaluation Scenarios

The comprehensive performance assessment framework encompasses three distinct operational scenarios specifically designed to evaluate controller capabilities under diverse environmental conditions that accurately represent the operational challenges encountered in practical photovoltaic installations. Each scenario provides specific insights into different aspects of maximum power point tracking performance, collectively establishing complete characterization of integrated system behaviour.

IV.2.4.1 **Scenario 1: Constant Environmental Conditions**

The constant environmental conditions testing validates steady-state tracking accuracy, stability characteristics, and ripple performance under idealized operational conditions without external environmental disturbances. This baseline scenario employs standard test conditions of 1000 W/m² solar irradiance and 25°C cell temperature, eliminating environmental variability effects to enable precise assessment of fundamental controller precision and stability characteristics.

This scenario enables detailed evaluation of steady-state oscillation magnitude, power extraction efficiency, and convergence characteristics without the complicating effects of environmental variations. The testing duration extends sufficiently to ensure complete system settling and statistical significance of performance measurements.

IV.2.4.2 **Scenario 2: Variable Irradiance Conditions**

Variable irradiance testing introduces systematic step changes in solar irradiance from 1000 W/m² to 900 W/m² and subsequently to 700 W/m², as illustrated in Figure 52, simulating cloud

transient effects that represent among the most challenging operational scenarios for maximum power point tracking systems. This scenario evaluates dynamic response characteristics including convergence velocity, overshoot behaviour, tracking accuracy during environmental transitions, and steady-state performance recovery.

The irradiance variation profile incorporates realistic transition rates and magnitude changes representative of actual meteorological conditions. The step changes are designed to evaluate controller performance across different operating power levels while maintaining clear delineation between steady-state and transient performance characteristics.

IV.2.4.3 **Scenario 3: Variable Temperature Conditions**

Variable temperature testing implements systematic step changes from 25°C to 35°C and subsequently to 45°C while maintaining constant irradiance at 1000 W/m², as depicted in Figure 55, representing thermal cycling effects typical of diurnal temperature variations encountered in practical photovoltaic installations. This scenario assesses controller adaptability to temperature-dependent characteristic variations and thermal sensitivity effects that significantly influence photovoltaic performance.

The temperature variation profile reflects realistic thermal time constants and temperature ranges encountered in field installations. The testing enables evaluation of controller performance across the typical operational temperature range while isolating temperature effects from irradiance variations.

IV.2.5 Quantitative Performance Assessment Methodology

The quantitative performance evaluation employs multiple complementary metrics to provide comprehensive characterization of maximum power point tracking effectiveness. The primary performance metric utilizes tracking efficiency, defined as the ratio between actual power extraction and theoretical maximum power availability:

$$\eta_{MPPT} = \frac{P_{out}}{P_{MPP}} \times 100\% \tag{58}$$

This fundamental metric provides direct quantification of energy harvest effectiveness while facilitating straightforward comparison between different control approaches across diverse operational conditions.

IV.3 Operational Verification of the Proposed Converter

Prior to maximum power point tracking integration, a thorough verification of the three-level quadratic boost converter's fundamental operational characteristics is essential to validate

design predictions and ensure a reliable test platform. This verification encompasses steady-state behavior analysis, dynamic response evaluation, and inherent voltage-balancing validation, collectively establishing the converter's suitability for advanced control strategies.

IV.3.1 Steady-State Behaviour Analysis

A representative test case was selected to evaluate the converter's steady-state performance: a 24 V DC input with a 0.60 duty cycle produces a theoretical output near ~450 V. As shown in Figure 46, simulation results confirm the predicted output voltage within 1 % of the theoretical value. Inductor current waveforms exhibit continuous conduction mode operation across both inductors, with peak-to-peak current ripple maintained below 10 % of nominal current, thereby satisfying design criteria for stable energy transfer.

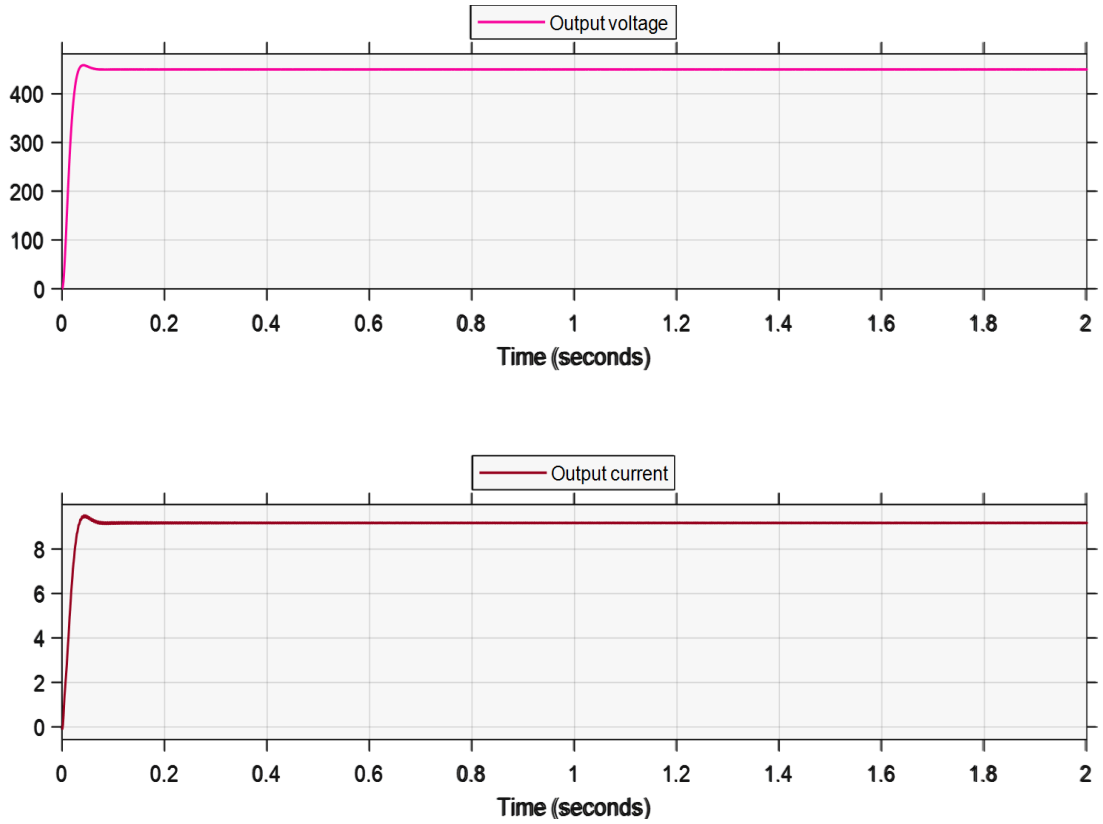

Figure 46 Output voltage and current.

IV.3.2 Dynamic Response Characterization

The converter's transient response evaluation demonstrates exceptional dynamic performance characteristics under controlled test conditions. Figure 46 presents the output voltage and current waveforms under steady-state operation, confirming stable operation at approximately ~450 V output with minimal ripple characteristics. The output voltage exhibits excellent stability

with peak-to-peak ripple maintained below 1% of the nominal value, while the output current demonstrates smooth waveform characteristics without significant distortion.

The switching behavior analysis, illustrated in Figure 47, reveals the switch voltage and output current relationships during normal operation. The switch voltage waveform demonstrates clean transitions between conducting and non-conducting states, with well-defined voltage levels that validate proper switching operation. The output current maintains continuous characteristics throughout the switching cycle, confirming continuous conduction mode operation as intended by the design specifications.

The dual-inductor configuration contributes significantly to the superior dynamic performance by providing enhanced energy storage capabilities and improved current sharing between the two boost stages. This arrangement results in reduced current stress on individual components while maintaining excellent dynamic response characteristics during input perturbations.

The switching transition analysis confirms proper operation between the fundamental switching states without excessive voltage overshoots or current discontinuities. The clean switching transitions validate the design methodology and demonstrate the effectiveness of the component specifications in achieving reliable operation.

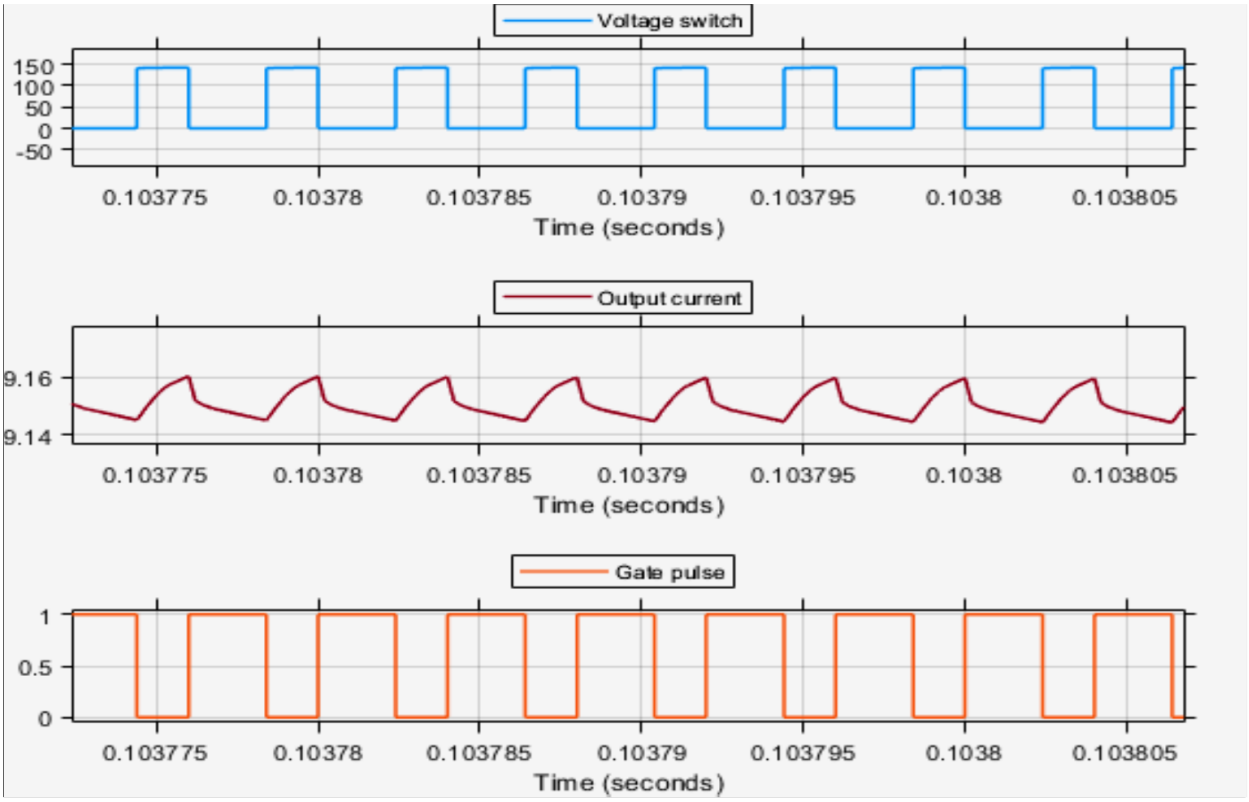

Figure 47 Switch voltage and output current

IV.3.3 Voltage Gain Verification and Stress Distribution

The steady-state operation validation confirms achievement of the theoretical voltage gain relationship, with the converter producing an 18.75:1 voltage transformation ratio under test conditions. Component stress analysis reveals well-distributed voltage and current stresses, with all switching elements operating within 60% of their rated specifications, providing substantial reliability margins.

IV.4 Advanced MPPT Control Strategies for the Proposed Converter

The implementation of sophisticated maximum power point tracking strategies represents the critical interface between environmental energy availability and optimal power extraction efficiency. The investigated control architectures span the spectrum from conventional algorithmic approaches to state-of-the-art artificial intelligence methodologies, each offering distinct advantages and limitations that influence their suitability for specific applications and operational requirements..

In the present study, four MPPT algorithms—representing conventional, intelligent, and hybrid paradigms—were implemented on the proposed Three-Level Quadratic Boost Converter (TLQBC) to ensure a comprehensive evaluation of control performance. However, this subsection focuses specifically on the NARX neural network and the Type-2 fuzzy logic controller, which represent the most advanced AI-based strategies investigated. Their modeling principles, control structures, and performance characteristics are discussed in detail to demonstrate their effectiveness in optimizing PV energy extraction and improving the dynamic response of the TLQBC system.

IV.4.1 NARX Neural Network-Based MPPT

The Nonlinear Autoregressive with Exogenous Inputs (NARX) neural network leverages past photovoltaic measurements to predict the optimal operating voltage for the three-level quadratic boost converter. Its structure, shown in Figure 48, comprises two hidden layers—12 neurons in the first layer and eight in the second—each employing hyperbolic tangent activation functions to capture smooth nonlinearities. The network's input vector at sample k includes:

- PV module voltages $V(k-1), V(k-2), V(k-3)$
- PV module currents $I(k-1), I(k-2), I(k-3)$
- Module temperature $T(k)$

The single output $V_{ref}(k)$ serves as the reference voltage for the converter's duty-cycle controller.

Offline Training:

- Dataset generation via high-fidelity simulations covering 200–1000 W/m² irradiance and 15–50 °C.
- Levenberg–Marquardt backpropagation minimizes mean squared error between predicted and actual MPP voltages.
- Early stopping with k-fold cross-validation prevents overfitting and ensures generalization to unseen conditions.

Online operation:

- At each sampling instant, the NARX outputs $V_{ref}(k)$ based on the latest measurement window.
- A proportional-integral compensator filters the residual error $e(k)= V_{ref}(k)-V(k)$, producing the final duty-cycle adjustment $\Delta D(k)$.
- Predictive capability reduces tracking delay below and minimizes energy loss during rapid irradiance fluctuations.

IV.4.2 Type-2 Fuzzy Logic Controller (FLC-T2)-Based MPPT

Building upon the performance limitations observed in the Type-1 Fuzzy Logic Controller (T1FLC), particularly its sensitivity to measurement noise and parameter uncertainty, this study offers the Type-2 Fuzzy Logic Controller (T2FLC) as an enhanced MPPT method. The T2FLC expands the typical fuzzy framework by introducing a second level of uncertainty into its membership functions, allowing it to better handle imprecise input data and nonlinear PV behaviour. This capacity makes it especially useful under variable irradiance and temperature settings when traditional or Type-1 fuzzy systems may display tracking oscillations or delayed convergence.

The Type-2 Fuzzy Logic Controller (T2FLC) is designed to regulate the duty ratio of the three-level quadratic DC–DC boost converter (TLQ-DC–DC-BC), ensuring that the photovoltaic (PV) system continuously works at its maximum power point (MPP). Structurally, the T2FLC bears many similarities with the Type-1 Fuzzy Logic Controller (T1FLC), with the key distinction resting in the output processing stage. Specifically, the T2FLC contains an additional type-

reduction process, which turns Type-2 fuzzy sets into Type-1 sets prior to the final defuzzification stage. This enables the controller to appropriately handle the uncertainties and nonlinearities inherent in solar energy conversion systems.

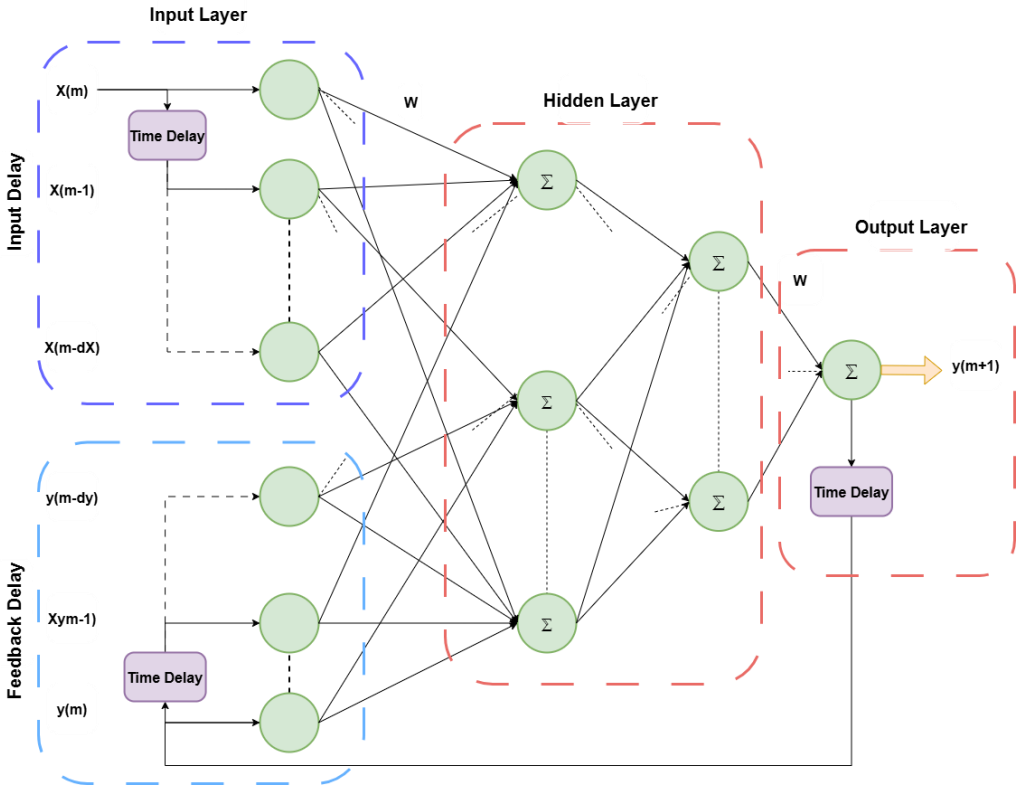

Figure 48 Structure of the NARX neural network

Fuzzifier, Fuzzy rule base, Inference engine, Type-reducer, and Defuzzifier are the five functional blocks that make up the T2FLC system's overall architecture, which is depicted in Figure 49.

The inputs of the fuzzifier are the change in power (ΔP) and the change in voltage (ΔV), indicating the dynamic fluctuations of the PV array under variable environmental conditions. As illustrated in Figure 50(a), both input variables are defined by seven membership functions (MFs) that span the whole universe of speech. Similarly, the output variable, corresponding to the duty-cycle adjustment (ΔD), likewise employs seven MFs, as indicated in Figure 50(b). The fuzzified inputs are next processed by the inference engine, which evaluates the rule-base matrix provided in Table 8. Each rule is triggered according to the degree of membership of the input variables, and the resulting aggregated fuzzy sets are subsequently sent to the type-reducer.

The type-reduction stage reflects the most distinctive aspect of the Type-2 fuzzy method. It compresses the Footprint of Uncertainty (FOU) associated with the Type-2 fuzzy sets into an

equivalent Type-1 set that can then be handled by the defuzzification process. Several algorithms have been developed for this purpose, including the Karnik–Mendel (KM) iterative method, Sugeno's Weighted Average (SWA), Centre of Sets (COS), and Modified Centre of Sums (MCOS) techniques. In this study, a cluster-centre-based type-reduction strategy is utilised, offering a good compromise between computational efficiency and output smoothness.

The type-reduction process can be mathematically expressed as follows [77]:

$$Y_{cos}(e) = [y_l, y_i] = \int_{y^1 \in [y_l^1, y_r^1]} .. \int_{y^M \in [y_l^M, y_r^M]} \int_{f^M \in \left[\underline{f}^1, \overline{f}^1\right]} .. \int_{f^M \in \left[\underline{f}^1, \overline{f}^1\right]} 1 \Big/ \frac{\sum_{i=1}^{M} y^i f^i}{\sum_{i=1}^{M} f^i} \qquad (59)$$

Where y_l and y_r are the leftmost and rightmost edges of the type-reduced interval, respectively. $Y_{cos}(e)$ represents the interval set of output values that y_l and y_r decide, and i=1,2,…,M is the total number of fuzzy rules. The Karnik–Mendel (KM) algorithm offers an iterative method for the efficient computation of y_l and y_r. The type-reduction operation produces a type-reduced set, called $Y_{cos}(e)$, which is then defuzzified to give a clear control output.

Since $Y_{cos}(e)$ is an interval type-reduced set, the defuzzification is done by averaging its border points. This gives the Type-2 fuzzy controller a clear output of:

$$\Delta D = \frac{y_l + y_r}{2} \qquad (60)$$

The final output ΔD determines the corresponding duty-cycle adjustment applied to the TLQBC, leading the operating point of the PV system toward the MPP. Through this structure, the suggested T2FLC offers improved tracking accuracy, smoother control behaviour, and enhanced robustness compared with the T1FLC, especially under fast-changing ambient and noisy measurement conditions.

The T2FLC demonstrates significant flexibility to parameter and measurement errors, giving a more dependable MPPT performance under dynamic settings. The next subsection gives a comparative analysis of all implemented MPPT algorithms, highlighting the quantitative gains gained by the T2FLC and the NARX-NN controllers relative to the conventional techniques.

IV.5 Performance Evaluation Under Diverse Operating Conditions

The effectiveness of the four MPPT controllers was evaluated under the three operating scenarios defined in Section 4.2. Key performance metrics included tracking speed (time to reach the MPP following a change), steady-state accuracy (voltage/current ripple and deviation from MPP), and tracking efficiency (ratio of extracted power to theoretical MPP power). Representative

simulation results for PV power, voltage, current, and efficiency are presented to illustrate controller performance in each case.

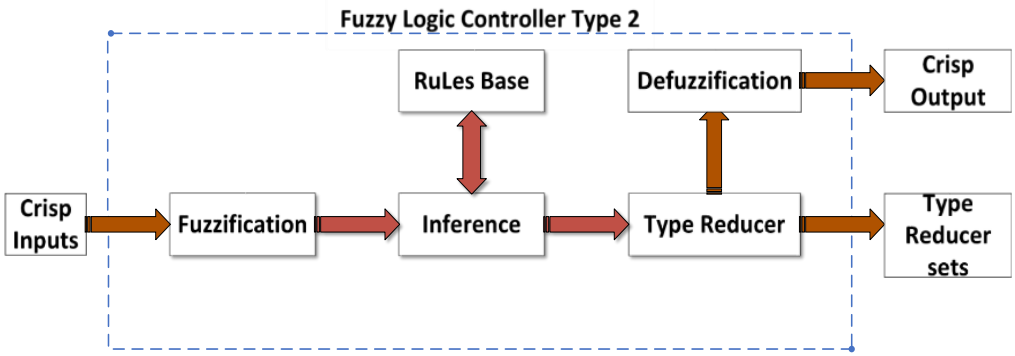

Figure 49 Overall architecture of T2FLC system.

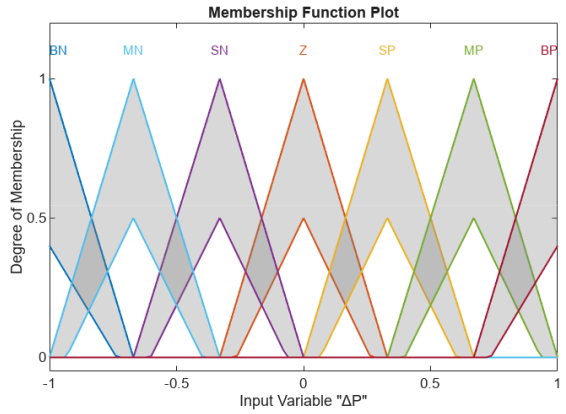

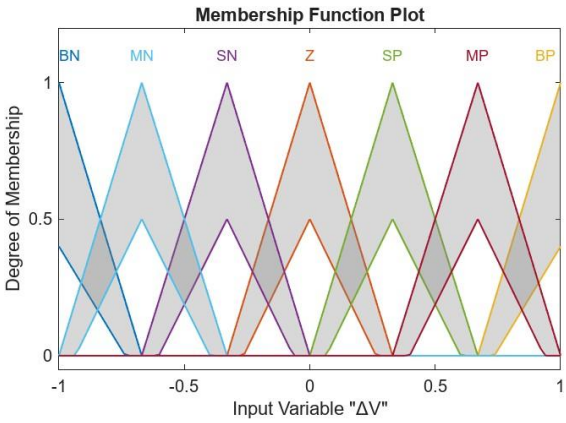

(a)

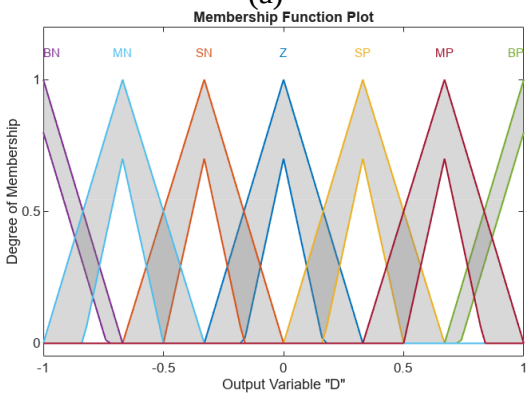

(b)

Figure 50 Type-2 fuzzy logic membership functions for: (a) input variables (ΔP and ΔV); (b) output variable.

Table 8 Fuzzy logic rules.

Rules		***ΔP***						
		BN	MN	SN	Z	SP	MP	BP
	BN	BP	BP	MP	Z	MN	BN	BN
	SN	MP	SP	SP	Z	SN	SN	MN
	BP	BN	BN	MN	Z	MP	BP	BP
	Z	BN	MN	SN	Z	SP	MP	BP
	MN	BP	MP	SP	Z	SN	MN	BN
	MP	BN	MN	SN	Z	SP	MP	BP
	SP	MN	SN	SN	Z	SP	SP	MP

IV.5.1 Constant Irradiance and Temperature

The first test considered fixed conditions of 1000 W/m² irradiance and 25 °C temperature. Figure 51(a) shows the PV output power obtained using the four MPPT strategies. At steady state, the NARX-NN, T1-FLC, and T2-FLC controllers achieved stable power output, while the IC algorithm exhibited pronounced oscillations. The NARX-NN method demonstrated the fastest convergence to the MPP, minimal oscillation, and the highest dynamic efficiency. In contrast, the T1-FLC required a longer settling time but effectively suppressed steady-state oscillations, outperforming the IC controller in stability.

Figure 51(b) illustrates the PV output voltage. The NARX-NN exhibited the most responsive and stable voltage behavior, owing to its predictive capacity and adaptive regulation. Conversely, the IC method produced significant voltage ripples, underscoring its limited capability in maintaining a stable operating point.

Figure 51(c) shows the PV current under the same conditions. All intelligent controllers (NARX-NN, T1-FLC, T2-FLC) delivered nearly identical steady-state current values, with the T1-FLC achieving the highest average current. The IC controller, however, introduced visible current ripples, reflecting its weaker control performance.

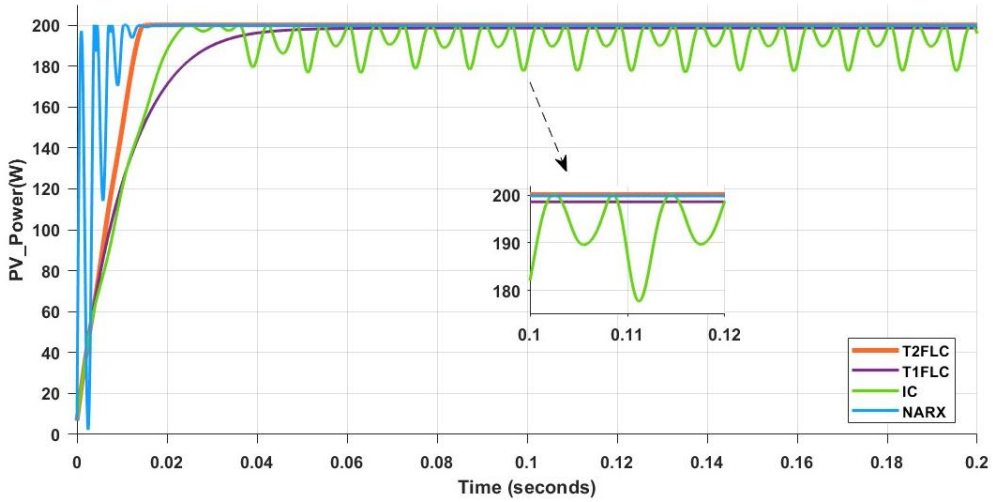

(a)

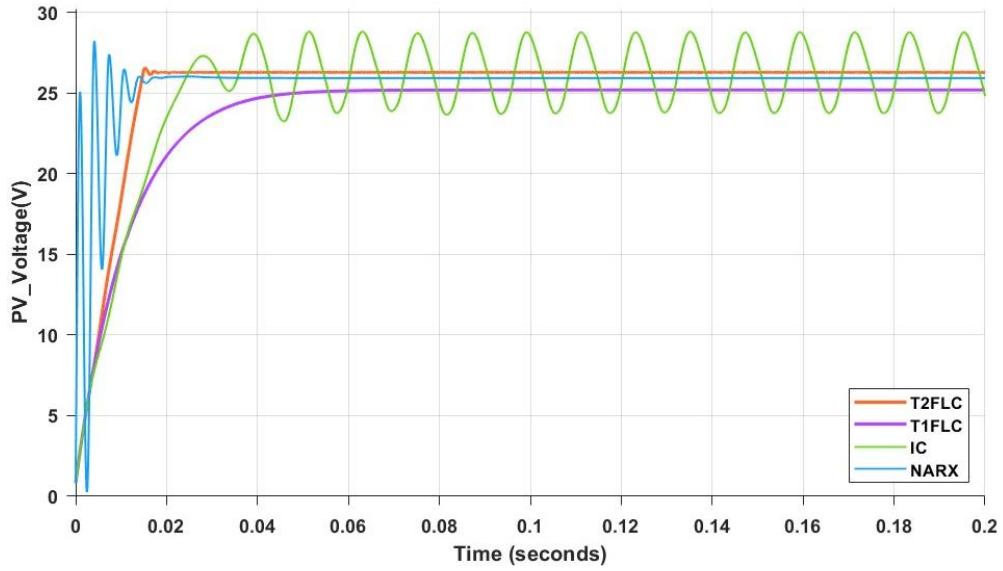

(b)

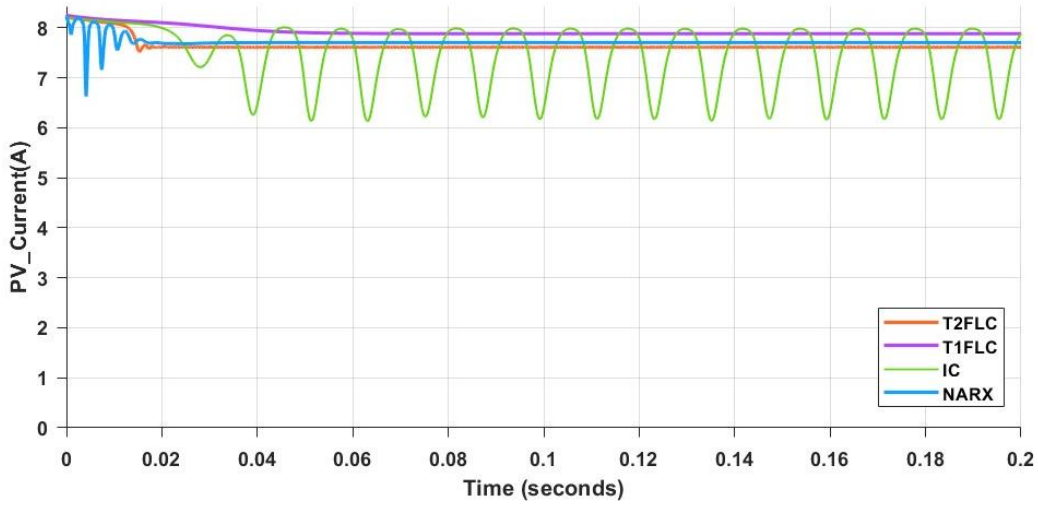

(c)

Figure 51 PV output constant irradiance and T: (a) PV energy output, (b) PV voltage output, and (c) PV current output.

IV.5.2 Variable Irradiance (Constant Temperature)

The second test introduced step changes in irradiance from 1000 → 900 → 700 W/m², with constant temperature at 25 °C (profile shown in Figure 52). Figure 53(a) compares the PV power responses. All controllers followed the irradiance profile, but the IC algorithm displayed delayed response and significant power ripple. The NARX-NN achieved the fastest dynamic tracking with minimal power loss during each transition. The T2-FLC also performed well, slightly outperforming the others in steady-state accuracy, while the T1-FLC response lagged slightly behind NARX-NN and T2-FLC.

Figure 53(b) presents the PV voltage. The NARX-NN controller quickly adjusted to each irradiance step, maintaining close alignment with the new MPP voltage. The T2-FLC and T1-FLC tracked the MPP with modest delays, while the IC method showed large oscillations and slower settling.

Figure 53(c) illustrates PV current. The NARX-NN again exhibited the most stable and rapid current regulation. The IC controller introduced pronounced current ripples, whereas the T1-FLC and T2-FLC achieved smoother tracking with only minor overshoot or undershoot.

The tracking efficiency curves in Figure 54 confirm these observations. The T2-FLC achieved the highest overall accuracy, maintaining ~99.9% efficiency in steady state and ~99.5% during transients. The NARX-NN achieved nearly equivalent results, with peak efficiency of ~99.8% and a brief dip to ~96.3% at the lowest irradiance. The T1-FLC delivered moderate performance (~97.8% average efficiency), while the IC algorithm lagged behind at ~95.6%. Overall, the T2-FLC proved most robust in accuracy, while the NARX-NN offered superior transient response.

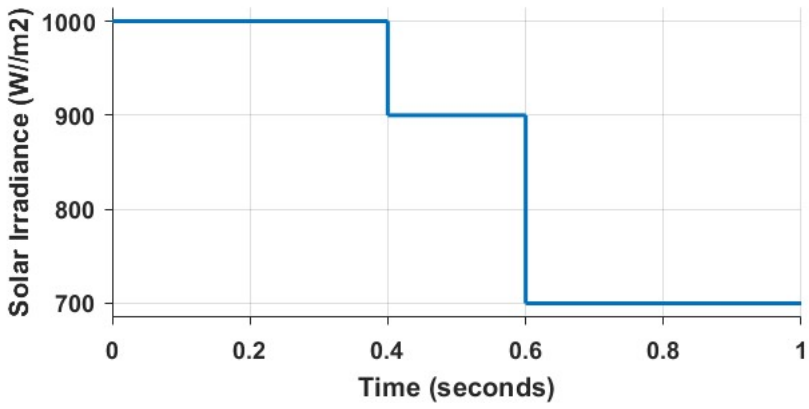

Figure 52 Changing PV irradiance.

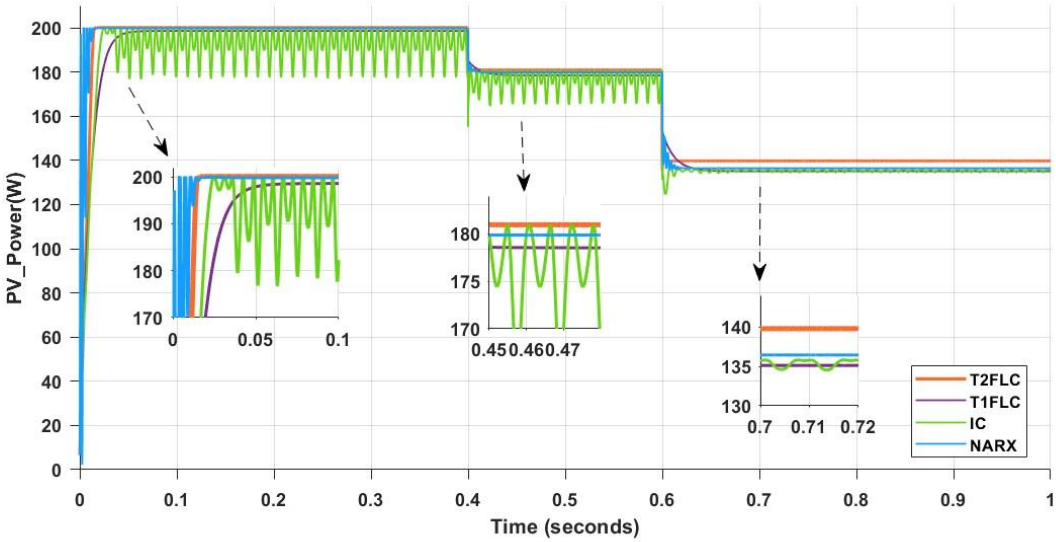

(a)

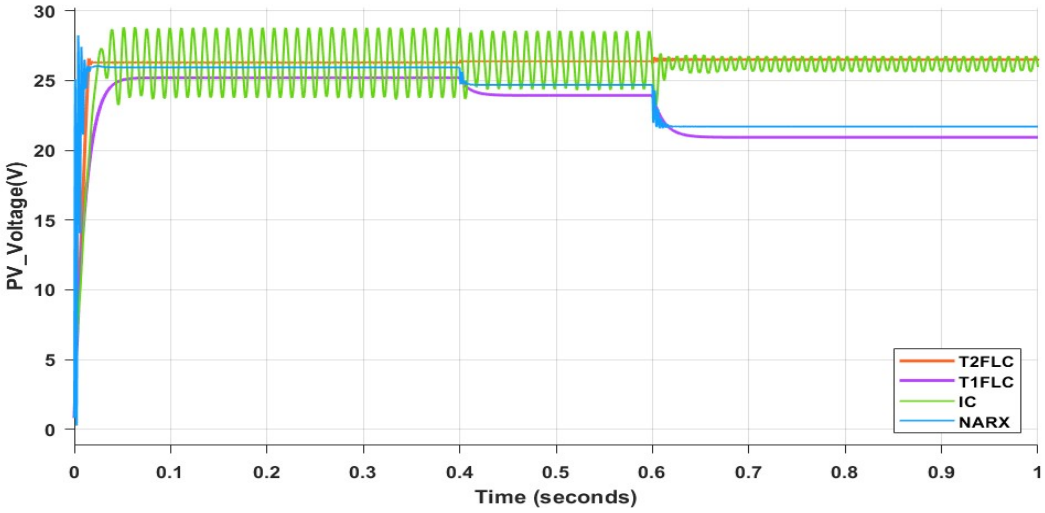

(b)

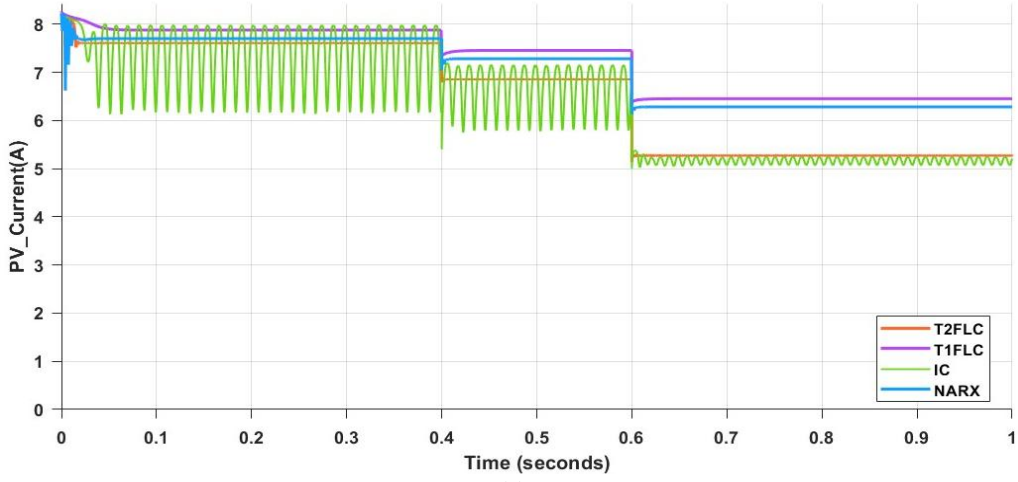

(c)

Figure 53 PV output under fluctuating irradiance conditions: (a) PV energy output, (b) PV voltage output, and (c) PVcurrent output.

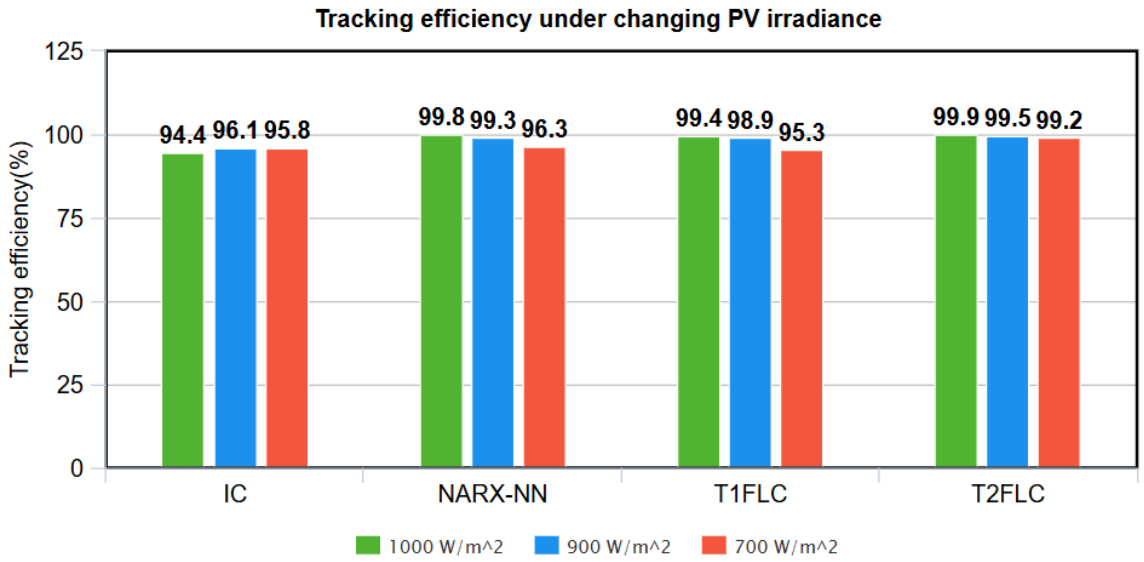

Figure 54 Tracking efficiency under changing PV irradiance.

IV.5.3 Variable Temperature (Constant Irradiance)

As shown in Figure 55, the third test considered step changes in temperature from 25 °C to 35 °C and then to 45 °C, with irradiance fixed at 1000 W/m². Figure 56(a) shows the PV output power for each controller. As expected, power decreased with rising temperature. The NARX-NN achieved the fastest response to each transition, rapidly converging to the new MPP with minimal overshoot. The T2-FLC consistently produced slightly higher output during 0.6–1.0 s, whereas the IC method suffered from slow adaptation and significant fluctuations.

Figure 56(b) depicts the PV voltage. With temperature increases, the operating voltage dropped across all controllers. The NARX-NN maintained the most stable voltage trajectory, while the IC algorithm exhibited considerable ripple.

Figure 56(c) presents the PV current response. Again, the NARX-NN produced the smoothest and most rapid adaptation. The IC controller's current fluctuated markedly during each temperature change. Both the T1-FLC and NARX-NN maintained higher average current compared to the IC and T2-FLC.

Tracking efficiency results are summarized in Figure 57. The T2-FLC achieved ~99.7% average efficiency, the highest among the fuzzy methods. The NARX-NN reached ~99.8% at 25 °C, ~99.3% at 35 °C, and ~96.4% at 45 °C, demonstrating robust adaptability across the temperature range. In contrast, the T1-FLC achieved ~97.8% average efficiency, while the IC method delivered only ~93.4%, confirming its limited suitability for temperature-varying conditions.

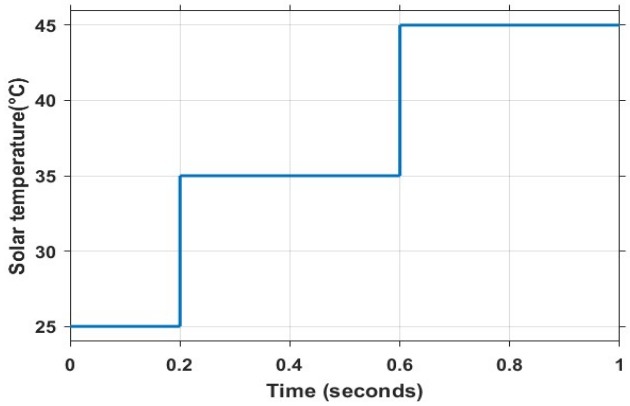

Figure 55 Changing PV temperature.

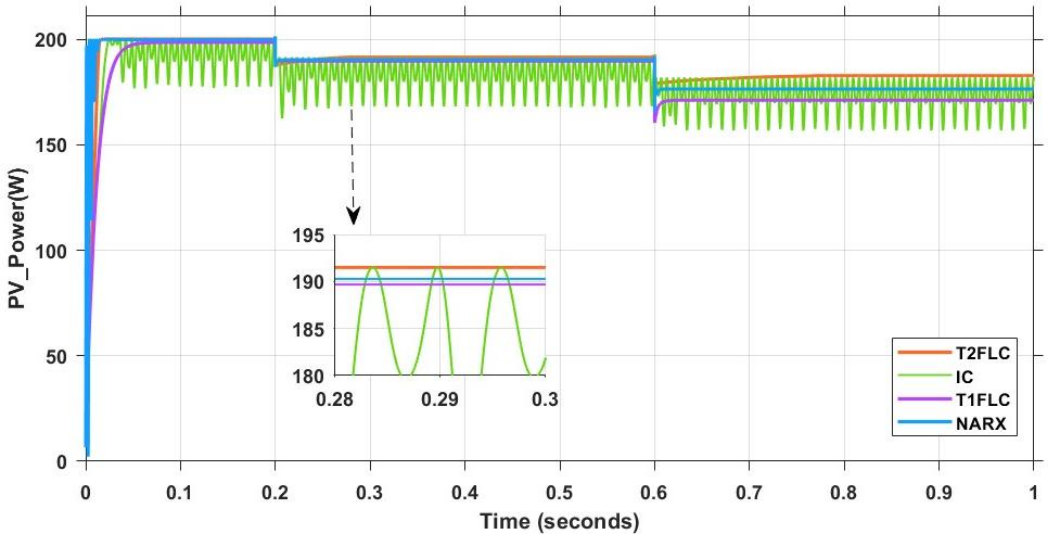

(a)

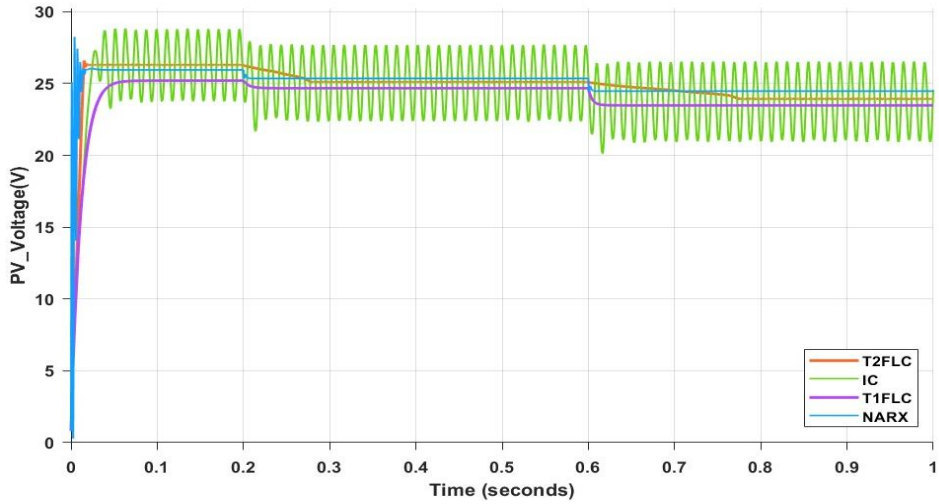

(b)

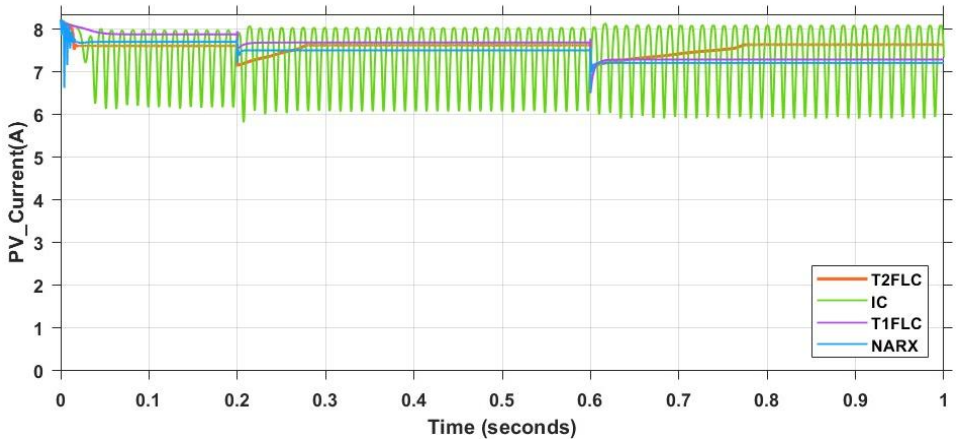

(c)

Figure 56 PV output under varying temperature conditions: (a) PV energy output, (b) PV voltage output, and (c) PV current output.

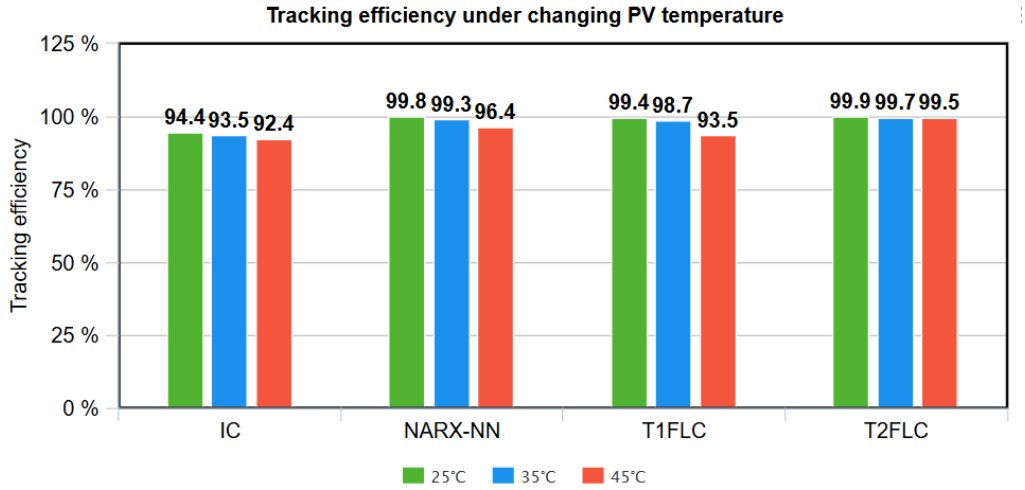

Figure 57 Tracking efficiency under changing PV temperature.

IV.6 Comparative Evaluation of MPPT Controllers

The comparative analysis of the four MPPT algorithms highlights clear distinctions in efficiency, dynamic response, stability, and computational requirements.

Tracking efficiency. The interval type-2 fuzzy controller (T2-FLC) achieved the highest average tracking efficiency (~99.5%), closely followed by the NARX-NN (~98.2%). The type-1 fuzzy logic controller (T1-FLC) delivered intermediate performance (~97.1%), while the incremental conductance (IC) algorithm had the lowest efficiency (~94.4%).

Tracking speed. In terms of rise and settling times, the NARX-NN exhibited the most rapid response, with a rise time of only 0.63 ms compared to 17.65 ms for IC and 23.71 ms for T1-FLC. Its settling time (≈0.014 s) was also the shortest. The T2-FLC offered moderate dynamic speed

(rise ≈11.47 ms; settling ≈0.015 s), faster than IC and T1-FLC but still slower than NARX-NN. The IC algorithm was the slowest and most oscillatory, confirming that simplicity comes at the cost of responsiveness.

Ripple and stability. Under both steady-state and transient conditions, the intelligent controllers (NARX-NN, T1-FLC, T2-FLC) effectively suppressed oscillations, while the IC method exhibited pronounced power and voltage ripples. The smallest steady-state error (deviation from the exact MPP) was observed with the NARX-NN and T2-FLC approaches, reflecting their superior accuracy.

Computational complexity. The T2-FLC requires type-reduction and the handling of interval fuzzy sets, making it computationally "high-complexity." The NARX-NN demands offline training, but once deployed, its online operation involves only lightweight neural computations; thus, its runtime complexity is comparable to IC ("low-complexity"). The T1-FLC falls in between ("medium-complexity"), as it avoids type-reduction but still requires fuzzification and inference operations.

Overall, the NARX-NN demonstrated the best dynamic performance with fast rise and settling times, coupled with high efficiency. The T2-FLC delivered the highest steady-state accuracy but at the expense of increased computational burden and slightly slower response. The T1-FLC provided a balanced compromise between simplicity, smoothness, and accuracy, while the IC algorithm proved least effective, serving primarily as a baseline reference.

Table 9 Performance metrics of MPPT controllers. Tracking efficiency is average over all tests; rise/settling times are typical values after a step change

Controller	**Tracking Efficiency (%)**	**Rise Time (ms)**	**Settling Time (s)**	**Remarks**
IC	94.4	17.65	0.028	Largest steady-state ripple, slow response.
NARX-NN	98.2	0.63	0.014	Fastest response, high efficiency.
T1FLC	97.1	23.71	0.042	Moderate accuracy, smoother output than IC.
T2FLC	99.5	11.47	0.015	Highest accuracy, highest complexity.

IV.7 Integrated System Performance Analysis

The integration of the photovoltaic array with the TLQ boost converter demonstrates the synergistic interaction between the high-gain, multilevel converter topology and the advanced MPPT controllers. In steady-state conditions, under constant irradiance and temperature, the converter delivers a stable boosted DC output with minimal ripple across all controllers. Once the MPPT algorithm locks onto the maximum power point (MPP), the output voltage and current remain well regulated. For example, in Test (i), both the NARX-NN and fuzzy controllers maintained nearly ripple-free operation, whereas the IC algorithm introduced more noticeable fluctuations.

During transient scenarios involving abrupt irradiance or temperature variations, the system adapts rapidly to the new operating point. The TLQ topology, with its dual inductors and switched-capacitor network, ensures efficient energy transfer, enabling the controller commands to propagate swiftly to the output. Simulation results confirm that the DC link voltage remained stable throughout dynamic tests, preventing undervoltage events. The high inherent gain of the converter ensured continuous regulation, even when the input power decreased significantly. Notably, the NARX-NN and T2-FLC controllers consistently achieved energy extraction efficiencies above 95%, indicating that nearly all available PV energy was successfully delivered to the load.

Furthermore, the intelligent controllers significantly reduced voltage ripples and overshoot compared to the IC algorithm. As illustrated in Figure 51 and summarized in Table 9, the peak-to-peak output voltage ripple under NARX-NN and T1-FLC control remained below 2% of the nominal output, whereas the IC method exhibited ripples of 5–10%. This reduction is particularly advantageous for downstream inverters and DC bus applications, where stable voltage is essential. In addition, the converter maintained its theoretical gain ratio (≈3×) across all operating conditions, validating both the robustness of the topology and the accuracy of the derived state-space model.

Overall, the integration of the TLQ boost converter with advanced MPPT strategies enables a photovoltaic system that combines high voltage gain, low ripple, and superior tracking performance. The converter's natural capacitor self-balancing minimizes control complexity, allowing the MPPT algorithms to focus entirely on maximizing PV power extraction. Simulation findings demonstrate that this architecture delivers enhanced efficiency, fast dynamic response, and reliable stability without introducing practical drawbacks, thereby making it an effective solution for high-performance PV energy conversion.

IV.8 Critical Discussion of Results

The comparative evaluation of the four MPPT controllers highlights distinct trade-offs between computational complexity, transient performance, and steady-state accuracy.

The NARX-NN controller consistently demonstrated the fastest dynamic response and strong overall efficiency. Its data-driven recurrent structure enabled predictive adaptation to environmental changes, with a rise time of approximately 0.63 ms, which is several orders of magnitude faster than that of the IC or T1FL methods. This capability translates into near-instantaneous MPP tracking during rapid irradiance fluctuations, thereby minimizing power loss. The NARX-NN achieved an average tracking efficiency of 98.2% (Table 9). Importantly, its implementation in real time is computationally light once training is complete, requiring only a small number of forward neural operations per cycle. However, its performance depends heavily on the quality of offline training data, and retraining may be necessary if PV characteristics drift over time due to aging or partial shading effects.

The Type-2 fuzzy logic controller (T2FL) achieved the highest steady-state accuracy, with an average efficiency of 99.5%, and proved especially robust under conditions of parameter uncertainty. The additional degrees of freedom provided by interval type-2 fuzzy sets reduced residual tracking errors, enhancing stability in noisy or uncertain environments. Nonetheless, this benefit comes at the cost of increased computational overhead, as the type-reduction process adds significant complexity. Its rise time of approximately 11.5 ms is moderate, making it less suitable for highly dynamic scenarios. T2FL is therefore most appropriate in applications where precision and robustness outweigh fast transient response, and where higher-end digital controllers can be used to accommodate its computational requirements.

The Type-1 fuzzy logic controller (T1FL) represents a balance between simplicity and adaptability. Without type-reduction, its computational load is considerably lower than that of T2FL, while still providing better nonlinear handling than IC. It produced smoother outputs with fewer oscillations, though at the expense of slower convergence compared to NARX-NN. Its tracking efficiency was measured at ≈97%, positioning it as a practical compromise in systems where moderate complexity and reliability are acceptable but extreme precision or ultrafast response is not required.

The incremental conductance (IC) method, while conceptually straightforward and computationally inexpensive, proved the least effective overall. With an efficiency of only 94–95% and the slowest transient behavior, it exhibited significant oscillation around the MPP due to

its fixed-step perturbation mechanism. These oscillations were further amplified by the high-gain TLQ converter, where small duty-cycle variations produce disproportionately large output voltage swings. IC thus remains best suited for low-cost, resource-limited applications where implementation simplicity is the overriding priority.

These findings align with trends reported in the literature: neural-network-based approaches outperform classical algorithms in dynamic conditions, while fuzzy logic controllers improve steady-state performance and robustness. The magnitude of improvement is notable—NARX-NN reduced rise time by approximately 96–97% relative to IC and T1FL.

A key limitation of this work is that all evaluations were conducted in simulation environments. Real-world systems inevitably introduce additional challenges such as sensor noise, component parasitics, and partial shading, which may influence controller behavior. For instance, T2FL may prove even more advantageous in noisy settings, while NARX-NN may require adaptive retraining or online learning strategies. Future work should therefore extend this analysis to hardware implementation, where practical efficiency, computational latency, and converter non-idealities can be fully assessed.

IV.9 Conclusion

This chapter presented a detailed investigation of advanced maximum power point tracking (MPPT) strategies applied to a three-level quadratic boost converter (TLQBC) for photovoltaic (PV) systems. The TLQBC was modeled and validated, confirming its ability to achieve high voltage gain with inherently balanced capacitors and reduced ripple, making it a robust platform for high-performance PV applications.

Four MPPT controllers—Incremental Conductance (IC), Type-1 fuzzy logic (T1FL), Interval Type-2 fuzzy logic (T2FL), and NARX neural network (NARX-NN)—were designed, implemented, and compared under constant and dynamic operating conditions. The results revealed that conventional IC control, while simple, suffers from oscillations, low tracking accuracy, and poor dynamic performance. The fuzzy-based controllers improved stability and reduced ripples, with T2FL achieving the highest steady-state accuracy (~99.5%). The NARX-NN controller delivered the fastest dynamic response, achieving rapid convergence with minimal overshoot, making it particularly effective under fast irradiance and temperature variations.

Overall, the study demonstrates that integrating intelligent MPPT methods with the TLQBC significantly enhances PV system efficiency, stability, and adaptability. The findings suggest that NARX-NN is best suited for highly dynamic environments, while T2FL provides superior

precision under steady or uncertain conditions. T1FL represents a balanced compromise between simplicity and robustness, whereas IC remains a baseline reference.

These insights provide a strong basis for further research into real-time hardware implementation and hybrid intelligent MPPT approaches, aimed at maximizing PV energy extraction under real-world conditions.

General Conclusion

General Conclusion

This thesis has systematically addressed the challenge of maximizing photovoltaic energy yield through co-design of high-gain converters and advanced MPPT control. In Chapter I, a comprehensive review of high-gain DC–DC converter topologies was conducted, classifying existing designs by their power flow configuration, use of magnetic or capacitive energy transfer, isolation, and switching strategies. Key topologies (coupled inductors, cascaded boosts, switched-capacitor networks, etc.) were analysed with respect to their voltage gain, efficiency, and dynamic behaviour under PV loading. This survey identified the most promising converter principles for PV, and established design criteria for converters that must support intelligent MPPT and handle rapid load changes.

Chapter II examined state-of-the-art optimization and control techniques for PV systems. Various MPPT algorithms were reviewed, including classical methods (P&O, Incremental Conductance), bio-inspired metaheuristics (Particle Swarm Optimization, Grey Wolf, etc.), and artificial intelligence approaches (fuzzy logic, neural networks). Their advantages and limitations under partial shading and fast irradiance fluctuations were discussed. In particular, the chapter highlighted that AI-based controllers (e.g. fuzzy and neural networks) can achieve higher tracking precision and faster convergence, albeit at the cost of increased complexity and tuning requirements. This set the stage for adopting an intelligent, learning-based controller in the present work.

In Chapter III, detailed modelling and design of high-gain converter architectures were undertaken. First, standard boost and quadratic boost converters were modelled and their voltage conversion ratios derived. Then, a new converter topology – the TLQBC – was proposed. The TLQBC combines a quadratic boost stage with a three-level switched-capacitor cell, resulting in an exceptionally high voltage gain and inherent capacitor voltage balancing. State-space equations were developed and the converter was designed for a target PV application. Performance comparison simulations demonstrated that the TLQBC achieves significantly higher gain with lower capacitor stress than conventional boosts at the same duty ratio. In summary, Chapter III established the TLQBC as a robust high-gain DC–DC stage, validating its efficacy through modeling and preliminary tests.

Chapter IV focused on the control of the TLQBC based PV system using advanced MPPT strategies. First, the operation of the TLQBC was verified under constant conditions, confirming its theoretical gain and balanced operation. Next, four MPPT controllers were implemented and compared: the traditional Incremental Conductance (IC) algorithm, a standard

Mamdani-type fuzzy logic controller (T1FL), an interval type-2 fuzzy logic controller (T2FL), and the novel NARX neural-network controller. These controllers were tested in simulation under various scenarios (steady irradiance, step changes in irradiance or temperature, and realistic time-varying profiles). The results showed that the simple IC controller achieved only moderate accuracy with large oscillations, while the fuzzy controllers greatly reduced steady-state ripples. Notably, the T2FL controller achieved the highest steady-state power accuracy (~99.5%). The proposed NARX-NN controller delivered the fastest dynamic response and smoothest convergence to the MPP, with minimal overshoot. For example, compared to IC and T1FL, the NARX algorithm reduced rise-time by over 94% and improved average tracking efficiency by several percent. In aggregate, the TLQ converter together with intelligent MPPT realized a more efficient and stable PV system: the integration of these advanced methods significantly enhanced energy capture across all test conditions.

The achievements of this work are twofold. First, the thesis introduced and validated a novel converter architecture (TLQBC) that provides very high voltage gain with balanced operation, thus overcoming key limitations of conventional boost converters. Second, it demonstrated that a NARX-based MPPT controller can dramatically improve MPPT performance for high-gain PV systems. The NARX controller's data-driven, recurrent structure allows it to predict the optimal operating point based on past PV behavior. Simulation results indicated that the NARX-MPPT achieved near-optimal tracking efficiency (~99.8% peak) with greatly reduced dynamic losses. In contrast, the traditional controllers lagged in either speed or accuracy. These findings underscore the potential of combining high-gain hardware and intelligent control: the proposed approach yielded high energy extraction and robust operation, moving solar PV systems closer to their theoretical performance limits. Overall, this research contributes to more efficient and reliable PV systems, directly supporting the broader goal of expanding clean solar power. By improving the conversion efficiency of PV arrays and enabling faster, more accurate tracking, the methods developed here help increase the usable energy from each panel, reduce losses, and enhance system stability. In the context of global energy transition, such improvements play a valuable role in boosting renewable generation (cf. the decarbonization benefits of widespread PV deployment).

The present work has limitations that suggest avenues for future research. All results were obtained in simulation; practical implementation will require hardware prototyping and experimental validation. Future work should focus on building a physical TLQ-boost converter prototype and implementing the NARX-MPPT algorithm on real-time hardware (e.g. DSP or

FPGA) to assess its performance under real PV conditions. Factors such as non-ideal losses, component tolerances, and digital control latency must be evaluated in practice. Additionally, while the NARX network was trained offline in this study, online or adaptive training strategies could enhance robustness to changing conditions. Combining the NARX approach with other optimization techniques (e.g. hybrid reinforcement learning or heuristic tuning of its parameters) could further improve resilience against disturbances. Field tests on grid-connected systems and integration with storage or battery charging scenarios would also be important to validate the system in a complete energy context. Finally, exploring other machine learning strategies or multi-objective optimizations (for example, minimizing component stress or maximizing lifespan) may yield further gains. By addressing these topics—hardware realization, real-time control, grid validation, and advanced ML integration—the future work will extend the impact of this research and bring the proposed solutions closer to practical deployment.

Bibliography

[1]: International Energy Agency – Photovoltaic Power Systems Programme (IEA-PVPS), Trends in Photovoltaic Applications 2024, IEA-PVPS Task 1 Report, Oct. 2024.

[2]: Machín, Abniel, and Francisco Márquez. "Advancements in photovoltaic cell materials: silicon, organic, and perovskite solar cells." Materials 17.5 (2024): 1165.

[3]: Souheyb Mohammed Belhadj et al., “Control of three-level quadratic DC-DC boost converters for energy systems using various technique-based MPPT methods,” Scientific Reports, vol. 15, p. 14631, 2025.

[4]: Luis E. Zubieta, “A high efficiency unidirectional DC/DC converter for integrating distributed resources into DC microgrids,” in IEEE ICDC, 2015.

[5]: S. Bhaskar et al., “Survey of DC-DC non-isolated topologies for unidirectional power flow in fuel cell vehicles,” IEEE Access, vol. 8, pp. 178130–178166, 2020.

[6]: Furqan A. Abbas et al., “A Comprehensive Review and Analytical Comparison of Non-Isolated DC-DC Converters for Fuel Cell Applications,” Energies, vol. 16, no. 8, p. 3493, 2023.

[7]: Preeti Sharma, “Advancing renewable energy: A quadratic high-efficiency high gain step-up DC/DC converter,” e-Prime, vol. 10, p. 100847, 2024.

[8]: Amir Ghorbani Esfahlan, “Non-isolated common-grounded high step-up DC-DC converter with continuous source current suitable for low power applications,” Scientific Reports, vol. 15, p. 5062, 2025.

[9]: Hasanpour, “A novel soft-switching quadratic high voltage gain trans-inverse DC/DC converter,” IET Pow. Electron., vol. 17, no. 16, pp. 2714–2729, 2024.

[10]: Chen, Shin-Ju, et al. "Interleaved High Voltage Gain DC-DC Converter with Winding-Cross-Coupled Inductors and Voltage Multiplier Cells for Photovoltaic Systems." Electronics 13.10 (2024): 1851.

[11]: Tong, Yan, et al. "Bidirectional DC-DC Converter Topologies for Hybrid Energy Storage Systems in Electric Vehicles: A Comprehensive Review." Energies 18.9 (2025): 2312.

[12]: Khaligh, Alireza, and Zhihao Li. "Battery, ultracapacitor, fuel cell, and hybrid energy storage systems for electric, hybrid electric, fuel cell, and plug-in hybrid electric vehicles: State of the art." IEEE transactions on Vehicular Technology 59.6 (2010): 2806-2814.

[13]: Esteban, Francisco D., et al. "Nonlinear control for a DC–DC converter with dual active bridges in a DC microgrid." International Journal of Electrical Power & Energy Systems 146 (2023): 108731.

[14]: Tuluhong, Ayiguzhali, et al. "Recent Developments in Bidirectional DC-DC Converter Topologies, Control Strategies, and Applications in Photovoltaic Power Generation Systems: A Comparative Review and Analysis." Electronics 14.2 (2025): 389.

[15]: Hu, Weihao, et al. "Application of artificial intelligence in dual-active-bridge (DAB) converters." 2024. 83-126.

[16]: Iqbal, Mohammad Tauquir, et al. "Explicit discrete modelling of bidirectional dual active bridge DC–DC converter using multi-time scale mixed system model." IET Power Electronics 13.18 (2020): 4252-4260.

[17]: Coelho, Sergio, Vitor Monteiro, and Joao L. Afonso. "Topological advances in isolated DC–DC converters: High-efficiency design for renewable energy integration." Sustainability 17.6 (2025): 2336.

[18]: Sugali, Harinaik, and Shelas Sathyan. "Design and analysis of isolated high step-up Y-source DC/DC resonant converter for photovoltaic applications." Energy Sources, Part A: Recovery, Utilization, and Environmental Effects 45.1 (2023): 1604-1623.

[19]: Mahafzah, Khaled A., et al. "A novel synchronized multiple output DC-DC converter based on hybrid flyback-cuk topologies." Batteries 8.8 (2022): 93.

[20]: Rodríguez, Juan, et al. "High step-down isolated PWM DC–DC converter based on combining a forward converter with the series-capacitor structure." IEEE Access 11 (2023): 131045-131063.

[21]: Azeem, Syed Waqar, et al. "A ZVZCS Full-Bridge Converter Suitable for Renewable Energy-Based MVDC Collection System." IEEE Access 12 (2024): 32434-32444.

[22]: Pastor, Marek, et al. "Soft-switching full-bridge DC-DC converter with energy recovery capacitor snubber." Energies 16.4 (2023): 1591.

[23]: Mohammadi Jouzdani, Marzieh, Mahdi Shaneh, and Tohid Nouri. "Design of an Interleaved High Step-Up DC-DC Converter with Multiple Magnetic Devices for Renewable Energy Systems Applications." International Transactions on Electrical Energy Systems 2022.1 (2022): 2645938.

[24]: Shaabani, Maryam, et al. "A hybrid switched-inductor/switched-capacitor DC-DC converter with high voltage gain using a single switch for photovoltaic application." Energies 16.14 (2023): 5524.

[25]: J. Han, T. Liu, F. Wang, "A Hybrid Coupled-Inductor and Switched-Capacitor DC-DC Converter for Wide Voltage Gain in Renewable Systems," IEEE Access, vol. 12, pp. 44321–44332, 2024.

[26]: Hinov, Nikolay, and Tsvetana Grigorova. "A Comprehensive Analysis of Losses and Efficiency in a Buck ZCS Quasi-Resonant DC/DC Converter." Journal of Low Power Electronics and Applications 15.2 (2025): 34.

[27]: Chen, Shin-Ju, et al. "High Step-Up Interleaved DC–DC Converter with Voltage-Lift Capacitor and Voltage Multiplier Cell." Electronics 14.6 (2025): 1209.

[28]: Alkhaldi, Abdulaziz, Ahmad Elkhateb, and David Laverty. "Voltage lifting techniques for non-isolated dc/dc converters." Electronics 12.3 (2023): 718.

[29]: Ramanathan, Girish Ganesan, and Naomitsu Urasaki. "Non-isolated interleaved hybrid boost converter for renewable energy applications." Energies 15.2 (2022): 610.

[30]: Pilawa-Podgurski, Robert CN, and David J. Perreault. "Merged two-stage power converter with soft charging switched-capacitor stage in 180 nm CMOS." IEEE Journal of Solid-State Circuits 47.7 (2012): 1557-1567.

[31]: Rajesh, Ramachandran, and Natarajan Prabaharan. "Stability and reliability analysis of a non-isolated high gain DC-DC converter." IET Power Electronics 17.9 (2024): 1035-1050.

[32]: Yadav, Neelesh, et al. "Performance evaluation of step-up/down partial power converters based on current-fed dc-dc topologies." IEEE Transactions on Industry Applications 60.5 (2024): 7111-7124.

[33]: Rahimi, Ramin. Advanced Topologies of High Step-Up DC–DC Converters for Renewable Energy Applications. Ph.D. Dissertation, Missouri University of Science and Technology, Rolla, MO, USA, 2022.

[34]: Kapat, Santanu, and Philip T. Krein. "A tutorial and review discussion of modulation, control and tuning of high-performance dc-dc converters based on small-signal and large-signal approaches." IEEE Open Journal of Power Electronics 1 (2020): 339-371.

[35]: Wang, Jiulong, et al. "Review of bidirectional DC–DC converter topologies for hybrid energy storage system of new energy vehicles." Green Energy and Intelligent Transportation 1.2 (2022): 100010.

[36]: Jiang, Yunlei. Soft Switching Control and Loss Analysis for High Frequency Power Converters. Ph.D. Thesis, University of Cambridge, Cambridge, UK, 2022.

[37]: R. Maalandish, S. Ghaemi, and H. Rostami, "An Efficient Interleaved Coupled-Inductor Converter With Passive Clamping for Renewable Applications," IEEE Transactions on Industrial Electronics, vol. 71, no. 3, pp. 2350-2362, 2024.

[38]: Beiranvand, Reza, and Soheil Hasani Sangani. "A family of interleaved high step-up DC–DC converters by integrating a voltage multiplier and an active clamp circuits." IEEE Transactions on Power Electronics 37.7 (2022): 8001-8014.

[39]: Kumar, Pawan, Rajeev Kumar Singh, and Ranjit Mahanty. "Performance of MPPT-based minimum phase bipolar converter for photovoltaic systems." IEEE Transactions on Power Electronics 36.5 (2020): 5594-5609.

[40]: Ahmadi, Sayed Mohsen, et al. "A new forward-flyback converter without right half plane zero." IET Power Electronics 17.15 (2024): 2428-2438.

[41]: Rahimi, Ramin. Advanced Topologies of High Step-Up DC–DC Converters for Renewable Energy Applications. PhD Dissertation, Missouri University of Science and Technology, Rolla, MO, USA, 2022.

[42]: Rajesh, R. Mr. Design and Implementation of Non-Isolated High Gain DC-DC Converter for Photovoltaic Application. Ph.D. Thesis, SASTRA Deemed to be University, Thanjavur, India, 2024.

[43]: Deng, Junjun, et al. "Design of LLC resonant converters based on operation-mode analysis for level two PHEV battery chargers." IEEE/ASME Transactions on Mechatronics 20.4 (2014): 1595-1606.

[44]: Xu, DianGuo, et al. "A review of high frequency resonant DC-DC power converters: Topologies and planar magnetic technologies." Science China Technological Sciences 63.8 (2020): 1335-1347.

[45]: Asish, Jaldu, et al. "Analysis of Non-Minimum Phase Fourth-Order Buck Boost Converter." 2023 7th International Conference on Computer Applications in Electrical Engineering-Recent Advances (CERA). IEEE, 2023.

[46]: Goudarzian, Alireza, Adel Khosravi, and Heidar Ali Raeisi. "Analysis of a step-up dc/dc converter with capability of right-half plane zero cancellation." Renewable Energy 157 (2020): 1156-1170.

[47]: Amudhavalli, Dhanaraj, Nalin Kant Mohanty, and Ashwin Kumar Sahoo. "Interleaved quadratic boost converter integrated with Dickson voltage multiplier with energy storage for high power photo voltaic applications." International Journal of Power Electronics and Drive Systems 12.2 (2021): 957-967.

[48]: Silva-Vera, Edgar D., et al. "Quadratic Boost Converter with Optimized Switching Ripple Based on the Selection of Passive Components." Electricity 5.4 (2024): 877-894.

[49]: Alghaythi, Mamdouh L., et al. "A Non-Isolated High Step-Up Interleaved DC-DC Converter with Diode-Capacitor Multiplier Cells and Dual Coupled Inductors." 2020 52nd North American Power Symposium (NAPS). IEEE, 2021.

[50]: N. Priyadarshi, A. K. Bhoi, R. C. Bansal, and A. Kalam, Eds., " DC-DC Converters for Future Renewable Energy Systems ". Springer, 2022.

[51]: Nouri, Tohid, Ebrahim Babaei, and Seyed Hossein Hosseini. "A generalized ultra step-up DC–DC converter for high voltage application with design considerations." Electric Power Systems Research 105 (2013): 71-84.

[52]: Rajesh, Ramachandran, Natarajan Prabaharan, and Eklas Hossain. "Design and analysis of a new high step-up converter using switched-inductor-capacitor voltage multiplier cells for photovoltaic application." IEEE Journal of the Electron Devices Society 12 (2023): 842-848.

[53]: Tian, Guosheng, et al. "Isolated High Step-Up Soft-Switching Quasi-Z-Source DC–DC Converter." IEEE Access 12 (2024): 49927-49936.

[54]: Spiazzi, Giorgio, et al. "An Isolated Bidirectional Soft-Switching DC-DC Converter for Wide Input/Output Voltage Range." Energies 17.23 (2024): 6121.

[55]: Jiang, Li, et al. "A new push-pull DC/DC converter topology with complementary active clamped." IEEE Transactions on Industrial Electronics 69.6 (2021): 6445-6449.

[56]: Alhuwaishel, Fahad M., and Nabil A. Ahmed. "Coupled inductor based boost microinverter with dual mode time sharing operation for renewable energy applications." IEEE Access 12 (2024): 73889-73905.

[57]: Abolghasemi, Mahdi, et al. "Recent advances of step-up multi-stage DC-DC converters: A review on classifications, structures and grid applications." Energy Reports 13 (2025): 3050-3081.

[58]: Chen, Shin-Ju, et al. "Interleaved High Voltage Gain DC-DC Converter with Winding-Cross-Coupled Inductors and Voltage Multiplier Cells for Photovoltaic Systems." Electronics 13.10 (2024): 1851.

[59]: Semiromizadeh, Javad, Hamed Izadi, and Ehsan Adib. "High step-up interleaved DC-DC converter for photovoltaic systems." IET Power Electronics 15.1 (2022): 33-42.

[60]: Ye, Haixiong, et al. "High step-up interleaved dc/dc converter with high efficiency." Energy sources, Part A: recovery, utilization, and environmental effects 46.1 (2024): 4886-4905.

[61]: Akhlaghi, Zahra, Amirhossein Karimi, and Ehsan Adib. "High step up DC–DC converter with low conduction losses and reduced switching losses." IET Renewable Power Generation 18.4 (2024): 654-662.

[62]: Luo, Fang Lin, and Hong Ye. "Positive output super-lift converters." IEEE Transactions on Power Electronics 18.1 (2003): 105-113.

[63]: de Souza, Alencar Franco, Fernando Lessa Tofoli, and Enio Roberto Ribeiro. "Switched capacitor DC-DC converters: A survey on the main topologies, design characteristics, and applications." Energies 14.8 (2021): 2231.

[64]: Mahafzah, Khaled A., et al. "A new smart grid hybrid DC–DC converter with improved voltage gain and synchronized multiple outputs." Applied Sciences 14.6 (2024): 2274.

[65]: Nhi, Nguyen Hong. " Fault-tolerant control scheme of modular multilevel converter in medium-voltage motor drive applications." (2024): 43-51.

[66]: Alkhaledi, Khaled, et al. "Multilevel converter to access maximum power from distributed energy source based smart grids." Frontiers in Energy Research 11 (2023): 1125461.

[67]: Xiao, Bailu, et al. "Three-phase modular cascaded H-bridge multilevel inverter with individual MPPT for grid-connected photovoltaic systems." 2013 Twenty-Eighth Annual IEEE Applied Power Electronics Conference and Exposition (APEC). IEEE, 2013.

[68]: Reddy, D. Chinna Kullay, S. Satyanarayana, and Vaishnavi Ganesh. "Design of hybrid solar wind energy system in a microgrid with MPPT techniques." International Journal of Electrical and Computer Engineering 8.2 (2018): 730-740.

[69]: Sharma, Amit Kumar, et al. "Role of metaheuristic approaches for implementation of integrated MPPT-PV systems: a comprehensive study." Mathematics 11.2 (2023): 269.

[70]: D. Rekioua and E. Matagne, Optimisation of Photovoltaic Power Systems: Modelisation, Simulation and Control. Springer, 2012.

[71]: Alombah, N. H., et al. (2025). Multiple-to-single maximum power point tracking for photovoltaic systems under partial shading conditions. Scientific Reports, 15, Article 8752.

[72]: Ashwini, M., et al. (2025). Design and comprehensive analysis of adjustable step size perturb and observe MPPT algorithm. Scientific Reports, 15, Article 7234

[73]: Et-Torabi, K., et al. (2025). Experimental Validation of Intelligent MPPT Control for Photovoltaic Systems Using Fractional Open-Circuit Voltage Method. Engineering, Technology & Applied Science Research, 15(1), 9657-9662.

[74]: Naderi, E., et al. (2024). A high gain interleaved MPPT converter using modified switched inductor boost cell. International Scholarly and Scientific Research & Innovation, 18(5), 217-225

[75]: S. Mohammed belhadj, B. Meliani, M. Rivera, P. Wheeler, E. Zerdali and S. Zaidi, "Three-level DC-DC converter with fuzzy logic-based MPPT controller for photovoltaic applications," 13th International Conference on Power Electronics, Machines and Drives (PEMD 2024), Nottingham, UK, 2024, pp. 639-645, doi: 10.1049/icp.2024.2222.

[76]: Doubabi, Hajar. Contribution à l'amélioration de l'efficacité de la chaîne de conversion photovoltaïque. Diss. Université de Reims Champagne-Ardenne, 2021.

[77]: Belhadj, Souheyb Mohammed, et al. "Control of multi-level quadratic DC-DC boost converter for photovoltaic systems using type-2 fuzzy logic technique-based MPPT approaches." Heliyon 11.3 (2025).

[78]: E. B. Elnaghi, M. Asghar, and M. Ramzan, "Experimental validation of an adaptive Type-2 fuzzy logic MPPT controller for photovoltaic systems," Scientific Reports, vol. 15, Article 10188, 2025.

[79]: X. Li, J. Zhao, and Z. Wang, "High-speed feedforward neural network MPPT for photovoltaic systems under rapid irradiance changes," IEEE Transactions on Sustainable Energy, vol. 16, no. 2, pp. 345–353, Apr. 2025

[80]: Li, Y., Zhao, P., & Wang, L. (2025). Real-time implementation of NARX neural MPPT controllers on a DSP platform. Solar Energy, 234, 45–58.

[81]: A. Musa, A modified particle swarm optimization based maximum power point tracking for photovoltaic converter system, Ph.D. thesis, Universiti Teknologi Malaysia, Johor Bahru, Malaysia, 2015.

[82]: Mammeri, E., et al. "New MPPT Hybrid Controller Based on Genetic Algorithms and Particle Swarm Optimization for Photovoltaic Systems." Int. J. Circuits Syst. Signal Process 17 (2023): 83-91.

[83]: Dagal, Idriss, AL-Wesabi Ibrahim, and Ambe Harrison. "Leveraging a novel grey wolf algorithm for optimization of photovoltaic-battery energy storage system under partial shading conditions." Computers and Electrical Engineering 122 (2025): 109991.

[84]: Hadj Salah, Zahra Bel, et al. "A new efficient cuckoo search MPPT algorithm based on a super-twisting sliding mode controller for partially shaded standalone photovoltaic system." Sustainability 15.12 (2023): 9753.

[85]: Zhang, Xiang, et al. "A hybrid global maximum power point tracking control method based on particle swarm optimization (PSO) and perturbation and observation (P&O)." Electric Power Systems Research 248 (2025): 111967.

[86]: Mohammad Noor, Siti Zaliha. Single-Phase Single-Stage String Inverter for a Grid-Connected Photovoltaic System with Integrated Perturb and Observe–Fuzzy Logic Control MPPT Technique. Ph.D. Thesis, Universiti Teknologi MARA (UiTM), Shah Alam, Malaysia, 2018.

[87]: Kumar, Sandeep, Raunak Jangid, and Kapil Parikh. " Comparative performance analysis of ANFIS and ANN algorithms based MPPT energy harvesting in solar PV system "

[88]: Seguel, Julio López, S. I. Seleme Jr, and Lenin MF Morais. "Comparison of the performance of MPPT methods applied in converters Buck and Buck-Boost for autonomous photovoltaic systems." Ingeniare: Revista Chilena de Ingenieria 29.2 (2021): 229-244.

[89]: Villegas-Mier, César G., et al. "Artificial neural networks in MPPT algorithms for optimization of photovoltaic power systems: A review." Micromachines 12.10 (2021): 1260.

[90]: NM, Jothi Swaroopan. "MPPT of solar PV systems using PSO memetic algorithm considering the effect of change in tilt angle." Scientific Reports 15.1 (2025): 1-17.

[91]: de Oliveira, Fernando Marcos, et al. "Development of an MPPT-based genetic algorithm for photovoltaic systems versus classical MPPT techniques in scenarios with partial shading." Inventions 9.3 (2024): 64.

[92]: Mrhar, Oumaima, Khalid Kandoussi, and Mohamed Eljouad. "A new hybrid MPPT algorithm combining P&O and fuzzy logic techniques." International Journal of Power Electronics and Drive Systems (IJPEDS) 16.1 (2025): 497-508.

[93]: Aldulaimi, Mahmood Yaseen Mohammed, and Mesut Çevik. "AI-Enhanced MPPT Control for Grid-Connected Photovoltaic Systems Using ANFIS-PSO Optimization." Electronics 14.13 (2025): 2649.

[94]: Green, Martin A. "Solar cells: operating principles, technology, and system applications." (1981).

[95]: Mlazi, Nsulwa John, et al. "Mathematical modeling and extraction of parameters of solar photovoltaic module based on modified Newton–Raphson method." Results in Physics 57 (2024): 107364.

[96]: Doubabi, Hajar, and Issam Salhi. "Design and dSPACE Implementation of a Simplified Fuzzy Control of a DC-DC Three-Level Converter." Journal of Electrical and Computer Engineering 2021.1 (2021): 5593572.

[97]: Erickson, R. W., & Maksimović, D. (2001). Fundamentals of Power Electronics (2nd ed.). Springer Science & Business Media.